

DYNAMIC ORIENTATION  
OF NUCLEI AT LOW TEMPERATURES

A study of the mechanisms of  
dynamic polarization in polarized targets

W. de BOER

1843 1725

C10057  
19180



P1843  
1725

DYNAMIC ORIENTATION  
OF NUCLEI AT LOW TEMPERATURES

A study of the mechanisms of  
dynamic polarization in polarized targets

PROEFSCHRIFT

TER VERKRIJGING VAN DE GRAAD VAN DOCTOR IN DE  
TECHNISCHE WETENSCHAPPEN AAN DE TECHNISCHE  
HOGESCHOOL TE DELFT, OP GEZAG VAN DE RECTOR  
MAGNIFICUS, IR. H.B. BOEREMA, HOGLERAAR IN DE  
AFDELING DER ELEKTROTECHNIEK, VOOR EEN COMMISSIE  
AANGEWZEN DOOR HET COLLEGE VAN DEKANEN,  
TE VERDEDIGEN OP DINSDAG 9 JULI 1974 TE  
14.00 UUR.

DOOR

WILLEM DE BOER

NATUURKUNDIG INGENIEUR  
GEBOREN TE STEENWIJKERWOLD

1843 1725

BIBLIOTHEEK TU Delft  
P 1843 1725



C 571918



1974  
CERN SCIENTIFIC REPORTS  
TYPING SERVICE

Dit proefschrift is goedgekeurd door de promotor:

PROF. DR. B.S. BLAISSE

ABSTRACT

A study has been made of the mechanisms of dynamic orientation of nuclei in organic materials at temperatures below 1 K and magnetic fields up to 50 kG.

After a description of the theory of dynamic polarization, the dynamic polarization experiments in diols, doped with paramagnetic  $\text{Cr}^{\text{V}}$ -complexes, are described. These measurements are compared quantitatively with a spin temperature model, in which it is assumed that the polarization of the nuclei is obtained via the thermal contact with a dynamically cooled electron spin-spin interaction reservoir. The role of such a reservoir was apparent from the transient behaviour of various nuclear spin systems, contained in the same sample. The observed high polarizations (80%-98% for protons,  $\sim 40\%$  for deuterons and  $\sim 50\%$  for carbon-13 nuclei) make this kind of material attractive for polarized targets.

We observed a pure tensor polarization of deuterons in a solid. This was obtained by slightly off-resonance irradiation of the proton spin system in partially deuterated diols. The results could be understood quantitatively in terms of the spin temperature theory.

At the end the dynamic polarization experiments with the free radical BDPA are described. The polarizations of different nuclei, measured as function of the microwave frequency, show clearly the contributions of different mechanisms of dynamic polarization.

In all the experiments mentioned above, the concept of a spin-spin interaction reservoir appears to be useful, even under conditions where the polarization of the spin system approaches one.

CONTENTS

	<u>Page</u>
LIST OF SYMBOLS	viii
INTRODUCTION AND SURVEY	1
CHAPTER I THE THEORY OF NUCLEAR DYNAMIC POLARIZATION	3
1. GENERALITIES	3
2. DYNAMIC POLARIZATION IN CASE OF NEGLIGIBLE ELECTRON SPIN-SPIN INTERACTIONS	5
3. DYNAMIC POLARIZATION IN CASE OF NON-NEGLIGIBLE ELECTRON SPIN-SPIN INTERACTIONS	8
3.1 Introduction	8
3.2 The spin temperature theory	9
3.3 Special cases	13
3.3.1 <i>Dynamic polarization at "high temperatures"</i>	13
3.3.2 <i>Dynamic polarization at "low temperatures" under strong saturation conditions</i>	14
3.3.3 <i>Dynamic polarization at "low temperatures" under weak saturation conditions</i>	19
4. SPIN LATTICE RELAXATION	21
4.1 Electron spin lattice relaxation	21
4.2 Nuclear spin lattice relaxation	22
5. DESCRIPTION OF THE DEUTERON SPIN SYSTEM	23
CHAPTER II EXPERIMENTAL TECHNIQUES	25
1. GENERAL ASPECTS	25
2. NUCLEAR MAGNETIC RESONANCE EQUIPMENT	27
3. ELECTRON SPIN RESONANCE EQUIPMENT	28
4. SAMPLE PREPARATION	29
CHAPTER III DYNAMIC POLARIZATION IN DIOLS DOPED WITH Cr <sup>V</sup> -COMPLEXES	32
1. ELECTRON SPIN RESONANCE MEASUREMENTS	32
2. MAXIMUM POLARIZATION VALUES OF PROTONS, DEUTERONS, AND CARBON-13 NUCLEI	33
2.1 Absolute values of the polarization	33
2.2 Relative values of the polarization	34
2.3 Comparison of the polarizations with the equal spin temperature hypothesis	35
2.4 Polarization versus microwave frequency	36

	<u>Page</u>
3. TRANSIENT BEHAVIOUR OF THE VARIOUS SPINS	37
3.1 Polarization build-up with microwave irradiation	37
3.2 Attainment of equilibrium with unequal initial spin temperatures	39
3.3 Thermalization within the deuteron spin system	41
3.4 Proton spin lattice relaxation	44
4. COMPARISON WITH THE SPIN TEMPERATURE THEORY	45
CHAPTER IV A PURE TENSOR POLARIZATION OF A DEUTERON SPIN SYSTEM	49
1. INTRODUCTION	49
2. SIMPLE ESTIMATES FROM THE SPIN TEMPERATURE THEORY	49
2.1 Steady-state values of the proton polarization and deuteron alignment	49
2.2 Transient behaviour of P(H) and A(D)	51
2.2.1 <i>Thermal mixing rate</i>	51
2.2.2 <i>Spin lattice relaxation in the rotating frame</i>	51
3. EXPERIMENTAL RESULTS	51
4. DISCUSSION	58
CHAPTER V DYNAMIC POLARIZATION EXPERIMENTS WITH THE FREE RADICAL BDPA	60
1. INTRODUCTION	60
2. RESULTS	61
FINAL CONCLUSIONS	66
ACKNOWLEDGEMENTS	68
REFERENCES	69
APPENDIX	75

LIST OF SYMBOLS

$\alpha$	inverse spin temperature of the electron Zeeman energy in the rotating frame.
$\alpha_0$	value of $\alpha$ under thermal equilibrium conditions.
$\alpha_{\text{lab}}$	inverse spin temperature of the electron Zeeman energy in the laboratory frame.
$\alpha_{\text{H}}$	inverse spin temperature of the proton Zeeman energy in the rotating frame.
$\beta$	inverse spin temperature of a nuclear Zeeman reservoir.
$\beta_{\text{H}}$	inverse spin temperature of the proton spin-spin interaction reservoir.
$\beta_{\text{f}}$	steady-state value of $\beta_{\text{H}}$ after saturation of the proton spin system with an RF field.
$\beta_{\text{i}}$	value of $\beta_{\text{H}}$ before saturation of the proton spin system with an RF field.
$\gamma$	inverse spin temperature of the electron spin-spin interaction reservoir.
$\gamma_{\text{D}}$	inverse spin temperature of the deuteron Zeeman energy.
$\gamma_{\text{e}}$	gyromagnetic ratio for electrons.
$\gamma_{\text{n}}$	gyromagnetic ratio for nuclei.
$\delta$	frequency difference.
$\Delta$	difference between the electron Larmor frequency and the microwave frequency.
$\Delta_{\text{n}}$	difference between the proton Larmor frequency and the RF frequency.
$\epsilon$	dipolar coupling coefficient.
$\nu$	irradiation frequency.
$\nu_{\text{C}}$	carbon-13 Larmor frequency.
$\nu_{\text{D}}$	deuteron Larmor frequency.
$\nu_{\text{e}}$	electron Larmor frequency.
$\nu_{\text{H}}$	proton Larmor frequency.

$\nu_n$	nuclear Larmor frequency.
$\nu_L$	frequency corresponding to the local, internal magnetic fields.
$\nu_Q$	frequency, characterizing the deuteron quadrupole interactions.
$\rho$	density matrix.
$\rho_0$	density matrix of an electron spin system in thermal equilibrium with the lattice.
$\Sigma$	normalization constant of a density matrix.
$\tau_{\pm}$	proton polarization time constant in case of a resolved solid-state effect.
$\tau(D,D)$	decay time of pure deuteron alignment.
$\tau(H,D)$	thermal mixing time between protons and electrons.
$\tau_{mix}$	thermal mixing time of $\alpha_H$ and $\beta_H$ .
$\tau_{nS}$	time constant for the relaxation of the nuclear Zeeman energy to the electron spin-spin interaction reservoir.
$\tau_{RF}$	common relaxation time of $\alpha_H$ and $\beta_H$ in the rotating frame.
$\tau_{Sn}$	time constant for the relaxation of the electron spin-spin interaction energy to the nuclear Zeeman reservoirs.
$\underline{\mu}$	magnetic dipole moment.
$\mu_B$	Bohr magneton.
$\Omega$	parameter related to the heat capacity of an electron spin-spin interaction reservoir.
$\Omega_n$	parameter related to the heat capacity of the reservoir consisting of the proton spin-spin interaction energy plus deuteron quadrupole interaction energy.
$a$	ratio of spin lattice relaxation times of the electron Zeeman reservoir and the electron spin-spin interaction reservoir.
$A$	alignment.
$A(D)$	deuteron alignment.
$A$	constant.
$ a\rangle,  b\rangle,  c\rangle, \text{ and }  d\rangle$	eigen functions of an electron plus a proton.
$b$	constant.
$c$	constant.
$C$	constant.
$C_{SS}$	heat capacity of an electron spin-spin interaction reservoir.

$C_{Zn}$	heat capacity of a nuclear Zeeman reservoir.
$d$	diffusion barrier.
$e$	electrons.
ESR	electron spin resonance.
$E_m$	energy of the Zeeman level, characterized by $m$ .
$f$	leakage factor.
$g$	$g$ -factor.
$g_1, g_2, g_3$	principal values of $g$ -tensor.
$g_i$	$g$ -factor of a particular spin of an inhomogeneous spin system.
$g(\nu)$	ESR line-shape function.
$h$	constant of Planck.
$\hbar$	constant of Planck, divided by $2\pi$ .
$H$	external magnetic field.
$2H_1$	amplitude of an RF field.
$H$	Hamiltonian.
$H_L$	local internal magnetic field.
$H^*$	Hamiltonian in rotating frame for an inhomogeneous electron spin system.
$h(\nu)$	proton NMR line-shape function.
$H_{II}$	Hamiltonian for nuclear spin-spin interaction energy.
$H_{IZ}$	Hamiltonian for nuclear Zeeman energy.
$H_{RF}$	Hamiltonian corresponding to an oscillating magnetic field.
$H_{SI}$	Hamiltonian for interaction between an electron and nuclear spin system.
$H_{SS}$	Hamiltonian for electron spin-spin interaction energy.
$H_{SS}^0$	secular part of $H_{SS}$ .
$H_{SSH}$	Hamiltonian for proton spin-spin interaction energy.
$H_{SZ}$	Hamiltonian for electron Zeeman energy.
$H_Q$	Hamiltonian for deuteron quadrupole interaction energy.
$H_{ZD}$	Hamiltonian for deuteron Zeeman energy.
$H_{ZH}$	Hamiltonian for proton Zeeman energy.
$H_{lab}$	Hamiltonian in the laboratory frame.

$H_{\text{rot}}$	Hamiltonian in the rotating frame.
$\underline{I}$	spin operator for nuclei.
$I$	value of a nuclear spin.
$I_x, I_y, I_z$	x, y, and z components of $\underline{I}$ .
$I_+, I_-$	raising and lowering operators for nuclear spins.
$J^+$	intensity of the $m = 1$ to $m = 0$ transition within the deuteron spin system.
$J^-$	as $J^+$ , but now for the $m = 0$ to $m = -1$ transition
$k$	Boltzmann constant.
$m$	magnetic quantum number ( $\langle I_z \rangle$ ).
$n$	nuclei.
$n_e$	number of electrons.
$n_H$	number of protons.
$n_n$	number of nuclei
$n_m$	fraction of spins with energy $E_m$ .
NMR	nuclear magnetic resonance.
$P$	polarization.
$P_e$	electron polarization.
$P_n$	nuclear polarization.
$P_0$	electron polarization at thermal equilibrium.
$P(^{13}\text{C})$	carbon-13 polarization.
$P(\text{D})$	deuteron polarization.
$P(\text{H})$	proton polarization.
$\dot{Q}$	heat transfer per second between sample and bath.
$\underline{r}$	vector joining two spins.
$R$	half the average distance between two electron spins.
$R$	$J^+/J^-$ .
RF	radio frequency.
$\underline{S}$	spin operator for electrons
$S$	value of an electron spin
$S_x, S_y, S_z$	x, y and z component of $\underline{S}$ .
$S_+, S_-$	raising and lowering operators for electron spins.
$S_1$	saturation parameter for the allowed transitions of an electron spin system.

$S^{\pm}$	saturation parameters for the forbidden transitions.
$s^{\pm}$	saturation parameters for the "double" forbidden transitions, involving an electron spin and two proton spins.
$S_4$	nuclear spin lattice relaxation time divided by the time constant of the relaxation of the nuclear Zeeman energy to the electron spin-spin interaction reservoir.
$S_{D1}^{\pm}, S_{D2}^{\pm}$	saturation parameters for the "double" forbidden transitions, involving an electron spin and two deuteron spins.
$T(C)$	spin temperature of the carbon-13 spin system.
$T(D)$	spin temperature of the deuteron spin system.
$T(H)$	spin temperature of the proton spin system.
$T_{1D}$	deuteron spin lattice relaxation time.
$T_{1H}$	proton spin lattice relaxation time.
$T_{1e}$	electron spin lattice relaxation time
$T_{1SS}$	relaxation time of the electron spin-spin interaction reservoir.
$T_{2e}$	transverse relaxation time of a homogeneous electron spin system.
$U$	unitary matrix.
$W_0$	transition probability for the allowed transitions within an electron spin system due to a microwave field.
$W_e^{\pm}, W_n^{\pm}$	transition probabilities for the forbidden transitions due to a microwave field.
$x$	$A(D) - \frac{3}{4} P(D)^2$ ;
$X$	$v_Q [3 \cos^2 (\theta) - 1]$ .

## INTRODUCTION AND SURVEY

Dynamic polarization by electron-nucleus dipolar coupling has been studied for many years now. The interest in these experiments comes from two sides: at first from the mechanisms of dynamic polarization itself<sup>1-7)</sup>, and secondly from the side of nuclear and high-energy physics. In these fields dynamic polarization is used for the production of polarized targets, in which the spins of the nuclei under study have a certain degree of orientation, for example protons having their spins mainly parallel or antiparallel to the direction of an external magnetic field. Oriented nuclei can be used, amongst other things, to study the role of the spin in the interaction between the elementary particles, to determine quantum numbers (spins and parities), or to test invariance properties of interactions. We shall not attempt to describe the many experiments carried out on these interesting subjects, but refer the reader to some conference proceedings<sup>8,9)</sup>.

This study will mainly be concerned with the mechanisms of dynamic polarization in organic materials under conditions which are suitable for obtaining high polarizations, i.e. at low temperatures and in high magnetic fields. These materials are doped with suitable paramagnetic impurities, of which the spin of the "free" electron can easily be oriented in a magnetic field owing to its strong magnetic moment; this in contrast to the nuclei, for which the magnetic moments are in general three orders of magnitude smaller than for electrons. Then the thermal disturbances prevent any appreciable degree of orientation, even in a magnetic field of 25 kG and at temperatures of about 0.5 K. However, by microwave irradiation of the electron spin system it is possible to transmit the high degree of ordering of the electrons to the nuclei, thus increasing the nuclear polarization.

Several schemes, effects, or mechanisms of dynamic polarization have been proposed and most of them were experimentally verified<sup>4,5,10-18)</sup>. In the case of a solid it is in general not easy to find out which mechanism is responsible for dynamic polarization, because several mechanisms may act simultaneously. The situation is especially complicated by the magnetic interactions between similar spins, which may be appreciable in a solid. In the early theories of dynamic polarization in solids, these spin-spin interactions were normally neglected or only partially taken into account [see the contributions of Overhauser<sup>11)</sup>, Bloembergen and Sorokin<sup>16)</sup>, Abragam and Proctor<sup>17)</sup>, and Jeffries<sup>2)</sup>]. However, later on the important role of especially the electron spin-spin interactions has been demonstrated several times in dynamic polarization experiments [see reviews by Borghini<sup>4)</sup>, Atsarkin and Rodak<sup>5)</sup>, and Wenckebach and Poullis<sup>6)</sup>]. It appears that the experiments described further on can only be understood by taking these spin-spin interactions into account.

In Chapter I we will summarize the theory of dynamic polarization in terms of the spin temperature theory. The latter forms the basic framework for the theory of magnetic resonance in solids. In this theory the spin-spin interactions are taken into account by the

introduction of a separated reservoir<sup>19,20</sup>), possessing its own degrees of freedom and its own temperature under suitable conditions. The concept of such a reservoir led to the prediction of several rather unexpected results, which were experimentally verified at first for nuclear spin systems [see reviews and contributions by Abragam<sup>1</sup>), Goldman<sup>3</sup>), Provotorov<sup>19</sup>), Anderson and Hartman<sup>21</sup>), Philippot<sup>22</sup>), Jeener<sup>23</sup>), Hebel<sup>24</sup>) and others] and later for electron spin systems [Atsarkin and Rodak<sup>5</sup>)]. The influence of the electron spin-spin interaction reservoir can manifest itself clearly in the transient behaviour of various spin systems, as will be apparent from the experiments described in Chapter III. There the dynamic polarization experiments performed in diols, doped with paramagnetic Cr<sup>V</sup>-complexes, are described. These materials are used as a substance for polarized targets, because of the high polarizations obtained in them: about 80% to 98% for protons<sup>25-29</sup>), 40% for deuterons<sup>27</sup>), and 50% for carbon-13 nuclei<sup>27</sup>). Experimental evidence is given, showing that the high polarizations in these samples result mainly from "dynamic polarization by cooling of the electron spin-spin interaction reservoir". We made a quantitative comparison of the measurements with a spin temperature model of Borghini<sup>30</sup>). Several features, such as a steep temperature dependence of the polarization and an increase of the ratio of lattice to final spin temperature for spin temperatures below 2 mK, were found to be in agreement with experimental results obtained in a <sup>3</sup>He-<sup>4</sup>He dilution refrigerator, which was located in a 25 kG magnetic field.

In partially deuterated diols a new method of orientation of the deuteron spin system was found<sup>31,32</sup>). It allows one to vary the deuteron tensor polarization independently of its vector polarization. This occurs by off-resonance RF irradiation of the polarized proton spin system, of which the polarization can be enhanced beforehand by dynamic polarization. The spin temperature theory provides a quantitative explanation in terms of a thermal contact between the proton spin-spin interaction reservoir and a deuteron quadrupole interaction reservoir. These measurements are described in Chapter IV.

In Chapter V the experiments with the free radical 1,2-bis-diphenylene-1-phenylallyl (BDPA) are described. They were particularly interesting because the contributions of different mechanisms of dynamic polarization could be distinguished from one another, owing to the narrow electron spin resonance line of BDPA.

Until now most of the experimental verifications of the spin temperature theory were made under conditions where the "high temperature approximation" is valid. The extension of the theory toward low temperatures is questionable, because of the limited degrees of freedom of the spin-spin interaction reservoir at high polarizations<sup>22</sup>). The limits under which the concept of an electron spin-spin interaction reservoir is still valid, can only be determined by experiments. Under our experimental conditions, the use of this concept still provides an adequate description of the processes.

## CHAPTER I

### THE THEORY OF NUCLEAR DYNAMIC POLARIZATION

#### 1. GENERALITIES

The orientation of a system of spins  $I$  along an axis  $Oz$  can be described by so-called orientation parameters, which are defined as expectation values of irreducible spin tensors<sup>33</sup>). Here we will consider only the vector polarization  $P$ , which is defined as:

$$P = \langle I_z \rangle / I \quad (I.1)$$

and the tensor polarization or alignment  $A$ , defined as

$$A = \langle 3I_z^2 - I(I+1) \rangle / I^2 . \quad (I.2)$$

The orientation parameters of higher order in  $I_z$  are normally null or very small, and can be neglected in practice. For spin  $I = \frac{1}{2}$  the alignment is always zero and the orientation coincides with the (vector) polarization.

If a spin  $I$  is subjected to a magnetic field  $H$  in the direction  $Oz$ , then the Zeeman interaction  $H_{ZI} = -\underline{\mu} \cdot \underline{H}$  establishes a set of  $2I+1$  sublevels with energy  $E_m = -m\hbar\gamma H$ ;  $\mu = |\gamma| \hbar I = g\mu_B I$  is the magnetic dipole moment,  $|\gamma|$  is the gyromagnetic ratio,  $\hbar$  is Planck's constant, divided by  $2\pi$ , the symbol  $m = \langle I_z \rangle$ ,  $g$  is the spectroscopic splitting factor, and  $\mu_B$  is the Bohr magneton. Later we will use the subscripts  $e$  for electrons and  $n$  for nuclei in the above-mentioned definition of  $\gamma$ ;  $\gamma_e$  is negative and  $\gamma_n$  is positive for the nuclei considered.

The polarization of an assembly of identical nuclei with  $I = \frac{1}{2}$  is easily calculated from Eq. (I.1) to be

$$P = n_+ - n_- , \quad (I.3)$$

where  $n_+$  is the fraction of the spins in the  $m = +\frac{1}{2}$  state and  $n_-$  the fraction with  $m = -\frac{1}{2}$ .

If the spins are in internal equilibrium, they can be characterized by a temperature  $T_S$ . The distribution of the different spins over the magnetic sublevels is then given by the Boltzmann law:

$$\frac{n_-}{n_+} = \exp (-E_m / kT_S) . \quad (I.4)$$

From Eqs. (I.3) and (I.4) the polarization for  $I = \frac{1}{2}$  is found to be

$$P = \tanh (\mu H / kT_S) . \quad (I.5)$$

This formula is a special case of the general Brillouin formula for arbitrary spin value:

$$P = \frac{2I+1}{2I} \coth \left[ \frac{2I+1}{2I} \left( \frac{\mu H}{kT} \right) \right] - \frac{1}{2I} \coth \left( \frac{1}{2I} \frac{\mu H}{kT} \right) . \quad (I.6)$$

It should be noted that if the polarization value is the one of thermal equilibrium with the lattice, the levels of highest energy are always less populated than the lower ones. Later it will appear possible, by dynamic polarization methods, to create situations in which the highest levels are more populated than the lower ones. If one assumes Eq. (I.4) to be still valid, this situation corresponds to negative spin temperatures. The spin system is then of course not in equilibrium with the lattice, because negative temperatures are only defined for systems with an upper bound in the energy spectrum.

Equation (I.5) shows that large magnetic fields and low temperatures are favourable for high polarizations. However, for example for protons at a temperature of 0.5 K in a 25 kG magnetic field, the polarization  $P_n$  is only 0.00511. For a free electron the magnetic moment is about three orders of magnitude larger than for protons and the polarization  $P_e$  is -0.9975 under the conditions mentioned.

Therefore to obtain a high nuclear polarization, the "brute force" method, which consists of just cooling the sample in an external magnetic field and waiting for thermal equilibrium, is rather impractical, at least in diamagnetic materials, because temperatures in the mK region need to be maintained for a relatively long time (the nuclear spin lattice relaxation times in diamagnetic materials are typically in the order of weeks or more at high fields and low temperatures).

In paramagnetic, ferromagnetic or antiferromagnetic materials one may use the large internal magnetic fields, sometimes as large as  $10^6$  Gauss, to orient nuclei<sup>34-37</sup>). A review of the possibilities and applications of the different static nuclear orientation methods are described, for example, by Shirley<sup>38</sup>). Another method of nuclear orientation, which does not rely on thermodynamical properties, is optical pumping; this has been successfully applied to  $^3\text{He}$  gas under reduced pressure and to a few solids<sup>39,40</sup>). Solid  $^3\text{He}$  has been polarized by adiabatic compressional cooling down to the mK region up to a polarization of about 50%<sup>41</sup>).

We will not describe these different methods here, but will proceed to a description of the dynamical methods, to which we will restrict ourselves in the following. "Dynamic" refers to the fact that in these cases a non-equilibrium between the spin system and the lattice is created in contradistinction to the static methods.

The basis for the dynamic methods can be described as follows: assume that the sample contains, besides the nuclei of interest, some other type of spin species with a higher magnetic moment, for example the unpaired electrons of free radicals, ions having an unpaired electron in one of the outer shells, or some other type of paramagnetic complex. As mentioned before, these electrons can be polarized to nearly 100% under moderate experimental conditions. As a consequence of the interaction between the different spin species, this high degree of ordering of the electron spins can be transmitted to the nuclei under suitable conditions, thus enhancing their polarization.

Most of these methods make use of transitions between the different energy levels, which can be induced by resonant oscillating magnetic fields (RF or microwave fields). An essentially different method consists of a rotation of the external magnetic field<sup>42,43</sup>; however, because of its limited use, we will not elaborate further on this subject.

The first dynamic polarization scheme involving microwave pumping of nuclear spins was invented by Overhauser<sup>11</sup>) for the polarization of nuclei in metals, and was experimentally verified by Carver and Slichter<sup>44</sup>). It was later extended to the case of liquids and paramagnetic ions involving strong hyperfine<sup>14,45,46</sup>) and dipolar coupling<sup>16,17,47-49</sup>). In the following we will consider only the case of a dipolar coupling between the electron and nuclear spins and discuss the different mechanisms, which may give rise to dynamic polarization under such conditions.

## 2. DYNAMIC POLARIZATION IN CASE OF NEGLIGIBLE ELECTRON SPIN-SPIN INTERACTIONS

The spin Hamiltonian of an assembly of identical nuclei diluted with paramagnetic centres in the presence of a magnetic field, can be written as

$$H = H_{SZ} + H_{IZ} + H_{SS} + H_{II} + H_{SI} + H_{RF}, \quad (I.7)$$

where the first two terms refer to the electron and nuclear Zeeman energies; the latter terms correspond to the spin-spin interactions between electrons, nuclei, and electrons-nuclei, respectively.  $H_{RF}$  refers to the possible presence of an oscillating magnetic field. The specific form of the different terms can be found in standard works<sup>1-3</sup>). We did not write the term corresponding to the interaction with the lattice, which is complicated since it involves the phonon spectrum of the lattice, but we will treat this interaction in a phenomenological way by describing the return to thermal equilibrium by a single exponential function, which is usually observed. This will be discussed in more detail in Section 4 of this chapter. Also the interaction with the crystalline field will be neglected, since we will deal only with electron spins for which  $S = \frac{1}{2}$ , so this interaction then causes only a shift of the energy levels, but does not change the distance between the levels.

Before discussing the various terms of the Hamiltonian, we first consider briefly the simple case of a system consisting of one proton and one electron. Only four terms need to be considered:

$$H_{SZ} + H_{IZ} + H_{SI} + H_{RF} \quad (I.8)$$

The term  $H_{SI}$  is assumed to coincide with the dipolar interaction between the magnetic moments of the electron spin  $S$  and the proton spin  $I$ :

$$H_{SI} = \frac{\hbar^2 \gamma_e \gamma_n}{r^3} \left[ \underline{S} \cdot \underline{I} - \frac{3(\underline{S} \cdot \underline{r})(\underline{I} \cdot \underline{r})}{r^2} \right]; \quad (I.9)$$

the vector  $\underline{r}$  joining the spins is assumed to have the polar angles  $\theta$  and  $\phi$ .  $H_{SI}$  contains terms proportional to the various bilinear products of spin operators:  $S_z I_z$ ,  $S_z I_{\pm}$ ,  $S_{\pm} I_z$ ,  $S_{\pm} I_{\pm}$ , and  $S_{\mp} I_{\pm}$ , where  $S_{\pm} = S_x \pm i S_y$ , etc. The diagonal terms shift the energy levels

slightly, while the off-diagonal terms cause also an admixing of the eigenstates of the Zeeman energy, denoted by  $| - + \rangle$ ,  $| - - \rangle$ ,  $| + + \rangle$ , and  $| + - \rangle$ . The most "powerful" off-diagonal term is  $S_z I_x$ , since it acts between levels separated by the nuclear Zeeman energy only. Using first-order perturbation theory, the admixed eigenfunctions read<sup>1,2)</sup>:

$$\begin{aligned} |a\rangle &= | - + \rangle + \epsilon^* | - - \rangle \\ |b\rangle &= | - - \rangle - \epsilon | - + \rangle \\ |c\rangle &= | + + \rangle - \epsilon^* | + - \rangle \\ |d\rangle &= | + - \rangle + \epsilon | + + \rangle \end{aligned}$$

The dipolar coefficient  $\epsilon$  is equal to

$$\epsilon = \frac{3}{4} \frac{\hbar \gamma_e}{r^3 H} \sin \theta \cos \theta e^{-i\phi} \quad ; \quad (I.10)$$

the value of  $\epsilon$  is proportional to the ratio of the local internal field to the external field. For an external field of 25 kG and  $r = 2 \text{ \AA}$  it is typically  $10^{-2}$ . As a consequence of this mixing, the microwave field now has a certain probability to induce, besides the allowed transition, the so-called forbidden transitions, in which an electron and a proton spin flip simultaneously (see Fig. I.1)<sup>15-17)</sup>. By evaluating the matrix elements of  $H_{RF}$  between the admixed eigenstates, it is found that the ratio of the probabilities for a forbidden transition to an allowed transition is equal to  $4|\epsilon|^2$ . For reasons of energy conservation these forbidden transitions occur at a microwave frequency  $\nu = \nu_e \pm \nu_H$ . The forbidden ESR lines may be well separated from the main line in a high magnetic field. They can only be observed by sufficiently sensitive ESR spectrometers<sup>2)</sup>, because the intensity relative to the main line is a factor  $4|\epsilon|^2$  smaller.

It is just the possibility of these forbidden transitions which may cause dynamic polarization. This can be understood from simple arguments. At low temperatures most of the electrons are in the lowest energy states. Application of microwave power at the frequencies of the forbidden transitions may then induce flip-flop transitions to the upper states

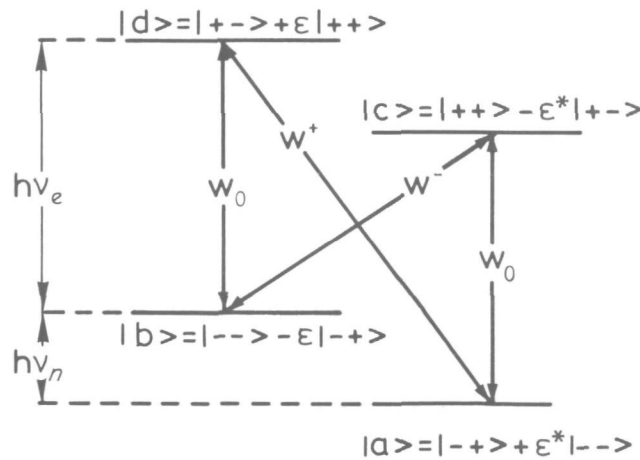


Fig. I.1 Energy level diagram of a simple pair of an electron and a proton.

(|a⟩ → |d⟩ and |b⟩ → |c⟩ in Fig. I.1). After a simultaneous flip-flop, the electron returns to its equilibrium state in a time of about that of the electron spin lattice relaxation time, which is of the order of milliseconds. It is then ready to flip the next nucleus in the same direction, if there are many nuclei surrounding one electron spin. However, once a nuclear spin has flipped, it stays pointing in the same direction for a time of the order of the spin lattice relaxation time, which is normally several seconds. Because of a favourable ratio between the nuclear and electron spin lattice relaxation times, the final polarization may be greatly enhanced. Of course, for nuclei far away from the electron, the polarization build-up would be extremely slow, because the transition probability for the forbidden transitions falls down with  $|\epsilon|^2$ , that is with the sixth power of the distance to the electron. Fortunately, there is another mechanism, known as spin diffusion<sup>50</sup>), which can "transport" the polarization of the nuclei near the electron to the distant nuclei. These processes occur through flip-flop processes between the nuclear spins, which are allowed through the dipolar coupling between them (terms  $I_{\pm}^i I_{\mp}^j$  in  $H_{II}$ ). This spin diffusion is normally very fast, because energy and angular momentum are both conserved. For example, an inhomogeneity in the polarization of protons diffuses over a distance of 100 Å in a few seconds. In fact, owing to this fast spin diffusion, one is allowed to speak about one single spin temperature within a spin system. Complications, which arise if the cross-relaxation between the nuclei is not very fast, will not be considered here, since this is seldom the case in organic materials.

The above-mentioned mechanism has been called the solid-state effect, which was first observed by Abragam and Proctor for the two nuclear spin systems in LiF<sup>17</sup>). It is called the resolved solid-state effect, if the forbidden transitions occur at a frequency outside the main line. The polarization versus microwave frequency then shows two peaks, namely at  $\nu_e - \nu_H$  and  $\nu_e + \nu_H$ . In the first case the protons are flipped from  $m = -\frac{1}{2}$  to  $m = \frac{1}{2}$  (|b⟩ → |c⟩ in Fig. I.1), that is a positive polarization is obtained; in the second case the opposite transitions occur (|a⟩ → |d⟩ in Fig. I.1) and a negative polarization is obtained.

If the forbidden lines are well separated from the main line, which implies that the broadening of the levels as a consequence of the spin-spin interactions is small, then the various processes can be described in a suitable way by rate equations. We will not write these rate equations now, but consider first the complications that may arise if the forbidden lines are not resolved from the main line.

In the case of completely inhomogeneous broadening -- that is, one can think of the electron spin resonance line as consisting of many independent spin packets with a slightly different Larmor frequency<sup>51</sup>) -- the application of microwave power saturates the forbidden transitions of two spin packets simultaneously, if the line is broader than the nuclear Larmor frequency; the net polarization will then be proportional to the difference of the intensity of the two packets, which causes opposite contributions to the polarization<sup>52</sup>). Therefore the net polarization will be always reduced. This mechanism was called the differential solid effect.

The assumption of independent spin packets is seldom justified in solids with high spin concentrations, because of the spin-spin interactions between the electron spins. The spin temperature theory, which takes correctly into account the existence of the spin-spin

interactions, may then be the proper approach to the problem, at least if the spin-spin interactions are sufficiently strong to maintain thermal equilibrium within the different parts of the spin system. For homogeneous spin systems this equilibrium is always obtained, while for inhomogeneous spin systems, thermal equilibrium may still be obtained if cross-relaxation [flip-flop transitions between the electron spins<sup>53)</sup>] is sufficiently fast compared with spin lattice relaxation. For intermediate cases of inhomogeneous lines with slow cross-relaxation there exists no adequate theory. A phenomenological model for such circumstances has been given in the literature under the name of cross-effect<sup>54,55)</sup>. This effect may then be effective, but it would not be the only effect. Furthermore, an experimental verification is difficult, because of the adjustable parameters in this theory.

In our experiments we are mainly dealing with inhomogeneous electron spin systems, in which the distribution of Larmor frequencies is caused by g-factor anisotropy and hyperfine interactions.

Fortunately, at low temperatures the electron spin lattice relaxation times are rather long, so that cross-relaxation is sufficiently fast for maintaining thermal equilibrium. Therefore the analysis of our results will be made in terms of the spin temperature theory, which is described in the next section.

### 3. DYNAMIC POLARIZATION IN CASE OF NON-NEGLIGIBLE ELECTRON SPIN-SPIN INTERACTIONS

#### 3.1 Introduction

In the classical theory of Bloembergen et al.<sup>53,56)</sup> about saturation and cross-relaxation in spin systems, the Zeeman levels are considered as being infinitely sharp, thus neglecting the broadening due to the spin-spin interactions. This is only justified in cases of liquids and gases, where the rapid motion of the atoms or molecules averages the spin-spin interactions to zero and the spins may be considered as being independent of each other.

However, in solids the spin-spin interactions are normally so strong that the whole ensemble of spins acts as a collective system with many degrees of freedom. For such a case, Redfield introduced the hypothesis that under strong saturation the whole spin system stayed in internal equilibrium, thus permitting its description by one single spin temperature<sup>57)</sup>. Provotorov solved the problem for an arbitrary degree of saturation<sup>19)</sup> and took the spin-spin interactions correctly into account in the theory of cross-relaxation<sup>20)</sup>. Since dynamic polarization is obtained by strong saturation of spin systems, Solomon extended the spin temperature theory to this problem, assuming Redfield's equal spin temperature hypothesis to be applicable<sup>58)</sup>; Borghini gave this theory in case of arbitrary saturation parameters<sup>4,7)</sup>. Several excellent reviews of the spin temperature theory have appeared since Redfield's original work describing the many beautiful verifications in the fields of cross-relaxation, adiabatic demagnetization in the rotating frame, dynamic polarization, spin lattice relaxation, and others (see reviews Refs. 3-6 and 23, 24).

In the next section we will summarize the results of the spin temperature theory, as far as they are important for the description of the mechanisms of dynamic polarization.

### 3.2 The spin temperature theory

We first consider a single spin system with dipolar interactions in an external magnetic field. Owing to the spin-spin interactions, the Zeeman levels have then a certain width of the order of the local internal fields  $H_L$ . The spin temperature theory is based on the segregation of the relatively weak spin-spin interactions into a separated reservoir<sup>19,20</sup>), which possesses its own temperature  $T_{SS}$ . This temperature may be different from the temperature of the Zeeman reservoir, denoted by  $T_Z$ . Then the spin system can be characterized by two temperatures: one for the Boltzmann distribution between the Zeeman levels, and a second one describing the ordering of the spins in the local fields. A pictorial illustration is given in Fig. I.2.

If the spin system is in thermal equilibrium with the lattice, the two temperatures are equal. However, under some experimental conditions they are different. For example,  $T_{SS}$  can be changed by slightly off-resonance irradiation of the spin system; it may become positive or negative, depending on the sign of  $\Delta = \nu_e - \nu$  (see Fig. I.2). Under such conditions Provotorov derived the evolution of the inverse spin temperatures of the Zeeman and spin-spin interaction reservoir, denoted by  $\alpha = h/kT_Z$  and  $\gamma = h/kT_{SS}$ , respectively:

$$\left(\frac{\partial}{\partial t}\right)_{RF} \alpha = -W_0(\alpha - \gamma) \quad (I.11)$$

$$\left(\frac{\partial}{\partial t}\right)_{RF} \gamma = +\frac{\Delta^2}{\nu_L^2} (\alpha - \gamma) \quad (I.12)$$

Here  $W_0 = \frac{1}{4} \gamma_e^2 H_1^2 g(\Delta)$ , where  $g(\Delta)$  is the shape function of the equilibrium absorption line,  $2H_1$  is the amplitude of the oscillating magnetic field and

$$\nu_L^2 = \gamma_e^2 H_L^2 \quad (I.13)$$

These equations are valid in a frame rotating with the frequency  $\nu$  of the oscillating field around the z axis. In this frame the time-dependent Hamiltonian is reduced to a static one, if the non-secular terms of the spin-spin interactions are neglected; that is,

$$H_{lab} = h\nu_e S_z + H_{SS}^0 + 2h\gamma_e H_1 S_x \cos(2\pi\nu t) \quad (I.14)$$

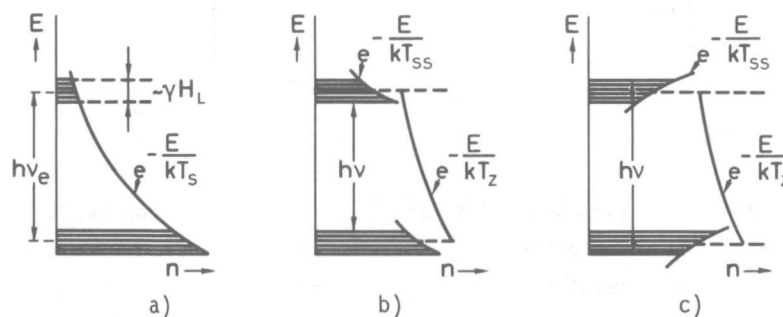


Fig. I.2a) The distribution of the populations  $n$  over the energy levels. In thermal equilibrium with the lattice this can be described by one single spin temperature  $T_S$ .  
 b) During RF irradiation at a frequency  $\nu$ , the spin system may be described by two spin temperatures,  $T_{SS}$  and  $T_Z$ . If  $\nu < \nu_e$  the populations become such that  $T_{SS} < T_Z$ , but  $T_{SS} > 0$ .  
 c) As in (b) but for  $\nu > \nu_e$ ; then  $T_{SS}$  may become negative.

is transformed into

$$H_{\text{rot}} = h\Delta S_z + H_{\text{SS}}^0 + 2h\gamma_e H_1 S_x . \quad (\text{I.15})$$

$H_{\text{SS}}^0$  refers to the secular part of the spin-spin interactions. From these equations it is easily seen that the evolution of  $\alpha$  and  $\gamma$  in the laboratory frame can be obtained from Eqs. (I.11) and (I.12) by replacing  $\alpha$  by  $\alpha_{\text{lab}} v_e/\Delta$ , while  $\gamma$  stays the same.

For the derivation of the above-mentioned formulae, the so-called high temperature approximation was used; it consists of taking only the linear terms in the density matrix

$$\rho = \frac{1}{\Sigma} \exp \left[ -\alpha v_e S_z - \gamma H_{\text{SS}}^0 \right] \quad (\text{I.16})$$

which then reduces to

$$\rho = \left[ 1 - \alpha v_e S_z - \gamma H_{\text{SS}}^0 \right] / \text{Tr } 1 . \quad (\text{I.17})$$

$\Sigma$  is the normalization constant and  $1$  is the unit matrix. Such an approximation is only valid at sufficiently high temperatures.

The extension of the theory toward low temperatures has only been done by taking second- or third-order terms into account<sup>59-61</sup>), or by neglecting the spin-spin interactions completely in the case where other sources of broadening of the Zeeman levels are dominant<sup>30</sup>). However, the form of the relaxation of the spin-spin interaction reservoir toward the lattice is still unknown.

Equation (I.11) expresses that in the rotating frame  $\alpha$  and  $\gamma$  will become equal to each other under strong saturation conditions. This result can also be stated in another way: since the "electron Larmor frequency in the rotating frame" is  $\Delta$  instead of  $v_e$  [see Eqs. (I.14) and (I.15)], there exists a possibility of thermal contact between the Zeeman reservoir and the spin-spin interaction reservoir, because their frequency spectra are similar, if  $\Delta = |v - v_e| \approx v_L$ . The "intermediary" between the reservoirs is then the microwave field. Another "intermediary" consists of the non-secular terms of the spin-spin interactions; however, in a high field these terms are negligible. Of course, in external magnetic fields of the order of the local internal fields, the non-secular terms cannot be neglected and one is not allowed to speak about two separated reservoirs, because they come rapidly into equilibrium with each other.

The second Provotorov equation can be derived from the first one by the principle of energy conservation. Energy can be conserved if the difference between the photon energy  $h\nu$  and the Zeeman energy  $h\nu_e$  is taken up by the spin-spin interaction reservoir. Such a change in the spin-spin interaction energy may be thought of as a rearrangement between the relative orientations of the spins via cross-relaxation transitions, thus changing  $T_{\text{SS}}$ .

If there are nuclei surrounding the electron spins, the situation becomes more difficult, because the density matrix now involves three spin temperatures in general<sup>4,62</sup>):

$$\rho = \frac{1}{\Sigma} \exp \left[ -\alpha v_e S_z + \beta v_n I_z - \gamma H_{\text{SS}}^0 \right] ; \quad (\text{I.18})$$

$\beta$  is the inverse spin temperature of the nuclei.

Summing up the contributions of spin lattice relaxation, the microwave-induced<sup>19)</sup> and cross-relaxation transitions<sup>20)</sup> of the electron spins, including the forbidden transitions<sup>7,63,64)</sup> in which a nuclear spin-flip also occurs, the following rate equations can be derived for spins one-half and using the high temperature approximation<sup>4,5)</sup>:

$$\begin{aligned} \dot{P}_e = & -W_0 \left[ P_e + \frac{1}{2} \gamma \Delta \right] - W_e^+ \left[ P_e - P_n + \frac{1}{2} \gamma (\Delta + \nu_n) \right] \\ & - W_e^- \left[ P_e + P_n + \frac{1}{2} \gamma (\Delta - \nu_n) \right] \\ & - \frac{1}{T_{1e}} \left[ P_e - P_0 \right] \end{aligned} \quad (I.19a)$$

$$\begin{aligned} \dot{P}_n = & -W_n^+ \left[ P_n - P_e - \frac{1}{2} \gamma (\Delta + \nu_n) \right] \\ & - W_n^- \left[ P_n + P_e + \frac{1}{2} \gamma (\Delta - \nu_n) \right] \\ & - \frac{1}{\tau_{nS}} \left[ P_n - \frac{1}{2} \gamma \nu_n \right] - \frac{P_n}{T_{1n}} \end{aligned} \quad (I.19b)$$

$$\begin{aligned} \frac{1}{2} \nu_L^2 \dot{\gamma} = & -W_0 \Delta \left[ P_e + \frac{1}{2} \gamma \Delta \right] - W_e^+ (\Delta + \nu_n) \left[ P_e - P_n + \frac{1}{2} \gamma (\Delta + \nu_n) \right] \\ & - W_e^- (\Delta - \nu_n) \left[ P_e + P_n + \frac{1}{2} \gamma (\Delta - \nu_n) \right] \\ & + \frac{\nu_L^2}{\nu_n} \frac{1}{\tau_{Sn}} \left[ P_n - \frac{1}{2} \gamma \nu_n \right] - \frac{1}{2} \nu_L^2 \frac{\gamma}{T_{1SS}} \end{aligned} \quad (I.19c)$$

In the high temperature approximation the electron and nuclear polarization, denoted by  $P_e$  and  $P_n$ , are related to  $\alpha$  and  $\beta$  by  $P_e = -\frac{1}{2} \alpha \nu_e$  and  $P_n = +\frac{1}{2} \beta \nu_n$  in case of spin one-half.  $P_0$  is the electron thermal equilibrium polarization. In these equations, small terms proportional to the thermal equilibrium values of  $\beta$  and  $\gamma$  have been neglected;  $W_n^+$  and  $W_e^+$  refer to the transition probabilities of the forbidden transitions;  $\tau_{Sn}$  and  $\tau_{nS}$  characterize respectively the relaxation of the spin-spin interaction reservoir to the nuclear Zeeman reservoirs and vice versa. The spin lattice relaxation times are denoted by  $T_{1n}$ ,  $T_{1e}$  and  $T_{1SS}$ . There exist the following relations between the different parameters<sup>5)</sup>:

$$\frac{\tau_{Sn}}{\tau_{nS}} = \frac{C_{SS}}{C_{Zn}} = \frac{n_e}{n_n} \cdot \frac{\nu_L^2}{\nu_n^2} \cdot \frac{S(S+1)}{I(I+1)} \quad (I.20)$$

and

$$W_e^+ = \frac{n_n}{n_e} \frac{I(I+1)}{S(S+1)} W_n^+ = f W_0 \quad (I.21)$$

Here  $C_{SS}$  and  $C_{Zn}$  denote respectively the heat capacities of the spin-spin interaction reservoir and the nuclear Zeeman reservoir. The "leakage factor"  $f$  is defined as:

$$f = \sum_k 4 |\epsilon_{ik}|^2, \quad (I.22)$$

where  $\epsilon_{ik}$  is the dipolar coupling coefficient between an electron spin  $i$  and a nucleus  $k$  [see Eq. (I.10)]. We assume, that the electron spins all have the same nuclear spin environment, thus the summation in Eq. (I.22) is independent of  $i$ . If the nuclear spin lattice relaxation proceeds via the forbidden transitions with the electron spins  $S$  (see Section 4.2 of this chapter), then the average value of  $4|\epsilon_{ik}|^2$  is  $T_{1e}/(n_e T_{1n})$ , so that  $f = (n_n/n_e)(T_{1e}/T_{1n})$ , at least at low values of  $P_e$ , because at high electron polarizations  $T_{1n}^{-1}$  should be multiplied by the factor  $(1 - P_e P_0)^{65}$  (see also Section 4.2).

For a homogeneous spin system,  $\tau_{nS}$  can be estimated from the expression<sup>6)</sup>

$$\tau_{nS}^{-1} \sim \frac{n_e}{n_n} f T_{2e}^{-1} \frac{\int_0^\infty g(\nu) g(\nu - \nu_n) d\nu}{g(\nu_e)}, \quad (I.23)$$

where  $T_{2e}$  is the transverse relaxation time of the electron spins.

The consequences of slightly off-resonance irradiation of an electron spin system are schematically represented in Fig. I.3: the cooling of the electron spin-spin interaction reservoir is transmitted to one or more nuclear Zeeman reservoirs by forbidden microwave-induced and cross-relaxation transitions.

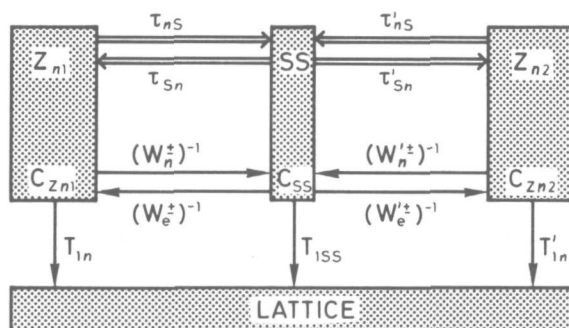


Fig. I.3 Scheme of thermal contact between the electron spin-spin interaction reservoir and the nuclear Zeeman reservoirs via the forbidden microwave-induced transitions (single arrows) and cross-relaxation transitions (double arrows). The various time constants of the processes are defined in the text.

In this way the absolute value of the spin temperatures of the nuclear Zeeman reservoirs may be appreciably lowered, thus giving rise to dynamic polarization in the presence of a magnetic field. If the thermal contact with the spin-spin interaction reservoir is strong enough, the final polarizations of different nuclear spin species will thus correspond to equal spin temperatures; they all become polarized simultaneously in a microwave frequency range around  $\nu_e$ . Such a behaviour differs appreciably from that of dynamic polarization by means of the resolved solid-state effect; in that case, not the spin temperatures but the polarizations of the different nuclei may become equal to the electron polarization. Furthermore, the optimum polarization then occurs at a microwave frequency, which is different for different nuclei.

### 3.3 Special cases

#### 3.3.1 Dynamic polarization at "high temperatures"

In this case the steady-state solutions of the electron and nuclear polarizations can be obtained from Eqs. (I.19) by putting the left-hand sides to zero. The expression for the nuclear polarization becomes simple, if the terms proportional to  $f$  are negligible<sup>4)</sup>:

$$P_n = P_e \frac{S^+ - S^- - \frac{\Delta\nu}{\Omega^2} S_1 [S^+ + S^- + S_4]}{\left[1 + S^+ + S^- + S_4\right] \left[1 + \frac{\Delta^2 + \Omega^2}{\Omega^2} S_1\right]} . \quad (\text{I.24})$$

The dimensionless saturation parameters are defined as

$$S_1 = W_0 T_{1e} , \quad S^{\pm} = W_n^{\pm} T_{1n} , \quad S_4 = T_{1n} / \tau_{nS} .$$

$\Omega^2 = a\nu_L^2 + M_2$ , where  $a = T_{1e}/T_{1SS}$  is a factor between 1 and 3<sup>7, 57, 61)</sup>. This expression of  $\Omega^2$  is valid for an inhomogeneous spin system with fast cross-relaxation, having a distribution of the Larmor frequencies characterized by the second moment  $M_2$ <sup>62)</sup>; for a homogeneous spin system  $M_2$  is zero.  $S_1$ ,  $S^+$ , and  $S^-$  are bell-shaped functions with their maxima at  $\nu_e$ ,  $\nu_e + \nu_n$ , and  $\nu_e - \nu_n$ , respectively. In the high temperature approximation these maxima are equal for spin one-half species, since

$$\frac{T_{1e}}{T_{1n}} = \frac{W_n^{\pm}}{W_0}$$

(see Section 4 of this chapter).

The numerator of Eq. (I.24) shows clearly the contributions from the solid effect, occurring through the forbidden transitions (term  $S^+ - S^-$ ) and from dynamic polarization via cooling of the electron spin-spin interaction reservoir by saturation of the allowed transitions, namely a term proportional to  $S_1$ , multiplied by a term  $[S^+ + S^- + S_4]$ ; this latter term determines the strength of the thermal contact between nuclei and electron spin-spin interactions (see Fig. I.3). In case of a resolved solid-state effect only  $S^-$  or  $S^+$  is present, if the microwave frequency is  $\nu_e - \nu_n$  or  $\nu_e + \nu_n$ , respectively. Assume the latter to be the case, then

$$P_n = P_e \frac{S^+}{1 + S^+} \approx |P_e| , \quad \text{if } S^+ \gg 1 . \quad (\text{I.25})$$

Thus under strong saturation,  $P_n$  becomes equal to  $P_e$  (or  $-P_e$ , if  $S^-$  is saturated).

On the contrary, if the forbidden and allowed transitions are strongly saturated simultaneously in case of an ESR line width larger than the nuclear Larmor frequency, the second term in the numerator of Eq. (I.24) will dominate, since this term is proportional to the square of the microwave power. The maximum polarization is then given by

$$P_n = \frac{-\Delta\nu}{\Delta^2 + \Omega^2} P_e , \quad (\text{I.26})$$

which is similar to Solomon's result<sup>58)</sup>.

$P_n$  reaches a maximum value of  $(\nu_n/2\Omega) P_e$  at  $|\Delta| = \Omega$ , which may be smaller or larger than  $P_e$  depending on the value of  $\Omega$ . It will in general not be larger than  $P_e$ , because of the small value of the product of the saturation parameters  $S_1(S^+ + S^- + S_0)$ , if  $\nu_n > 2\Omega$ . In case of low saturation, one expects to see a differential solid effect, since then the term  $(S^+ - S^-)$ , proportional to the microwave power (and not to its square) will be dominant. Such a behaviour was observed in copper tutton salts<sup>66</sup>): at low power a differential solid effect, and at high power dynamic polarization by cooling of the electron spin-spin interaction reservoir.

### 3.3.2 Dynamic polarization at "low temperatures" under strong saturation conditions

The extension of the spin temperature theory toward low temperatures causes difficulties, because of the higher order terms in  $\alpha$  and  $\gamma$ , which appear in the expressions for the expectation values of the various parts of the Hamiltonian. This causes among other things, that the form of the relaxation of the spin-spin interaction energy is unknown. Furthermore, the hypothesis of a spin-spin interaction reservoir separated from the Zeeman reservoir is questionable at low temperatures, because of the limited degrees of freedom of the former at low temperatures<sup>22</sup>). However, a relatively simple expression for the final spin temperatures is still possible, if the width of the Zeeman levels is mainly due to inhomogeneous broadening by g-factor anisotropy and/or hyperfine interactions<sup>30</sup>). Then the broadening due to the spin-spin interactions may be neglected. If the cross-relaxation is fast compared with the spin lattice relaxation, and assuming the concept of a spin-spin interaction reservoir to be still valid, then Redfield's equal spin temperature hypothesis may be applicable under strong saturation conditions. Since hyperfine interactions are negligible in our samples, we will not write the corresponding terms in the following. The equal spin temperature of the electron Zeeman reservoir and spin-spin interaction reservoir in the rotating frame is transmitted to the nuclei by the mechanisms indicated in Fig. I.3.

The Hamiltonian in the rotating frame  $H^*$  can be obtained from the one in the laboratory frame  $H$  by application of the unitary operator (if we neglect small differences in the directions of the quantization axis of  $S_z^i$  due to g-factor anisotropy)

$$U = \exp \left( -i2\pi\nu t \sum_i S_z^i \right)$$

and reads, if we neglect small terms arising from the microwave field and spin-spin interaction,

$$H^* = \sum_i h(\nu_i - \nu) S_z^i, \quad (I.27)$$

where  $h\nu_i = |g_i\mu_B H|$ .

During irradiation the density matrix changes from its thermal equilibrium value

$$\rho_0 = \frac{\exp(-\alpha_0 H)}{\text{Tr} \exp(-\alpha_0 H)} \quad (I.28)$$

to

$$\rho^* = \frac{\exp(-\alpha H^*)}{\text{Tr} \exp(-\alpha H^*)}, \quad (I.29)$$

where  $\alpha$  is the final inverse spin temperature and  $\alpha_0$  the thermal equilibrium one. The following relation for the steady-state value of  $\alpha$  can be obtained (see Appendix):

$$\text{Tr } \rho^* H^* = \text{Tr } \rho_0 H^* , \quad (\text{I.30})$$

which reduces to:

$$\sum_i \Delta_i P_i = \Delta P_0 , \quad (\text{I.31})$$

with

$$\Delta_i = \nu_i - \nu , \quad \Delta = \bar{\nu} - \nu , \quad \bar{\nu} = \sum_i \nu_i ,$$

$P_i = \tanh(\frac{1}{2} \alpha \Delta_i)$  and  $P_0 = \tanh(\frac{1}{2} \alpha_0 \bar{\nu})$  = the electron thermal equilibrium polarization.

In case of completely disoriented solids, the summation in Eq. (I.31) has to be done over all angles. Choosing a certain value of  $\alpha$ , the left-hand term in Eq. (I.31) becomes

$$(2\pi)^{-2} \int_0^{2\pi} \int_0^{2\pi} \Delta_i P_i \sin \theta \, d\theta \, d\phi , \quad (\text{I.32})$$

where

$$\Delta_i = \frac{g_i \mu_B H}{h} - \nu ,$$

with

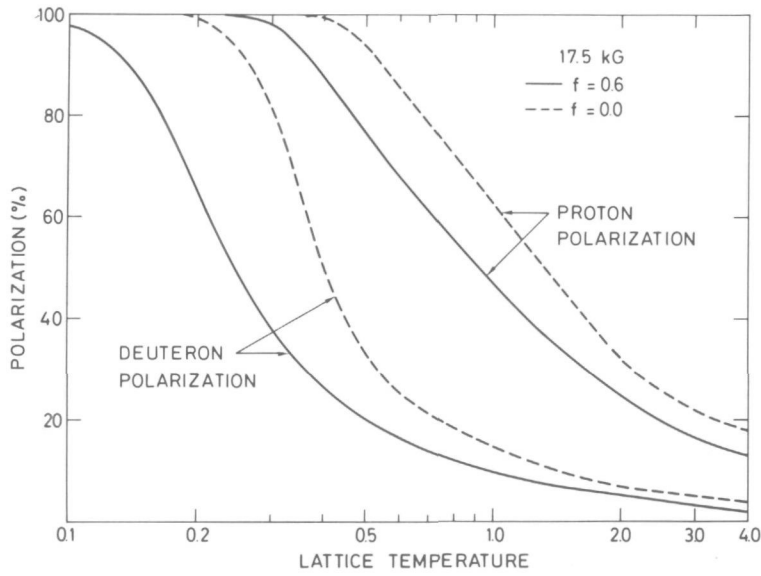
$$g_i = \left[ g_1^2 \cos^2 \theta + g_2^2 \sin^2 \theta \cos^2 \phi + g_3^2 \sin^2 \theta \sin^2 \phi \right]^{\frac{1}{2}} ;$$

$\theta$  and  $\phi$  are polar coordinates defining the orientation of the paramagnetic centre with respect to H. The principle values of the g-tensor  $g_1$ ,  $g_2$ , and  $g_3$  can be determined from electron spin resonance measurements. If the summation is done for a large range of  $\alpha$ 's, the value of  $\alpha$  for a certain value of  $\Delta P_0$  can easily be found by interpolation. Since we assumed that the nuclei would obtain the same spin temperature  $\alpha$ , the polarizations of the different nuclear species can be determined from the Brillouin formula.

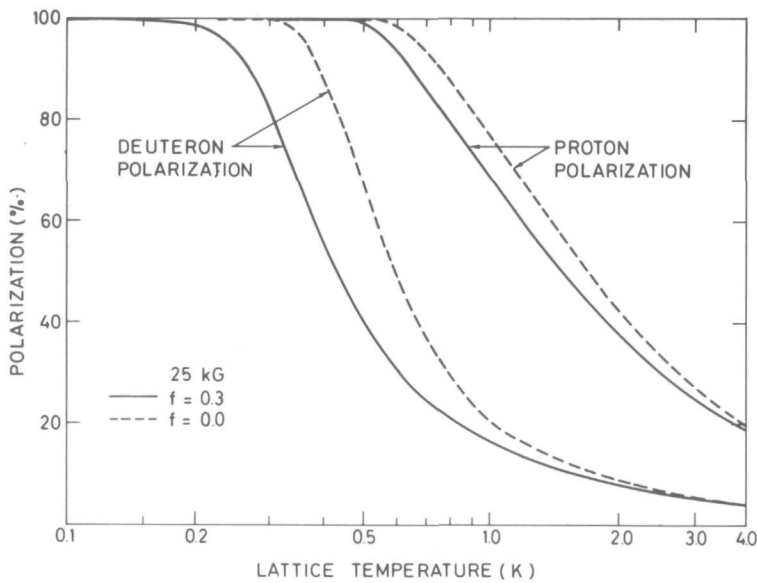
I made this calculation for the  $\text{Cr}^V$ -complex, for which the g-factor anisotropy is given in Chapter III. The maximum ratio of  $\alpha/\alpha_0$  as well as the corresponding values of the proton and deuteron polarizations are shown as function of temperature for different magnetic field values in the Figs. I.4-I.7. The curves were optimized with respect to microwave frequency. The value of  $\Delta$  at which optimum polarizations were obtained varied slightly as function of temperature. It changed, for example, from 160 to 200 MHz at 25 kG, if the lattice temperature decreased from 1 K to 0.4 K.

The finite nuclear spin lattice relaxation time causes a "leakage" of the polarization to the lattice. This was taken into account by adding a term (see also Appendix)

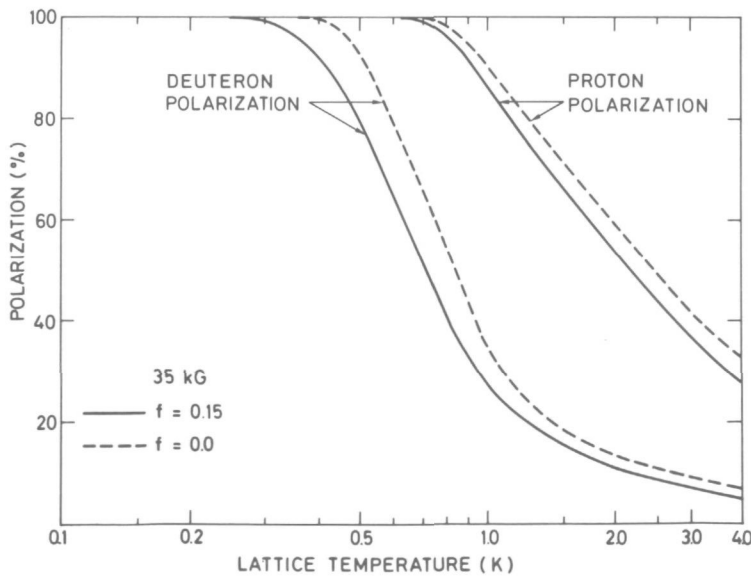
$$\sum_i f \nu_n P_n (1 - P_0 P_i)$$



a) The maximum proton and deuteron polarization in a 17.5 kG magnetic field versus temperature as calculated from Eq. (I.31). For the dashed curves the leakage term was taken to be zero, for the full curves the leakage factor was estimated from the measured relaxation times.

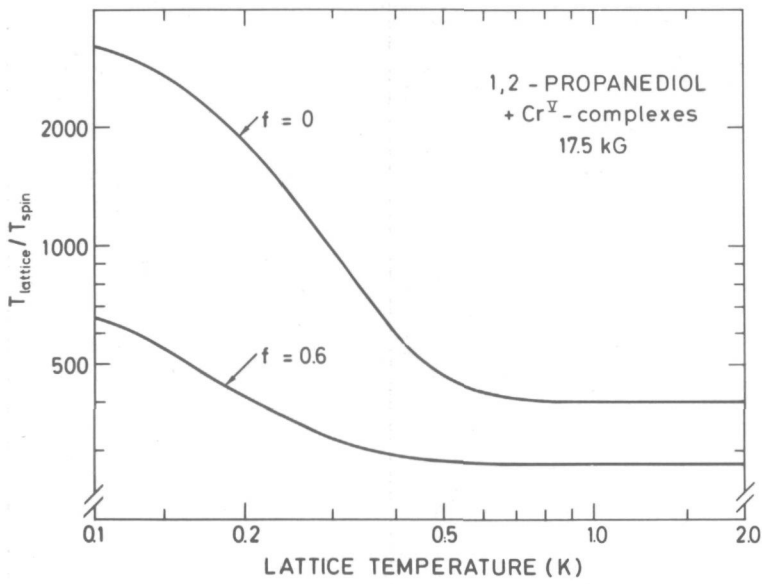


b) As in I.4a, but now for a 25 kG magnetic field.

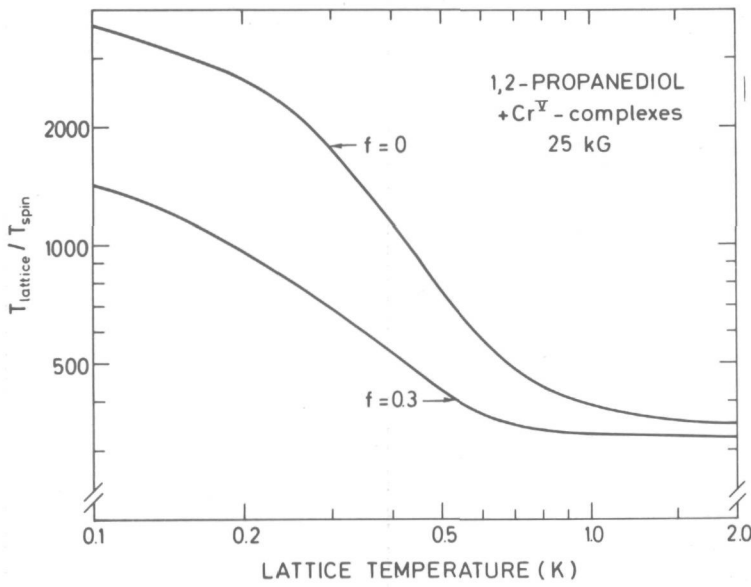


c) As in I.4a, but now for a 35 kG magnetic field.

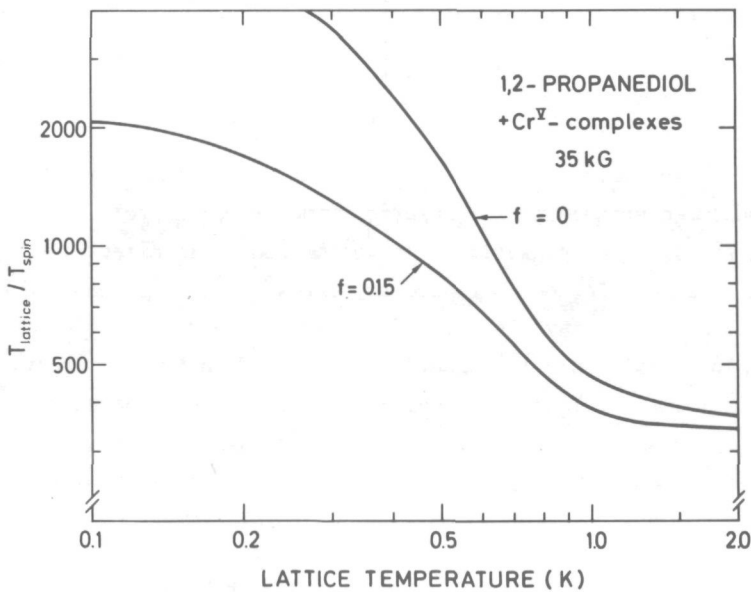
Fig. I.4



a) The ratio of the optimum inverse spin temperature and the inverse lattice temperature as function of temperature in a 17.5 kG magnetic field for two values of the leakage factor  $f$ .



b) As in I.5a, but for a 25 kG magnetic field.



c) As in I.5a, but now for a 35 kG magnetic field.

Fig. I.5

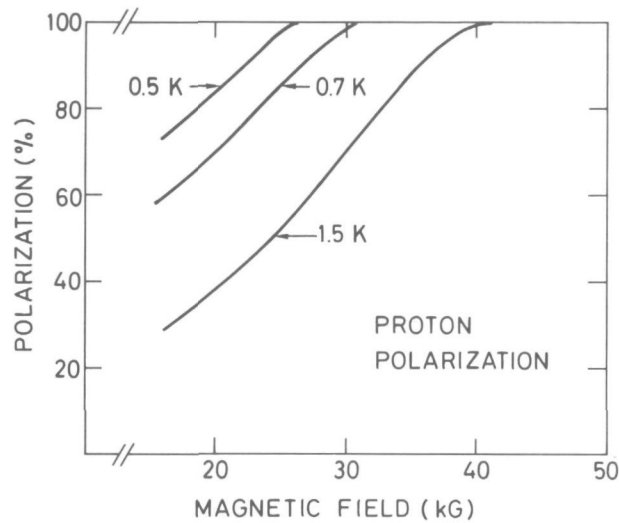


Fig. I.6 The optimum proton polarization as function of the magnetic field for three different temperatures. The leakage factor for each field value was estimated from the measured relaxation times.

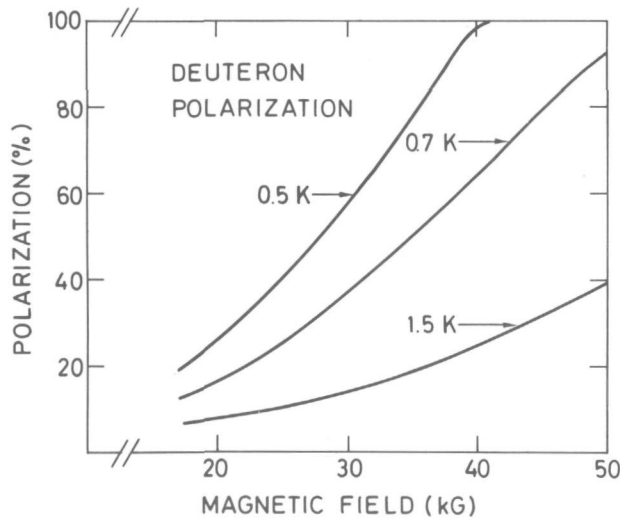


Fig. I.7 As in Fig. I.6, but now for the deuteron polarization.

to the left-hand side of Eq. (I.31). The value of the leakage factor was estimated from the spin concentrations and the measured spin lattice relaxation times (see Chapter III).  $T_{1n}^{-1}$  is by definition that part of the inverse relaxation time which occurs via direct interaction with the lattice. This value of  $T_{1n}^{-1}$  does not need to correspond to the measured inverse relaxation time, since the relaxation may also occur via the electron spin-spin interaction reservoir (see Section 4 of this chapter). However, it is difficult to separate this contribution from the observed inverse relaxation time. We therefore used the values of the measured relaxation times, which thus give a lower limit to the calculated polarizations. The dashed curves in the figures correspond to  $f = 0$ , which provides an upper limit of the polarizations. However, the real polarizations are expected to be closer to the lower limit.

The enhancement of the inverse spin temperatures tends to a constant value at high temperatures (see Fig. I.5), in agreement with Eq. (I.26). For temperatures below 0.5 K the enhancement starts to increase, which causes a rapid increase of the deuteron polarization.

Such an increase of the enhancement may seem rather surprising, since the right-hand side of Eq. (I.31) approaches a constant value when the polarization approaches one; then one would expect that  $\alpha$  approaches also a constant value, thus  $\alpha/\alpha_0$  would decrease. However, one should realize that the left-hand side of Eq. (I.31) shows also a "saturation" behaviour, so a small increase in  $\Delta P_0$  may cause a large increase of  $\alpha$ . Of course, the integration of Eq. (I.32) should be sufficiently precise for distinguishing such small effects (a relative accuracy of  $10^{-10}$  was needed at the lowest temperatures).

It is sometimes thought that the influence of the leakage factor will be negligible at low temperatures, because of the factor  $(1 - P_e P_0)$ . However, as can be seen from Fig. I.5b for example, the enhancement may be doubled at 0.5 K, if  $f$  varies from 0.3 to 0, and at lower temperatures the difference starts to be even more important.

This behaviour arises from the fact that we have an inhomogeneous ESR line with fast cross-relaxation; then electron spins with different Larmor frequencies have different polarizations in the rotating frame in spite of an equal spin temperature, namely  $P_i = \tanh(\frac{1}{2} \alpha \Delta_i)$ . Since  $P_i$  may be small, this causes the factor

$$\sum_i f \nu_n P_n (1 - P_e P_i)$$

to be not always negligible.

In Chapter III we will describe measurements which indicate both the increase of the enhancement at low temperatures and the important role of the leakage factor, even at low temperatures. It should be noted that large deuteron polarizations can be expected only if the proton polarization has reached almost complete polarization, at least if this mechanism of dynamic polarization is effective. This result clearly shows the difficulties involved in obtaining highly polarized deuteron targets.

### 3.3.3 Dynamic polarization at "low temperatures" under weak saturation conditions

There exists no exact theory for this case. However, by making a few simplifying assumptions, I believe a reasonable estimate of the polarization as function of the microwave frequency can be made, even at low temperatures.

The evolution of the electron polarization under microwave irradiation is given by Eq. (I.19a), which is valid at low values of  $P_e$ . However, under the condition

$$\frac{1}{2} \gamma \Delta \ll P_e, \quad (I.33)$$

which is true if the system is close to thermal equilibrium with the lattice, the term  $(P_e + \frac{1}{2} \gamma \Delta)$  may be replaced by  $P_e$ , and Eq. (I.19a) reduces to:

$$\dot{P}_e = -W_0 P_e - \frac{1}{T_{1e}} (P_e - P_0) \quad (I.34)$$

Here we assumed that terms proportional to  $f$  are negligible. Equation (I.34) is just the classical one in case of negligible spin-spin interactions, which is valid without restrictions on the temperature. The condition (I.33) will only be fulfilled under weak saturation conditions. In that case the spin-spin interaction reservoir will hardly be cooled. Therefore we used the high temperature approximation for the spin-spin interaction energy, which is an assumption, because the relaxation of the dipolar energy does not need to be exponential at low temperatures. Goldman et al.<sup>60)</sup> have given expressions for the dipolar energy, from which it is apparent that higher-order terms may be neglected at low values of  $\gamma$ .

Under these assumptions the steady-state solution of the proton polarization as function of microwave frequency is easily obtained from Eqs. (I.19b) and (I.19c):

$$P(H) = \frac{S^- - S^+ + \Delta \nu_H S_1 S_4 / \Omega^2}{1 + S^+ + S^- + S_4} \quad (I.35)$$

Here we replaced  $(P_e + \frac{1}{2} \gamma \Delta)$  by  $P_e \approx -1$  and neglected terms proportional to  $f$  and  $\gamma(\Delta \pm \nu_H)$ ;  $\nu_H$  denotes the proton Larmor frequency.

To be more specific, we now consider a homogeneous electron spin system in a 25 kG magnetic field, possessing a Lorentzian ESR line with a half-width of about 10 MHz. If this is compared with the Larmor frequencies of protons, deuterons, and carbon-13 nuclei, which are about 106, 16, and 26 MHz respectively, one expects a resolved solid-state effect only for protons, eventually accompanied with dynamic polarization by cooling of the electron spin-spin interaction reservoir. The expected proton polarization versus microwave frequency is schematically shown in Fig. I.8.

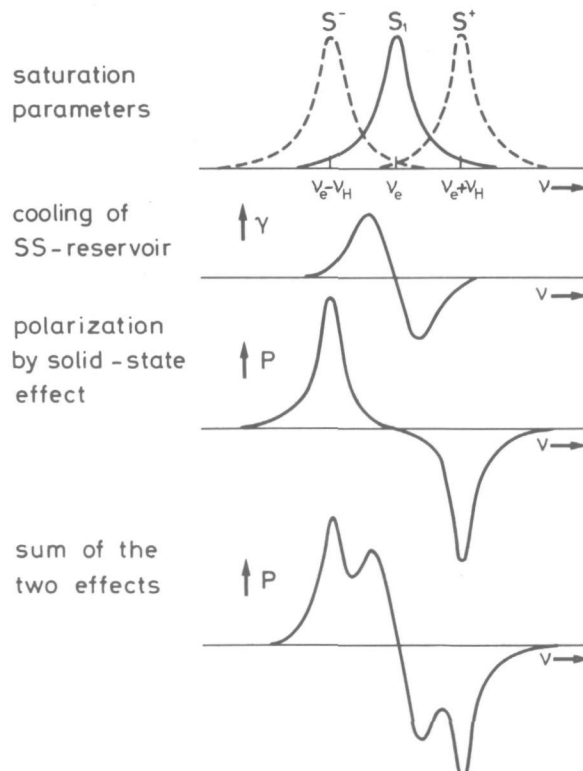


Fig. I.8 The polarization as function of microwave frequency arising from a cooling of the electron spin-spin interaction reservoir and a solid-state effect.

For deuterons and carbon-13 nuclei, the polarization arising from the thermal contact with the spin-spin interaction reservoir is expected to be dominant since

$$S_4 \gg S^{\pm} . \quad (\text{I.36})$$

This inequality follows from a simple estimate of  $S_4$ , using Eq. (I.23), and from the assumption of weak saturation. Then these nuclei will both obtain the same temperature as that of the electron spin-spin interaction reservoir, or

$$P(\text{D}) = \frac{2}{3} \gamma v_{\text{D}} = \frac{4}{3} \Delta v_{\text{D}} S_1 / \Omega^2 \quad (\text{I.37})$$

$$P(\text{C}) = \frac{1}{2} \gamma v_{\text{C}} = \Delta v_{\text{C}} S_1 / \Omega^2 . \quad (\text{I.38})$$

$v_{\text{D}}$  and  $v_{\text{C}}$  are the deuteron and carbon-13 Larmor frequencies. In order to obtain the right-hand side of these equations, we assumed again  $(P_e + \frac{1}{2} \gamma) \approx -1$  and  $f = 0$ . Furthermore, the terms proportional to  $\tau_{nS}^{-1}$  and  $\tau_{S_n}^{-1}$  can be taken as zero, because of the assumption of equal spin temperatures for the nuclei and the electron spin-spin interaction reservoir. From Eq. (I.19c) the steady-state solution of  $\gamma$  is then found to be  $2\Delta S_1 / \Omega^2$ . The expressions (I.35), (I.37), and (I.38) will be compared with the measurements of the polarization as function of microwave frequency in experiments with a free radical which exhibits such a narrow ESR line.

#### 4. SPIN LATTICE RELAXATION

In this section we will briefly consider the problem of spin lattice relaxation, which plays such an important role in dynamic polarization experiments. Especially the rapid increase of the nuclear spin lattice relaxation time  $T_{1n}$  at low temperatures decreases the leakage and makes it possible to obtain high polarizations.

It is well known that the nuclear spin lattice relaxation proceeds mainly via the interaction with the electron spin system, because the number of phonons "on speaking terms" with the low frequencies of the nuclear Zeeman reservoirs is extremely small at low temperatures<sup>6,7</sup>). We therefore consider first the field and temperature dependence of the electron spin lattice relaxation.

##### 4.1 Electron spin lattice relaxation

For the electron spin lattice relaxation, several processes are known to occur<sup>6,8</sup>). However, at low temperatures and in high magnetic fields normally the direct process dominates, which consists simply of an electron spin-flip accompanied by a photon absorption or emission<sup>6,9,70</sup>). The field and temperature dependence of this process are given by

$$T_{1e}^{-1} \propto H^5 \coth \left[ \frac{h\nu_e}{2KT} \right] , \quad (\text{I.39})$$

at least, if  $S$  is uneven (Kramers doublets).

#### 4.2 Nuclear spin lattice relaxation

Since the appearance of Bloembergen's original paper<sup>67)</sup>, the problem of nuclear spin lattice relaxation has been investigated many times<sup>1,2,71,72)</sup>. It was shown that the main cause for this process in solids with paramagnetic impurities was the fluctuating magnetic field at the nucleus created by the transitions within the electron spin system. The direct relaxation time of a nucleus at a distance  $r$  from a magnetic ion is proportional to

$$T_{1e}/|\epsilon|^2, \quad (\text{I.40})$$

where  $\epsilon$  is given by Eq. (I.10). This transition probability varies rapidly with the distance  $r$ . However, when the nuclear spin diffusion is fast, a homogeneous nuclear spin temperature is obtained. Then, in case of retarded spin diffusion, the single inverse relaxation time of the nuclear spins will be proportional to<sup>72,73)</sup>:

$$T_{1n}^{-1} \propto \left( \frac{\hbar \gamma_n}{H} \right)^2 (d^3 R^3)^{-1} \frac{(1 - P_e P_0)}{T_{1e}}. \quad (\text{I.41})$$

$R$  is defined as half the average distance between two electron spins, and  $d$  is the diffusion barrier which arises from the fact that at a distance shorter than  $d$  from the paramagnetic centre, the spin diffusion is slowed down as a consequence of the large internal fields acting there. However, this quenching of the diffusion may be largely reduced in presence of a spin-spin interaction reservoir, which can take up the difference in Zeeman energy between neighbouring nuclei. Sometimes a good agreement between theory and experiment is found, if  $d$  is taken as the shortest distance between a paramagnetic centre and the surrounding nuclei<sup>40,73-75)</sup>.

The factor  $(1 - P_0 P_e)/T_{1e}$  gives roughly the transition probability for an electron to perform a spin-flip per unit time. This factor, first observed by Schmugge et al.<sup>74)</sup>, becomes very small at low temperatures. It causes a steep increase of the nuclear spin lattice relaxation time at decreasing temperatures.

Another mechanism of nuclear relaxation is caused by the presence of the electron spin-spin interaction reservoir<sup>62,63)</sup> (see Fig. I.3). If there exists a strong thermal contact between the nuclei and this reservoir, then they obtain equal temperatures in a time of the order of  $\tau_{nS}$ . If this time is much shorter than  $T_{1n}$ , the common spin temperature will relax with a single time constant  $T_1'$  to the lattice temperature. From simple thermodynamical arguments,  $T_1'$  is found to be

$$T_1' = \frac{C_{Zn}}{C_{SS}} T_{1SS} \quad (\text{I.42})$$

at least in the high temperature approximation, where  $T_{1SS}$  is assumed to be  $T_{1e}/a$  with  $1 < a < 3$ <sup>7,57,61)</sup>.  $T_1'$  may become very long for small heat capacities of the spin-spin interaction reservoir ("dipolar bottleneck"). If  $T_{1SS}$  is different from the nuclear spin temperatures during relaxation, the situation is more complicated and one has to solve Eqs. (I.19), in which  $W_n^+$ ,  $W_e^+$  and  $W_0$  are set to zero. In general one then expects a non-exponential relaxation. This problem has been treated elsewhere<sup>76)</sup>.

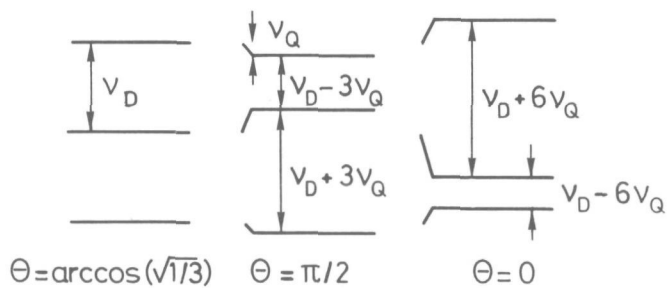
At high polarization values, the behaviour of  $T_{1SS}$  is not known. It is probably not simply proportional to  $T_{1e}$ , since the dipolar energy becomes a function of the Zeeman energy. Normally a behaviour different from that expected from the  $(1 - P_0 P_e)$  term is observed, when  $P_0$  is close to one<sup>29,77,79</sup>). However, as said before, in general it is difficult to calculate the contributions of the various mechanisms, not only because of uncertainties in important parameters such as  $T_{1SS}$  and  $d$ , but also because of the possible influence of clusters, unknown paramagnetic impurities, etc.

### 5. DESCRIPTION OF THE DEUTERON SPIN SYSTEM

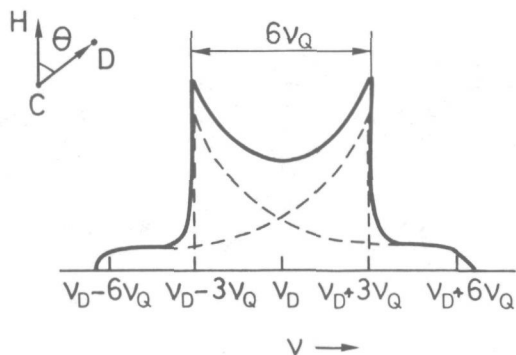
Let us briefly recall some properties of the deuteron spin system<sup>79</sup>). In an external magnetic field the energies of the three magnetic substates can be written as

$$E_m = -h\nu_D m + h\nu_Q \left\{ \left[ 3 \cos^2 (\theta) - 1 \right] \right\} \left\{ 3m^2 - I(I + 1) \right\} , \quad (I.43)$$

where  $\nu_D$  is the deuteron Larmor frequency (16.34 MHz in a 25 kG magnetic field),  $m = \langle I_z \rangle$ , and  $\nu_Q = 1/8 (e^2 q Q/h) = +19.5$  kHz for propanediol-D6, where  $eq$  is the deuteron quadrupole moment and  $eQ$  is the value of the electrical field gradient along the principal axis of the field gradient tensor, which can be assumed to coincide with a CD-bond;  $\theta$  is the angle between this axis and the direction of the magnetic field. In an amorphous solid, as is our case, all orientations of CD-bonds are equally probable. Therefore the magnetic levels are shifted, depending on the value of  $\theta$ . This gives rise to two transitions, which vary in energy according to the factor  $[3 \cos^2 (\theta) - 1]$  and in intensity according to the factor  $1/\cos (\theta)^1$ . These two transitions partially overlap each other, and the actual deuteron magnetic resonance (DMR) line is a superposition of them, as shown in Fig. I.9. The two



a) Energy level diagram of the deuteron spin system for three values of the factor  $(3 \cos^2 \theta - 1)$ , namely 0, -1, and 2, which corresponds to the centre, the peaks, and the pedestals of the deuteron line, respectively.  $\theta$  is roughly the angle between the direction of a CD-bond and an external magnetic field.



b) Theoretical deuteron line shape, which is the sum of the two possible transitions  $m = 0$  to  $m = 1$  and  $m = -1$  to  $m = 0$  (dashed lines). Some line broadening due to spin-spin interactions has been taken into account, which makes the line smoother. Otherwise the peaks would tend to infinity.

Fig. I.9

peaks correspond to  $\theta = 90^\circ$ , the pedestals to  $\theta = 0^\circ$ , while the right peak and left pedestal correspond to the  $m = 1$  to  $m = 0$  transition, whose intensity is  $J^+$ , and the other peak and pedestal to the  $m = 0$  to  $m = -1$  transition with intensity  $J^-$ . The intensities are proportional to the difference in populations  $n_m$  of the corresponding states, which satisfy the Boltzmann relations under thermal equilibrium conditions. We assume the sum of  $n_m$  to be normalized to 1. The vector polarization  $P(D) = \langle I_z \rangle$  is then given by  $n_1 - n_{-1} = c(J^+ + J^-)$ , and the tensor polarization or alignment  $A(D) = \langle 3I_z^2 - I(I+1) \rangle$  is equal to  $1 - 3n_0 = c(J^+ - J^-)$ . From the definitions it follows that under thermal equilibrium,  $A(D)$  and  $P(D)$  are related by  $A(D) \approx 3/4 P(D)^2$ , if  $A(D)$  is small. The constant  $c$  can be determined by measuring the thermal equilibrium signal at a known temperature. At high polarizations the intensities  $J^+$  and  $J^-$  become different and the asymmetry, defined as  $R = J^+/J^-$ , is related to  $P(D)$  by:

$$|P(D)| = (R^2 - 1)/(R^2 + R + 1) \quad , \quad (I.44)$$

as follows from the definitions.

## CHAPTER II

### EXPERIMENTAL TECHNIQUES

#### 1. GENERAL ASPECTS

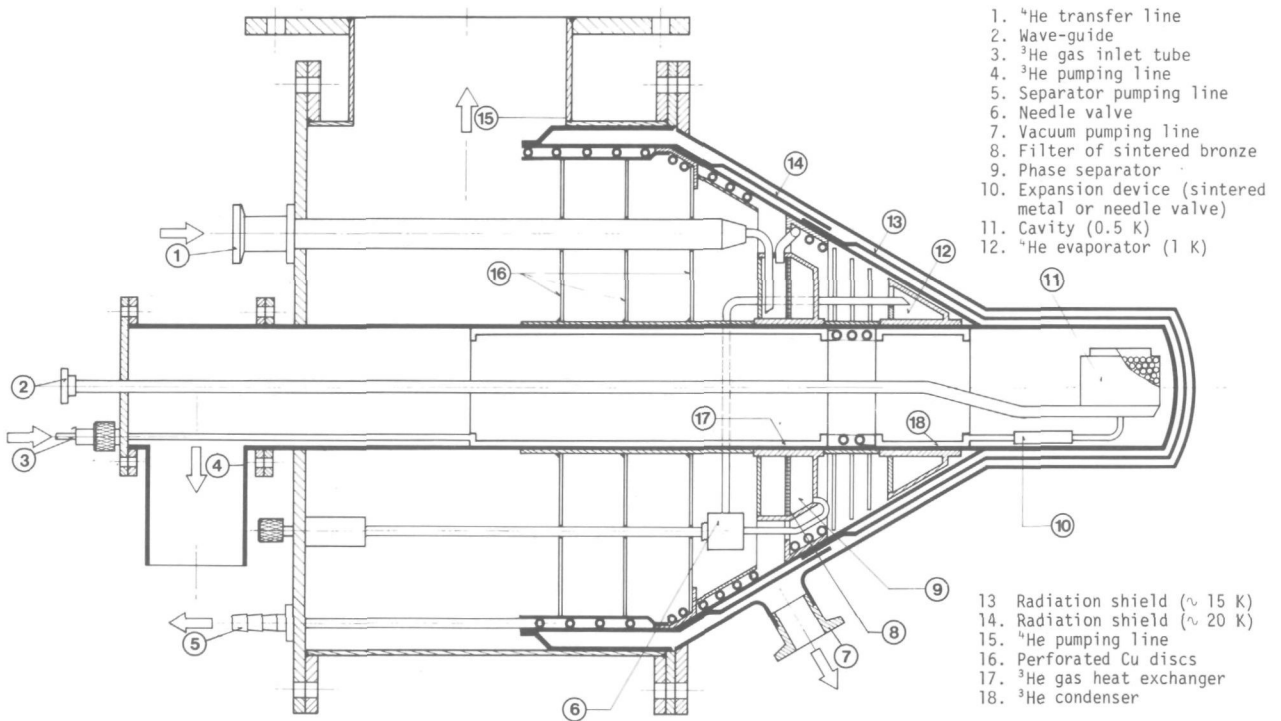
Nuclear dynamic polarization through the dipolar coupling with electron spins is obtained by placing the sample in a cavity and applying microwaves to it with a frequency near the electron Larmor frequency. Multimode cylindrical cavities were used, since single-mode cavities are too small in practice, if one uses microwaves in the millimetre range. The size of these cavities is not so critical, and cavities with a diameter of 3 cm and 15 cm long have been operated successfully.

The polarization can be determined by comparing the nuclear magnetic resonance absorption signal (NMR signal) at thermal equilibrium with the lattice, with that of the enhanced one, since the polarization is proportional to the surface of the NMR signal. The NMR spectrometer is described in the next section. Most of the experiments were done in a 25 kG magnetic field, obtained by a conventional iron magnet; some of them were done in a superconducting magnet operating at 50 kG. The field homogeneity was about  $3 \times 10^{-4}$  or better for small samples ( $< 3 \text{ cm}^3$ ).

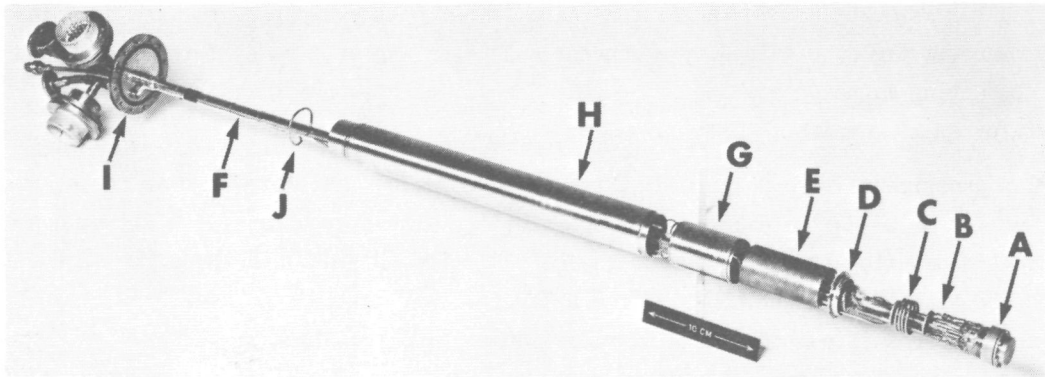
The experiments were performed at temperatures below 1 K, using  $^4\text{He}$  or  $^3\text{He}$  evaporation cryostats<sup>80)</sup> or a  $^3\text{He}$ - $^4\text{He}$  dilution refrigerator<sup>81)</sup>. These cryostats were all of a horizontal, continuous-flow-type with vapour-cooled radiation shields. In these cryostats, liquid  $^4\text{He}$  can be transferred continuously from a larger dewar into a separator. From the separator, cold  $^4\text{He}$  gas is pumped along the radiation shields, of which the lowest one is cooled to about 15 K. Via an expansion device (needle valve) the  $^4\text{He}$  liquid is transferred from the separator into an evaporator, which can act simultaneously as a cavity ( $^4\text{He}$  evaporation cryostat).

The  $^3\text{He}$  cryostats and dilution cryostat are inserted in a horizontal stainless-steel tube, which is precooled to about 1 K. The precooler is quite similar to the  $^4\text{He}$  cryostat described above. The  $^3\text{He}$  insert consists basically of a gas heat exchanger, condenser, expansion device, and cavity plus wave-guide. A sketch of a  $^3\text{He}$  cryostat with precooler is shown in Fig. II.1a.

The  $^3\text{He}$ - $^4\text{He}$  dilution cryostat is quite similar to the  $^3\text{He}$  cryostat, except that after the condenser a dilution unit is mounted (see Fig. II.1b). The cavity is located inside the mixing chamber (see Fig. II.1c). Microwave power is fed into it via a waveguide, which enters the dilution unit via the vacuum jacket pumping line. An FEP (fluorinated ethylene propylene) foil window in the waveguide near the mixing chamber makes the latter leak-tight. The cooling power available was respectively 1 W at 1 K, and 30-150 mW at 0.5 K in the

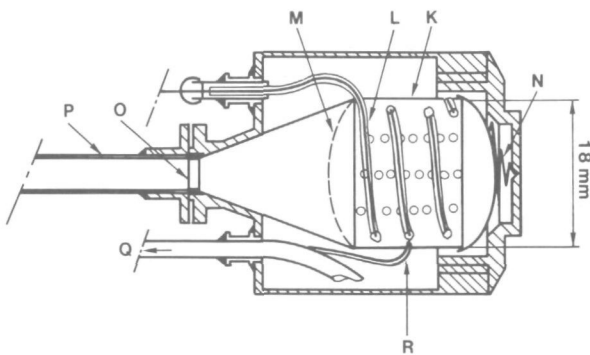


a) Sketch of a  $^3\text{He}$ -cryostat (not on the right scale; the horizontal dimensions are longer in practice and the walls thinner).



b) Photograph of the  $^3\text{He}$ - $^4\text{He}$  dilution refrigerator insert (from Ref. 81).

- |  |                               |                              |
|--|-------------------------------|------------------------------|
| A. Mixing chamber  | D. Vacuum jacket flange       | H. Gas heat exchanger        |
| B. Two discrete heat exchangers using sintered copper <sup>82,83</sup> ) | E. Still                      | I. Pumping line flange       |
| C. Tubular counter flow heat exchanger                                   | F. Vacuum jacket-pumping tube | J. $^3\text{He}$ -inlet tube |
|  | G. Condenser                  |                              |



c) The mixing chamber with cavity (from Ref. 78).

- |  |
|--|
| K. Microwave cavity  |
| L. NMR coil with teflon insulation the feed-through is made leak-tight with a mixture of Araldite + chalk powder (1:1 by weight) |
| M. Perforated FEP foil membrane  |
| N. Spring for holding the end cap of the cavity  |
| O. FEP foil window   |
| P. Wave-guide  |
| Q. Dilute stream outlet tube   |
| R. Concentrated stream inlet tube  |

Fig. II.1

evaporation-type cryostats, and varied from 0.2 mW at 0.1 K to 9 mW at 0.45 K in the dilution cryostat. These high cooling powers were not needed to obtain the maximum polarization in the samples, but they were of practical interest for a rapid build-up or reversal of the polarization. At temperatures below 0.5 K in a 25 kG field the microwave power for maximum polarization is about 1 mW per gramme of the sample. At higher temperatures the microwave power needed for optimum polarization increases rapidly (about 14 mW/g at 1 K). The reason for this is probably the rapid decrease of the spin lattice relaxation times at higher temperatures. The microwave power/g was calculated from the total microwave power absorbed in the cryostat, thus assuming that cavity losses are negligible compared with losses in the sample; this will be the case if the microwave frequency is near paramagnetic resonance (we used filling factors of the cavities between 50 and 70%). The microwave power for large targets (say 100 cm<sup>3</sup>) was normally obtained from carcinotrons, which provide a maximum output of several watts; for smaller samples a klystron was used, delivering typically 500 mW. The frequency of these sources could be varied slightly around their mean value of 70 GHz (or 140 GHz for the 50 kG measurements). The size of the samples in the experiments described later, was typically a few cm<sup>3</sup>. The organic samples that we studied are liquid at room temperature. They were mostly composed of pre-frozen spheres, formed by allowing liquid droplets to freeze on a liquid-nitrogen meniscus. The diameter of the spheres was between 1 and 2 mm; a bigger diameter would cause trouble for reasons of microwave heating<sup>84)</sup> and a finite penetration depth of the microwave field. The cavities were normally completely filled with these spheres. In experiments with the dilution cryostat, the samples were sealed in a 15  $\mu$ m thick FEP foil, because the sealing of the mixing chamber at room temperature prevented the use of pre-frozen spheres.

## 2. THE NUCLEAR MAGNETIC RESONANCE EQUIPMENT

The NMR signals of different nuclei were detected by continuous-wave magnetic resonance, using "Q-meters"<sup>85-87)</sup>. They were made out of a LC tuned series circuit, in which the capacitance outside the cryostat was connected to the coil in the cavity via a  $\frac{1}{2} \lambda$  cable. Normally one single coil with a diameter of 1 cm and about 4 to 6 turns was used for the different nuclei.

The signals are detected in the form of a change  $\Delta V$  in the RF power level  $V$  over the LC circuit. Care was taken that the ratio  $\Delta V/V$  was always smaller than 10% in order to make the "dispersion corrections" less than 3%<sup>86,87)</sup>; these small corrections were applied to the experimental results described further on. The RF power was always kept at a sufficiently low level to avoid saturation. These two requirements, linearity and non-saturation of the spin system can only be met by a low RF-field strength (say 1 mG) which implies that noise is not always negligible. Therefore the sensitivity of the system was improved by using a small computer as a digital averager (see Fig. II.2). As said before, the polarization is proportional to the surface of the NMR signal. Errors in this surface due to uncertainties in the base-line were negligible, because the latter was subtracted from the signal in a digital way.

Figure II.3 shows a thermal equilibrium signal of protons in 1,2 propanediol at 0.6 K and 25 kG after 500 $\times$  averaging.

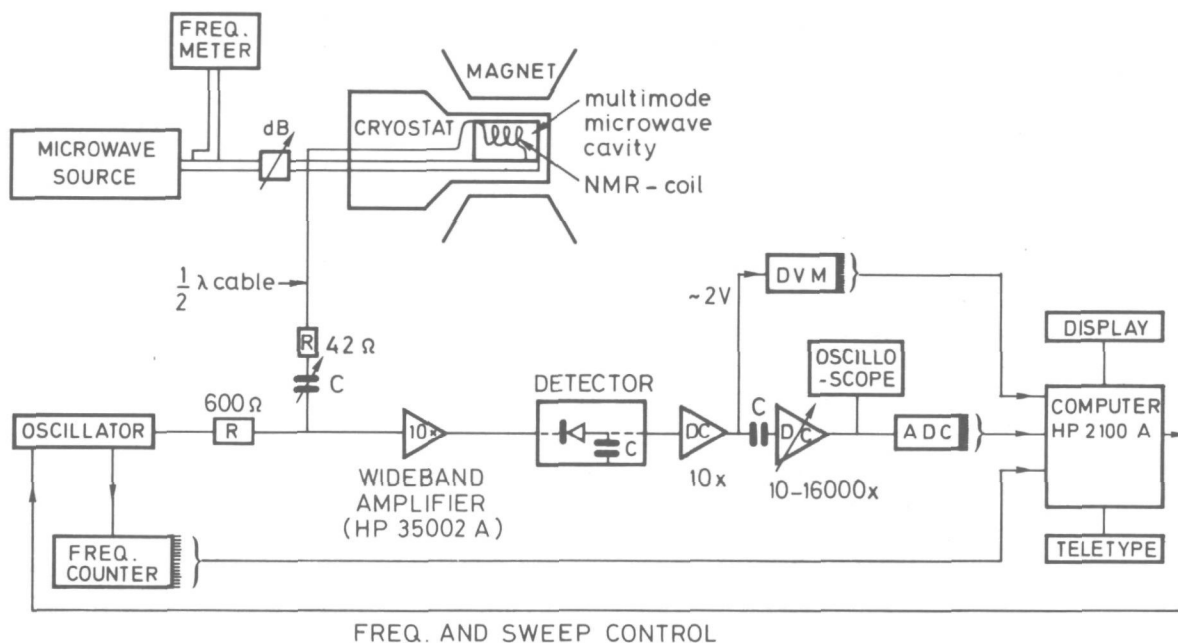


Fig. II.2 Basic elements of our experimental arrangement for dynamic polarization experiments.

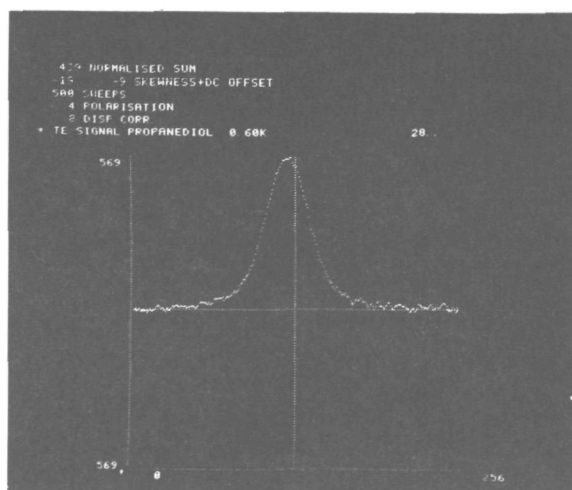


Fig. II.3

Thermal equilibrium signal of protons in 1,2-propanediol at a temperature of 0.6 K in a 25 kG magnetic field. The signal was photographed from the display screen of a HP 2100 computer after 500 times averaging. The frequency sweep on the horizontal axis is from 106.3 to 106.7 MHz.

### 3. THE ELECTRON SPIN RESONANCE EQUIPMENT

Two electron spin resonance spectrometers were available for the measurements of ESR line-shapes and electron spin lattice relaxation times. The first one is a commercial Varian E3 spectrometer, operating at 3 kG between room temperature and liquid-nitrogen temperature. The second one is a transmission-type spectrometer, which can be operated at 25 kG and 0.5 K. It consisted simply of a <sup>3</sup>He evaporation cryostat, equipped with a U-form waveguide. At one end of the waveguide, made of monel, a detection diode was mounted; at the other end a klystron, attenuator, phase shifter, and frequency meter. The use of a cavity or of modulation techniques was not necessary in the latter, because under the conditions mentioned the electron polarization is about |1|, and sufficient sensitivity can be

obtained for rather concentrated samples ( $\sim 10^{19}$  spins/cm<sup>3</sup>) by just placing them inside the cold part of the waveguide. The samples, sealed in FEP foil, were normally smaller than 20 mm<sup>3</sup>, thus avoiding too strong a variation of the microwave field strength during the sweep of the magnetic field through resonance.

Electron spin lattice relaxation times at 25 kG could be measured by the pulse relaxation method, in which the recovery of the signal is measured after saturation. The pulses were obtained with the aid of a Hitachi ferrite modulator, which has a maximum attenuation of about 20 dB and a switching time of a few microseconds. The computer was used for accumulating the recovery of the ESR signal, which made it possible for us to operate at low power levels in order to prevent sample heating and errors due to saturation during the recovery. Errors due to uncertainties in the base-line were negligible, because it was subtracted from the recovery signal in a digital way. A typical recovery signal is shown in Fig. II.4, obtained after 100× averaging.

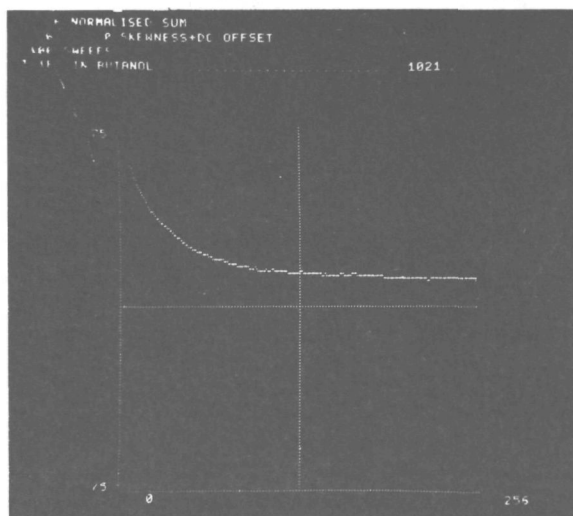


Fig. II.4

Recovery of the ESR signal in 1-butanol doped with 1% (by weight) of the free radical porphyrin at a temperature of 0.5 K in a 25 kG magnetic field. The time scan on the horizontal axis is 26.2 msec ( $T_{1e} = 3.3$  msec).

#### 4. SAMPLE PREPARATION

The experiments were mainly performed with two kinds of samples: diols doped with paramagnetic Cr<sup>V</sup>-complexes, and toluenes doped with the free radical BDPA. The chemicals which we used were obtained from Fluka AG, 9470 Buchs, Switzerland. The deuterated products were obtained from Merck, Sharp and Dohme, Ltd., P.O. Box 899, Quebec, Canada, or Roth, D-7500 Karlsruhe 21, Germany.

The Cr<sup>V</sup>-complex can be formed by slowly reducing hexavalent chromium compounds ( $K_2Cr_2O_7$ ,  $Na_2Cr_2O_7 \cdot 2H_2O$ ,  $(NH_4)_2CrO_4$ ,  $K_2CrO_4$ ,  $CrO_3$ ) with a diol (ethanediol, 1,2-propanediol, 2,3-butanediol, and others). This complex was discovered by Garif'yanov et al.<sup>88</sup>, who studied its ESR spectrum ( $S = \frac{1}{2}$ ). Since then much research has been carried out with the aim to understand the formation of this complex<sup>89-91</sup>. In the course of the oxidation reduction reaction, the Cr<sup>V</sup> is further reduced to Cr<sup>III</sup> ( $Cr^{VI} \rightarrow Cr^V \rightarrow Cr^{III}$ ). The Cr<sup>V</sup>-complex appeared to be a very suitable one for obtaining high polarizations, as was first proved by Glättli et al.<sup>25,92</sup>. However, getting very high polarizations requires a high Cr<sup>V</sup> concentration and a low Cr<sup>III</sup> content. This is related to the fact that Cr<sup>III</sup>

appreciably shortens the nuclear spin lattice relaxation time. For example, in a propane-diol sample, in which the ratio of  $\text{Cr}^{\text{V}}$  to  $\text{Cr}^{\text{III}}$  was about 1, we measured a relaxation time of 1 minute at 25 kG and 0.5 K, while it is about 1 hour if the  $\text{Cr}^{\text{III}}$  concentration is kept as low as possible.

The final concentrations of  $\text{Cr}^{\text{V}}$  and  $\text{Cr}^{\text{III}}$  not only depend on the reaction time and the temperature, but are also sensitive to the presence of water and light<sup>89,90,93</sup>). The first parameters we studied were the reaction time and the temperature in several solutions.

Typical reaction times at 70°C of some diols with potassium dichromate, which in each case yield about the same concentration of  $\text{Cr}^{\text{V}}$ -complexes, are: 10 minutes for ethanediol, 120 minutes for 1,2-propanediol, and 160 minutes for 2,3-butanediol. Longer reaction times or higher temperatures increase the  $\text{Cr}^{\text{V}}$  concentration, but also increase the  $\text{Cr}^{\text{III}}$  concentration. An obvious way to increase the  $\text{Cr}^{\text{V}}$  concentration with still a low concentration of  $\text{Cr}^{\text{III}}$  in the final solution would be to distil part of the diol out of the solution after a reaction time at which the  $\text{Cr}^{\text{III}}$  concentration is still low. A necessary condition for this purpose is, of course, that the solution has a boiling point at which the oxidation-reduction reaction is slow; if the reaction is fast at that temperature, then the  $\text{Cr}^{\text{V}}$  will still be converted into  $\text{Cr}^{\text{III}}$  during the distillation. The boiling points of the mentioned diols at 1 mm Hg pressure are: 53.0°C for ethanediol, 45.5°C for 1,2-propanediol, and 44.0°C for 2,3-butanediol. From the reaction times given above, it is clear that for ethanediol it will be more difficult to concentrate the solution by distillation without destroying the  $\text{Cr}^{\text{V}}$  complexes than it would be for the other diols. Therefore we used 1,2-propanediol. We did not use diols with more C-atoms, because it is known that the polarization in several diols, doped with  $\text{Cr}^{\text{V}}$  complexes, decreases with an increasing number of C-atoms<sup>94</sup>). We choose  $\text{K}_2\text{Cr}_2\text{O}_7$  as a  $\text{Cr}^{\text{VI}}$  compound, because the formation of  $\text{Cr}^{\text{V}}$  complexes is slow in this case; this makes it easier to concentrate the solution by distillation.

During the oxidation of the diols, water is formed. Bontchev et al.<sup>89</sup>) found that if the water is removed out of the solution by performing the reaction under vacuum, a rather large improvement of the  $\text{Cr}^{\text{V}}/\text{Cr}^{\text{III}}$  ratio could be obtained.

We prepared 1,2-propanediol samples in the following way: a mixture of 650 ml propane-diol and  $\text{K}_2\text{Cr}_2\text{O}_7$  (15:1 by weight) was stirred for 90 minutes at a constant temperature of 65°C of the surrounding water bath. The reaction flask was connected to a distillation column operating under 1 mm Hg pressure. The speed of distillation could be regulated by the position of the column, causing more or less reflux of the distilled propanediol. After 90 minutes there was about 200 ml of the solution left with a concentration of  $\sim 2.5 \times 10^{19}$  spins/cm<sup>3</sup>. The solution was then quickly concentrated five to six times by distilling, as quickly as possible, for 10 to 20 minutes, which yielded a concentration for optimum polarization (see Chapter III.2). This latter time should be as short as possible in order to prevent  $\text{Cr}^{\text{V}}$  to  $\text{Cr}^{\text{III}}$  conversion in the rather concentrated solution; it was kept under nitrogen atmosphere during further preparation of the sample in the form of frozen spheres. Originally we used also the photosensitive properties of the reaction in order to improve the  $\text{Cr}^{\text{V}}/\text{Cr}^{\text{III}}$  ratio<sup>28</sup>). However, by using a commercial distillation column, in which the solution could be concentrated more quickly and at lower temperatures, samples with similar properties could be obtained.

The concentration in the samples was measured by comparing the absorptive part of the EPR signals of a sample and a solution of propanediol with a known concentration of DPPH. The concentration of the  $\text{Cr}^{\text{V}}$  complexes obtained in this way is plotted against the peak-to-peak separation of the derivative of the EPR signal in Fig. II.5, from which it can be seen that the peak-to-peak separation is an accurate method for reading the concentration in this range. This figure shows a close resemblance to the curve obtained by other authors for  $\text{Cr}^{\text{V}}$ -complexes in ethanediol<sup>92)</sup> (dotted line in Fig. II.5).

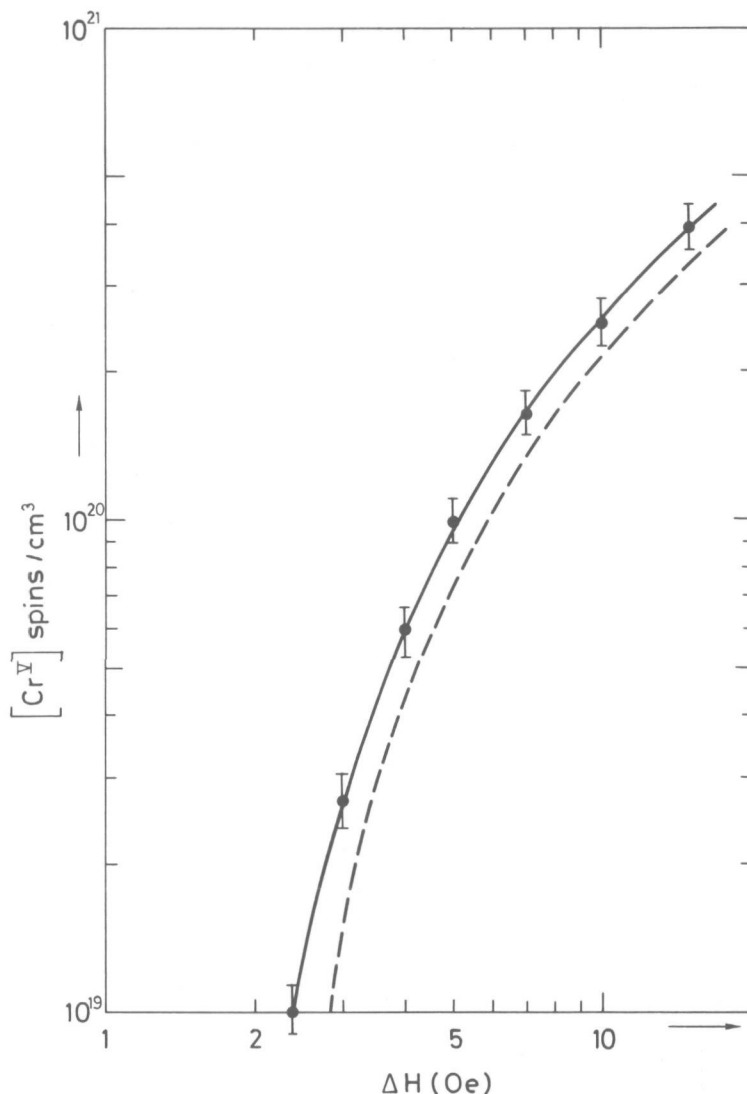


Fig. II.5 The peak-to-peak line width of the derivative of the ESR line versus the  $\text{Cr}^{\text{V}}$  concentration in 1,2-propanediol at room temperature in a 3 kG magnetic field. The dashed curve was obtained in ethanediol (from Ref. 92).

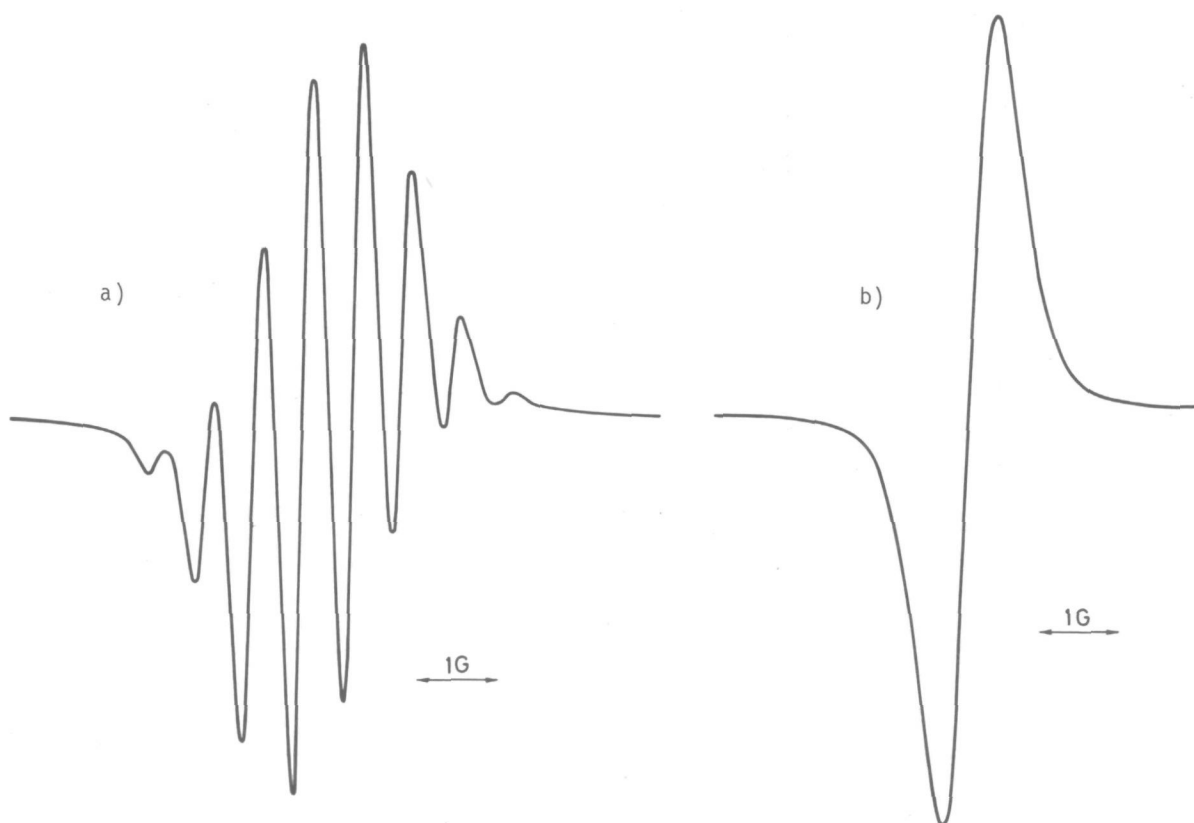
For an unknown reason the above-mentioned reaction is much more difficult in per-deuterated diols. We therefore used deuterated diols in which still two OH groups were present. Then the reaction appeared to occur with the same speed as in normal diols.

### CHAPTER III

#### DYNAMIC POLARIZATION IN DIOLS DOPED WITH Cr<sup>V</sup>-COMPLEXES

##### 1. ELECTRON SPIN RESONANCE MEASUREMENTS

The ESR spectrum of the Cr<sup>V</sup>-complex in ethanediol at 3 kG has been studied for the first time by Garif'yanov<sup>88</sup>). In a dilute solution it consists of a set of nine narrow lines separated by 0.3 G owing to the interaction with eight equivalent protons. Four other weak lines separated by 17 G were attributed to the hyperfine interaction with the <sup>53</sup>Cr nuclei (10% natural abundance). From the spectrum they deduced the most probable chemical structure of the complex and the fact of axial symmetry at the position of the Cr<sup>V</sup> ion. The structure in the main line disappears, when the Cr<sup>V</sup>-complexes are prepared in partially deuterated ethanediol-D4 (see Fig. III.1).



- a) ESR spectrum of a solution of ethanediol with a low concentration of Cr<sup>V</sup>-complexes ( $S = \frac{1}{2}$ ). The splitting results from the hyperfine interaction with neighbouring protons.
- b) ESR spectrum of a diluted solution of partially deuterated ethanediol-D4; since the Cr<sup>V</sup>-complexes are deuterated, the line width is drastically reduced compared with the spectrum given in Fig. III.1a.

Fig. III.1

Below  $-70^{\circ}\text{C}$  the solution becomes solid and the line width then increases from 7 to 14 G for a concentration of  $16 \times 10^{19}$  spins/cm<sup>3</sup>.

At 25 kG and 0.5 K the g-factor anisotropy is the dominant broadening mechanism. This spectrum is shown in Fig. III.2.

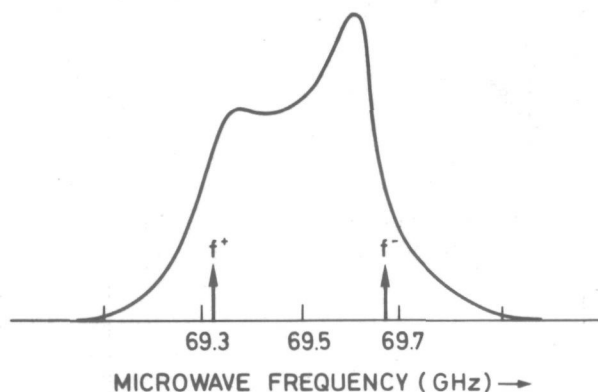


Fig. III.2

The ESR absorption spectrum of propanediol with a  $\text{Cr}^{\text{V}}$  concentration of  $16 \times 10^{19}$  spins/cm<sup>3</sup> in a 25 kG magnetic field at 0.5 K. The arrows indicate the microwave frequency, where optimum polarization is obtained ( $f^+$  for positive and  $f^-$  for negative polarization).

From the line shape the g-factor anisotropy can be deduced to be

$$\frac{\Delta g}{g} = \frac{g_{\perp} - g_{\parallel}}{g} \cong 4 \times 10^{-3} ,$$

where  $g \approx 1.985$ .

The electron spin lattice relaxation time in a sample with the above-mentioned concentration is rather long at 0.5 K and 25 kG, namely  $38 \pm 2$  msec.

## 2. MAXIMUM POLARIZATION VALUES OF PROTONS, DEUTERONS, AND CARBON-13 NUCLEI

### 2.1 Absolute values of the polarization

The optimum polarization values in diols doped with  $\text{Cr}^{\text{V}}$ -complexes have been widely studied under various experimental conditions, because of their interesting properties with regard to polarized targets. The results are listed in Table III.1. A few other organic materials have been included as well. Some crystals, in which dynamic polarization experiments have been performed, are lanthanum magnesium nitrate<sup>75)</sup>, ruby<sup>110)</sup>, tutton salts<sup>6)</sup>, rutile<sup>111)</sup>, calcium fluoride<sup>112)</sup>, and others.

In the following we will direct our attention to samples of propanediol and partially deuterated ethanediol-D4 or propanediol-D6. The concentration of  $\text{Cr}^{\text{V}}$ -complexes was chosen in the range where optimum polarization can be obtained (see Fig. III.3).

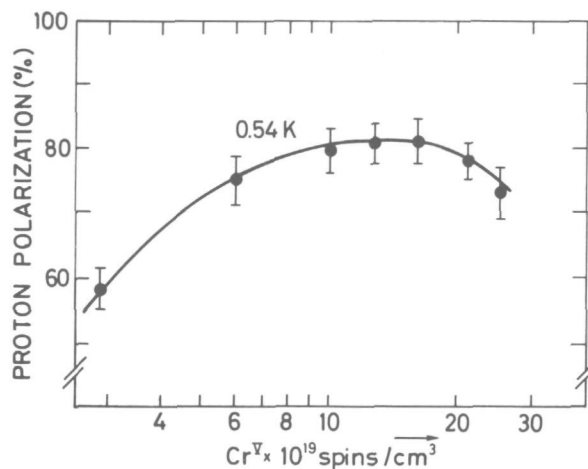


Fig. III.3

The optimum proton polarization versus Cr<sup>V</sup> concentration in 1,2-propanediol at a <sup>3</sup>He bath temperature of 0.54 K.

Table III.1

Substance (chemical formula)	Paramagnetic centres (concentration in spins/cm <sup>3</sup> )	Maximum polarization at 25 kG				Maximum proton polarization at 50 kG below 1.5 K	References
		~ 1 K	≤ 0.5 K				
Ethenediol (C <sub>2</sub> H <sub>6</sub> O <sub>2</sub> )	Cr <sup>V</sup> -complexes 5 × 10 <sup>19</sup> - 10 <sup>20</sup>	P(H) 50	P(H) 80-97	P(D) 40	P(C) 48	80	25-27, 61 95-97
1,2-propanediol (C <sub>3</sub> H <sub>8</sub> O <sub>2</sub> )	Cr <sup>V</sup> -complexes 5 × 10 <sup>19</sup> - 2 × 10 <sup>20</sup>	50	80-98	44	52	90	28, 29, 32, 98, 99
Hexanediol Pinacone (C <sub>6</sub> H <sub>14</sub> O <sub>2</sub> )	Cr <sup>V</sup> -complexes 10 <sup>19</sup> - 10 <sup>20</sup>	40	60-80	-	-	-	78, 92, 94
1-butanol (C <sub>4</sub> H <sub>10</sub> O)	Porphyrexide 3 × 10 <sup>19</sup>	40	70-85	25	21	80	100-108
Ammonia (NH <sub>3</sub> )	Cr <sup>V</sup> -complexes ~ 10 <sup>19</sup>	40	60-70	-	-	-	108, 109

## 2.2 Relative values of the polarization

The polarization values listed in Table III.1 were determined by comparison of the enhanced NMR signals with the thermal equilibrium ones. However, this method is not very accurate in the case of spin species with a low natural abundance, e.g. carbon-13 (1.1%). We therefore determined the carbon-13 polarization P(<sup>13</sup>C) in another way, namely by measuring the relative values of the polarization of different nuclei<sup>113</sup>). This was done by comparing NMR signals at a constant frequency and correspondingly different magnetic

field values: when the polarizations had reached their steady-state values, the microwave power was switched off and the dilution cryostat was cooled down to 120 mK in a few minutes, a time which is short compared to the relaxation times<sup>27</sup>). At 120 mK the relaxation times were longer than 100 h at 25 kG and longer than 3 h at the lowest field value. The polarizations were thus frozen in during their measurement, which lasted a few minutes. The relative values of the polarizations could then be calculated from the relative intensities of the NMR signals, the number of spins, their spin value and magnetic moment.

In 1,2-propanediol-D6 the ratios P(H) : P(D) : P(<sup>13</sup>C) were found to be equal to<sup>32</sup>)

$$1 : 0.445 \pm 0.02 : 0.53 \pm 0.03 \quad (\text{III.1})$$

in the case where the absolute values were equal to

$$P(\text{H}) = 98_{-3}^{+2}\% \quad \text{and} \quad P(\text{D}) = 44 \pm 4\% .$$

From these ratios and from the absolute value of P(H) we find

$$P(\text{D}) = 43.5 \pm 2\% \quad \text{and} \quad P(^{13}\text{C}) = 52 \pm 3\% .$$

The agreement between this value of P(D) and its absolute value of 44% gives confidence in the determination of P(<sup>13</sup>C) by this method.

### 2.3 Comparison of the polarizations with the equal spin temperature hypothesis

Since the electron spin lattice relaxation time of the inhomogeneous electron spin system is rather long, we might expect that cross-relaxation is fast compared with  $T_{1e}$ . Experimental evidence for this is described in the next section. In such a case dynamic polarization by cooling of the electron spin-spin interaction reservoir is expected to be dominant, because the line width of the ESR line is much broader than the nuclear Larmor frequencies. Under such conditions the different nuclear spin species will obtain an equal spin temperature. The polarizations and the spin temperatures are related by Brillouin functions, which reduce in the present case to

$$P(\text{H}) = \tanh \{h\nu_{\text{H}}/2kT(\text{H})\} , \quad (\text{III.2})$$

$$P(\text{D}) = \frac{4 \tanh \{h\nu_{\text{D}}/2kT(\text{D})\}}{3 + \tanh^2 \{h\nu_{\text{D}}/2kT(\text{D})\}} , \quad (\text{III.3})$$

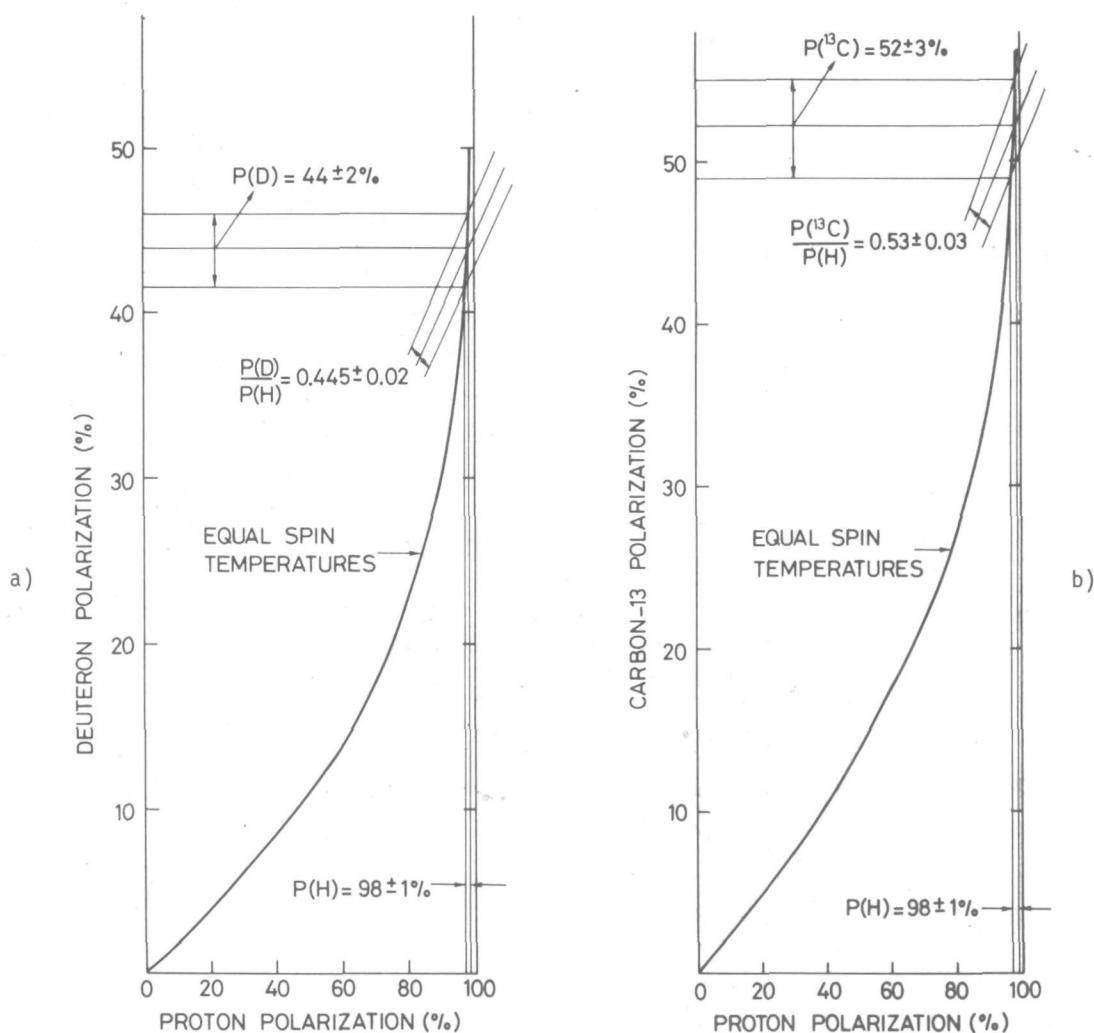
$$P(^{13}\text{C}) = \tanh \{h\nu_{\text{C}}/2kT(\text{C})\} . \quad (\text{III.4})$$

Assuming equal spin temperatures, we can replace the different temperatures in Eqs. (III.2)-(III.4) by a unique temperature  $T_{\text{S}}$ , and we see that each of the ratios P(D) : P(H) and P(<sup>13</sup>C) : P(H) determines the unique unknown  $T_{\text{S}}$  and thus makes it possible to calculate the absolute polarizations from their relative values only. With the ratios (III.1) one obtains

$$P(\text{H}) = 98 \pm 1\% \quad \text{and} \quad P(\text{D}) = 44 \pm 2\% , \quad (\text{III.5})$$

$$P(\text{H}) = 98 \pm 1\% \quad \text{and} \quad P(^{13}\text{C}) = 52 \pm 3\% . \quad (\text{III.6})$$

Figure III.4 illustrates how the equations can be solved graphically. The agreement between these results and the numbers obtained by the NMR calibration quoted in Section 2.2



- a) The deuteron versus proton polarization. The ratio of the deuteron and proton polarization was measured to be  $0.445 \pm 0.02$ . The line with this tangent crosses the curve, which corresponds to equal spin temperatures for the corresponding nuclear Zeeman reservoirs at values which coincide with the measured ones, thus confirming that the spin temperatures are equal within experimental errors.
- b) The same as in Fig. III.4a, but now for the carbon-13 versus proton polarization. The relevant numbers are indicated in the figure.

Fig. III.4

allows the conclusion that the spin temperatures were equal within experimental errors. Similar conclusions were drawn for experiments in 1-butanol<sup>106,107</sup>). The results (III.5) and (III.6) show how sometimes the proton polarization can be determined accurately without measuring thermal equilibrium signals, once the equality of the spin temperatures has been demonstrated.

#### 2.4 Polarization versus microwave frequency

Steady-state values of  $P(H)$  and  $P(D)$  in ethanediol-D4 were measured versus microwave frequency at a fixed temperature of 0.54 K, in a field of 25 kG, using a  $^3\text{He}$  evaporation cryostat and a microwave power of about 5 mW/g. The inverse spin temperatures  $1/T(H)$

and  $1/T(D)$ , deduced from the polarization values by using Eqs. (III.2) and (III.3), are shown in Fig. III.5. Again, the spin temperatures are seen to be equal within experimental errors. In particular, the maximum steady-state values of  $P(H)$  and  $P(D)$  occur at the same microwave frequency.

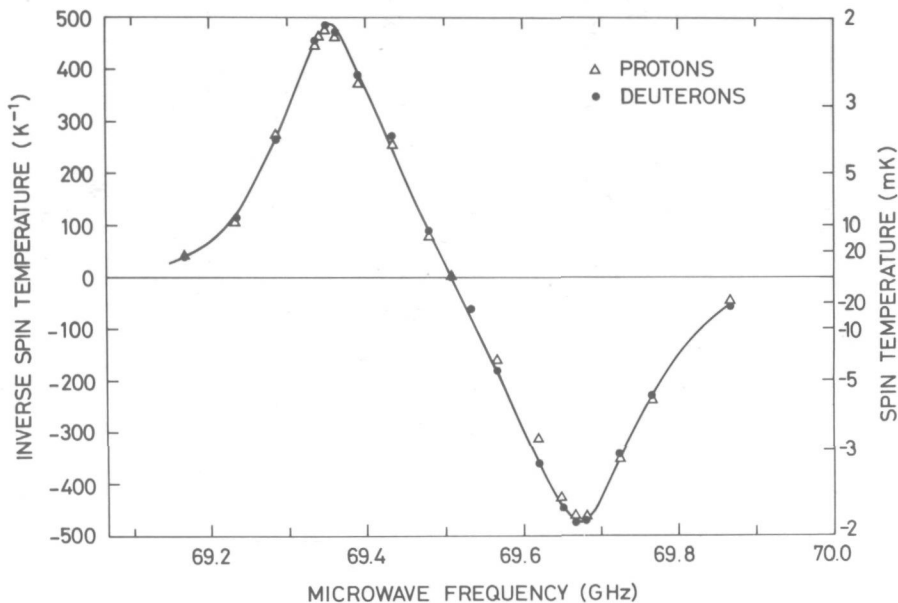


Fig. III.5

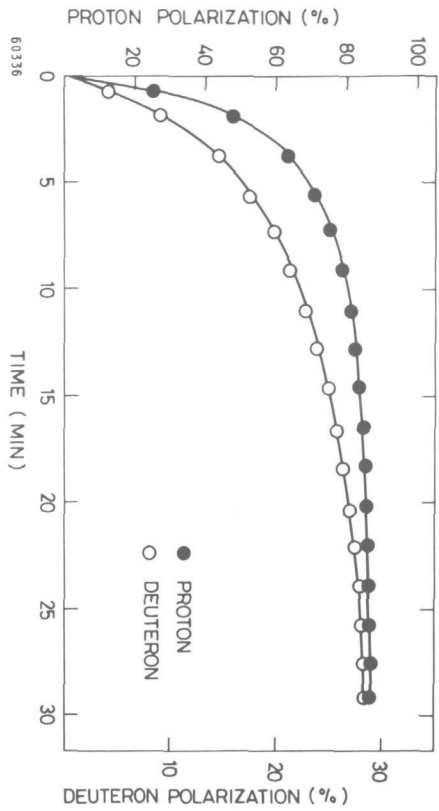
The inverse spin temperatures of protons and deuterons as a function of the applied microwave frequency at a  $^3\text{He}$  bath temperature of 0.54 K in a 25 kG magnetic field. They are seen to be equal at different microwave frequencies.

### 3. TRANSIENT BEHAVIOUR OF THE VARIOUS SPINS

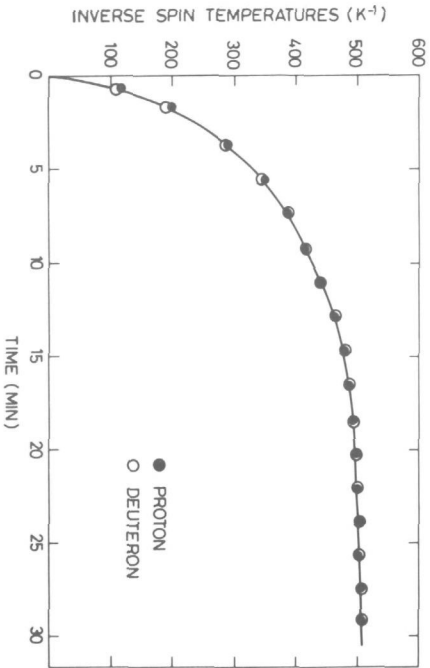
A series of measurements were made which show the existence of a thermal coupling between the different nuclear spin species, the strength of which depends on microwave power and temperature<sup>27</sup>).

#### 3.1 Polarization build-up with microwave irradiation

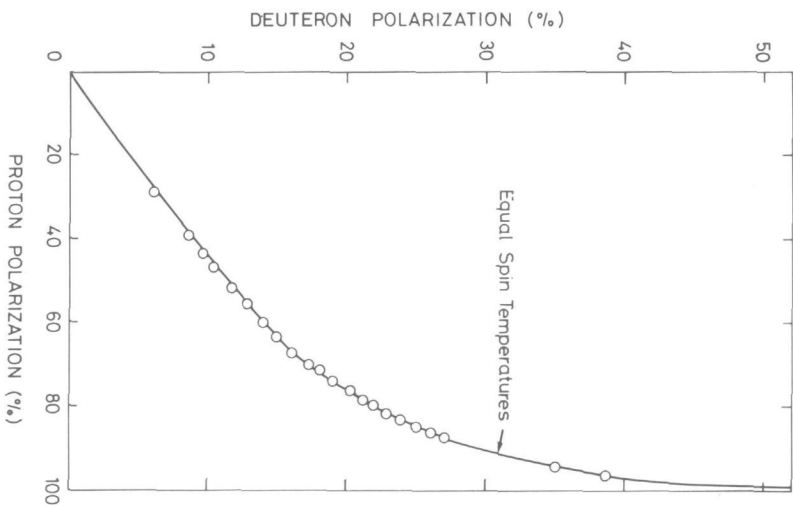
Starting from polarizations equal to zero, the microwave power was switched on and  $P(H)$  and  $P(D)$  in ethanediol-D<sub>4</sub> were monitored as a function of time. The evolution of  $P(D)$  is seen to be slower than that of  $P(H)$  (Fig. III.6a). The proton and deuteron "polarization times" are thus different. However, the corresponding spin temperatures, deduced by using Eqs. (III.2) and (III.3), were equal at each instant during polarization build-up, as can be seen from Fig. III.6b, where we plotted the inverse spin temperatures versus time. Note that the inverse spin temperatures are not directly proportional to the polarizations. The same results can be presented in another way: we draw a point on a "P(H)-P(D)" plot corresponding to instantaneous measured polarizations (Fig. III.6c). This point is seen to move in time along a curve which coincides with the curve deduced from the assumption of equal spin temperatures.



a) The evolution of the proton and deuteron polarization with time, when a microwave power of 3 mW/g is applied.



b) Inverse spin temperatures of protons and deuterons versus time as deduced from the polarization values of Fig. III.6a by using Eqs. (III.2) and (III.3). Contrary to the polarizations, the spin temperatures of the different nuclear species are seen to be equal at each time.



c) Deuteron versus proton polarization. The plotted points were determined during build-up of the polarization with a microwave power of 3 mW/g, except the three highest points which are steady-state values. The theoretical curve corresponds to equal spin temperatures for the different nuclei.

Fig. III.6

The polarization times in these samples were rather short. They correspond, in fact, to what can be expected if the polarization arises from a thermal contact with the electron spin-spin interaction reservoir<sup>29</sup>). Then each absorbed photon from the microwave field causes a cooling of the interaction reservoir by an amount  $h\Delta = h(\nu_e - \nu)$ ; thus the polarization time is directly related to the microwave power.

### 3.2 Attainment of equilibrium with unequal initial spin temperatures

After having polarized the nuclei to a high steady-state value, the microwave power was switched off and one of the polarizations, for example P(H), was reduced to zero by NMR saturation. The proton spins were thus heated up to a very high temperature, while the deuteron (and <sup>13</sup>C) spins remained polarized, i.e. remained very cold. The values of P(H) and P(D) were then monitored as a function of time. The proton and deuteron spin temperatures evolved towards one another with a time constant  $\tau(H, D)$ . The middle curve in Fig. III.7 shows the temperature dependence of  $\tau(H, D)$  in ethanediol-D4. For comparison we showed also the spin lattice relaxation times for protons and deuterons (upper curve); the lower curve will be discussed later. Similar observations have been done in other materials<sup>114-116</sup>); the thermal coupling is attributed to the contact with a common reservoir, in this case the electron spin-spin interaction reservoir, as is apparent from

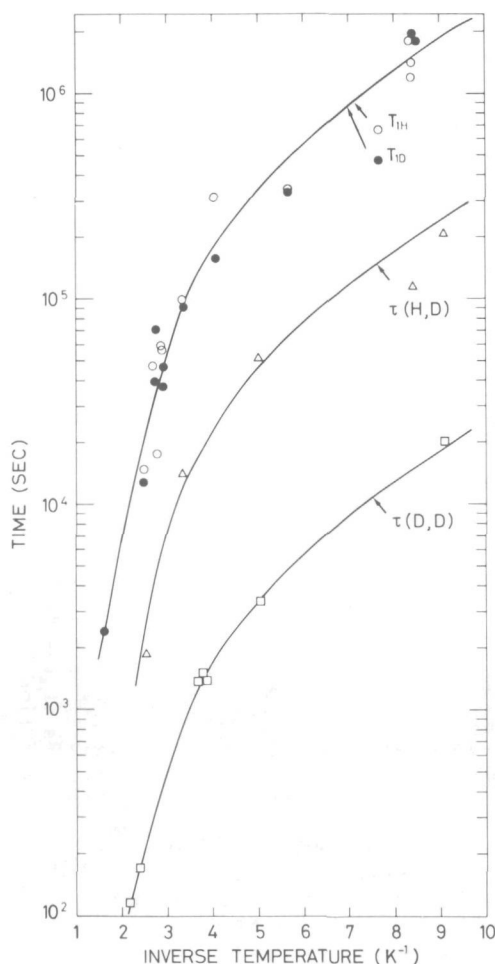
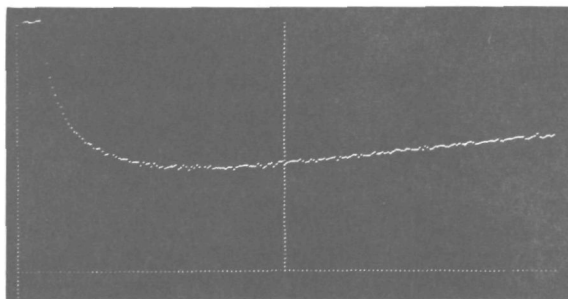


Fig. III.7

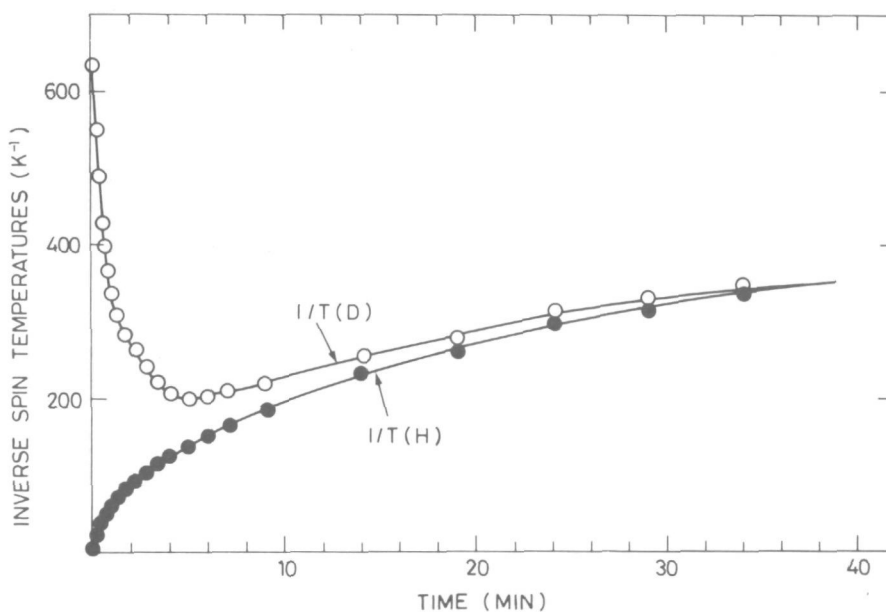
The following quantities are plotted as a function of temperature. Upper curve: Spin lattice relaxation times of protons  $T_{1H}$  (○) and deuterons  $T_{1D}$  (●). Owing to the thermal coupling between the different nuclei, which is much stronger than their coupling with the lattice, the decay of the polarizations of different nuclei occurred at about the same rate, but was not purely exponential. The points were obtained by the extrapolating the initial linear decay to zero. Middle curve: Proton-deuteron thermal mixing time  $\tau(H, D)$ . After saturating one of the spin systems, the decay of the other one was followed. This decay was much faster than the spin lattice relaxation and is attributed to the thermal coupling between different nuclei, which occurs via the electron spin-spin interaction reservoir. Lower curve: Relaxation time  $\tau(D, D)$  of the pure tensor polarization of deuterons (Section III.3.3).

a steep temperature dependence similar to that of the spin lattice relaxation time. The temperature and field dependence of the latter will be discussed in more detail in the next section. The fact that  $\tau(H, D) < T_{1H} \sim T_{1D}$  means that cross-relaxation within the electron spin system is so fast that the various parts rapidly reach thermal equilibrium, and their common temperature then varies more slowly towards that of the lattice.

We made another observation, which is important for the understanding of the mechanism of dynamic polarization: the spins were prepared in states defined by  $P(H) = 0$  and  $P(D) \neq 0$  as before: microwaves were then suddenly applied again. Figure III.8a shows the



- a) The evolution of the deuteron polarization after polarizing all the nuclei, switching off the microwave power, saturating the proton spin system, and switching microwave power on again (about 900  $\mu$ W) at time zero. The sharp decrease of  $P(D)$  is attributed to the improvement of the thermal contact between the hot proton spins and the cold deuteron spins. After re-establishment of the thermal equilibrium between the different nuclei, the deuteron polarization starts to increase again with a polarization build-up rate which is an order of magnitude smaller than the thermal mixing rate. The total time span for the 200 points is 500 sec.



- b) The inverse spin temperatures of protons and deuterons after polarizing all nuclei, saturating the proton spins with no microwave power on, and switching on the microwave power again (300  $\mu$ W) at time zero. The thermal mixing time is about three times longer than the one illustrated in Fig. III.8a, where a three times higher microwave power is used.

Fig. III.8

evolution of  $P(D)$  after saturation of the protons and application of a microwave power of about  $900 \mu\text{W/g}$  at  $69.32 \text{ GHz}$ . Instead of increasing,  $P(D)$  first decreased rapidly and then started to increase again with the normal polarization rate. We determined the inverse spin temperatures of protons and deuterons, doing the same experiment with  $300 \mu\text{W}$  microwave power/g. Figure III.8b shows that the deuteron and proton spin temperatures evolve towards one another with a time constant of about 2 min, which is about ten times shorter than the polarization time in this case.

This behaviour is attributed to the improvement of the thermal contact between the cold deuteron spins and the hot proton spins, owing to the application of the microwave power. The fact that the thermal mixing time is much shorter than the polarization time explains why, during polarization build-up, the spin temperatures of the different spin species were equal, as mentioned in Section 2.3.

The microwaves can improve the thermal contact in two ways, namely via the forbidden transitions and via a change in the factor  $1 - P_e P_0$ , which increases the probability of the cross-relaxation transitions. A consequence of the strong thermal coupling between nuclear spins is that the destruction of the polarization of one spin species by NMR saturation, which can occur in a few seconds, is followed by a rapid destruction of the polarization of the other spin species if microwaves are on. We have indeed observed such an effect.

### 3.3 Thermalization within the deuteron spin system

Besides the apparent strong thermal coupling between different nuclei, similar phenomena were observed within the inhomogeneous deuteron spin system<sup>27</sup>).

We used two ways to disturb thermal equilibrium within the deuteron spin system:

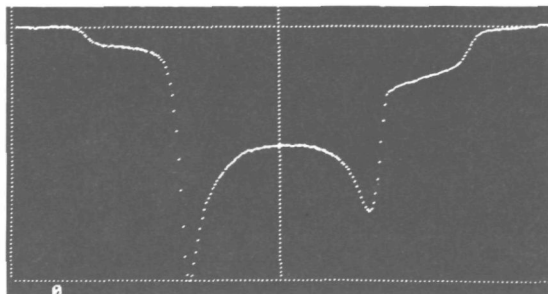
- a) burning a hole in the DMR line;
- b) producing alignment by proton RF irradiation, as described in the Chapter IV.

Both methods produced inhomogeneities in the populations of the magnetic substates, which had quite different lifetimes.

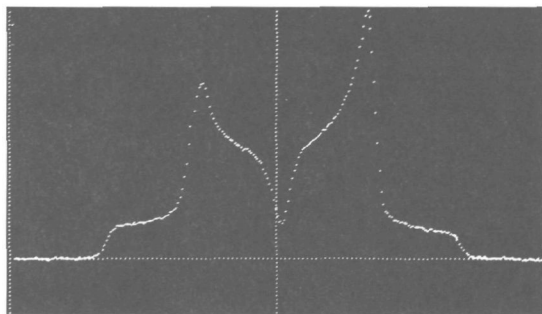
- a) Hole-burning was done by irradiating the sample for a few seconds with an RF field. A few examples are given in Fig. III.9, where we show respectively;
  - i) a polarized DMR signal;
  - ii) a DMR line, in which a hole was burned using one single RF frequency;
  - iii) same as (ii), but now with a frequency-modulated RF field;
  - iv) the recovery of a hole in the centre (the super-imposed pictures were taken 30 seconds one after another).

A narrow hole was found to be filled with a time constant of a few minutes, independent of temperature, and weakly dependent on its position within the DMR line.

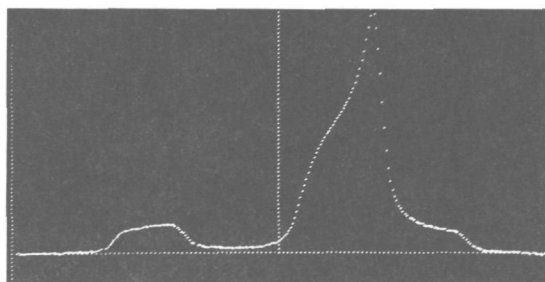
- b) The lifetime of the state obtained by RF alignment behaved quite differently, since it was much longer and highly temperature-dependent. In the absence of microwaves the application of an RF field slightly off the proton resonance frequency produced a change in the deuteron alignment (see next chapter); in particular, starting with unpolarized deuterons, the DMR line became antisymmetric, corresponding to a state with pure alignment  $A(D)$  and zero vector polarization  $P(D)$  (see Chapter IV). We



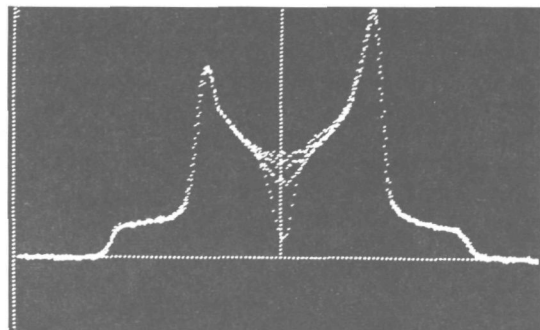
- a) The deuteron magnetic resonance line of 1,2-propanediol. This line shows remarkably well the features of the theoretical line shape (see Chapter I.5). The asymmetry is due to the polarization, which is -43% [see Eq. (I.44)]. The distance between the two peaks is 117 kHz.



- b) The inhomogeneous behaviour of the deuteron spin system made it possible to burn holes in the DMR line with a saturating RF field.



- c) As in Fig. II.9b, but with a frequency-modulated RF field.



- d) Recovery of a hole in the DMR line. The superimposed pictures were taken 30 sec after one another. It can be seen that the hole is filled from the edges, while the main part of the line is not affected.

Fig. III.9

describe the transient behaviour of the alignment, after the aligning RF field was turned off, by the parameter  $\tau(D, D)$  representing the decay of the alignment of the deuterons contributing to the peaks of the DMR line ("peak deuterons"). The temperature dependence of  $\tau(D, D)$  is depicted by the lowest line in Fig. III.7. We see that it has the same temperature dependence as the proton-deuteron thermal mixing time  $\tau(H, D)$  and the spin lattice relaxation time.

We interpret the relatively fast and temperature-independent recovery of a narrow hole burned in the DMR line as being due to pure deuteron cross-relaxation, involving for example two deuteron spin flips at the hole frequency and two other deuterons with frequencies on either side of the hole; energy and angular momentum can thus be conserved.

Such a mechanism is not efficient to produce the recovery of the deuteron spin system after pure RF alignment, since a change in the alignment corresponds to a change in the quadrupole energy (see Chapter IV). During relaxation this energy has to be taken up by the lattice or by the electron spin-spin interaction reservoir. This latter seems to occur, since the recovery time of the alignment  $\tau(D,D)$  is much shorter than  $T_{1D}$ , while the temperature dependence is about the same.

Applying microwave power to deuterons with pure alignment has two effects: the vector polarization increases and the alignment evolves rapidly towards its equilibrium value given by  $A(D) = (3/4)P(D)^2$  (see Chapter I.5). The thermalization of the deuteron spin system can thus be observed by computing the quantity

$$x = A(D) - \frac{3}{4} P(D)^2, \quad (\text{III.7})$$

as a function of time;  $x$  tends towards zero, when a spin temperature is established within the deuteron spin system. Figure III.10 gives various experimental curves of  $x$  versus time, taken with different microwave powers.

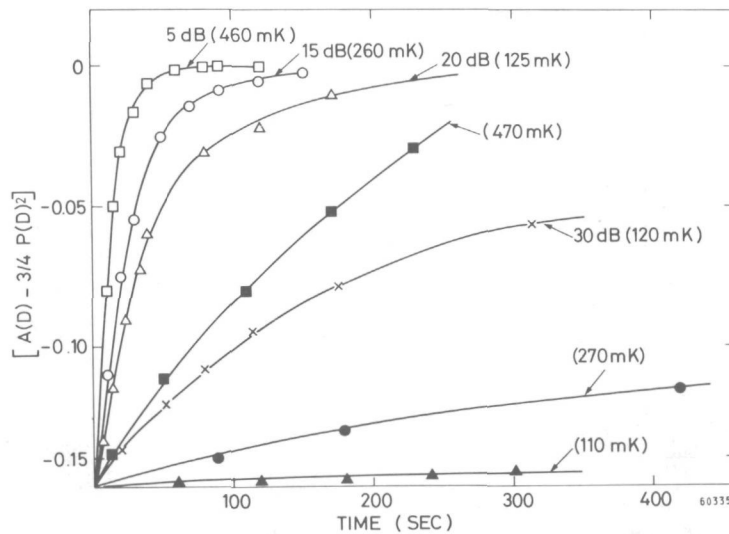


Fig. III.10

The evolution of the quantity  $x = A(D) - \frac{3}{4}P(D)^2$  at different temperatures and microwave power levels.  $A(D)$  is the peak deuteron alignment, which corresponds to the difference of the peak intensities of the DMR line. The relative microwave attenuation is indicated for the corresponding curves: 5 dB corresponds to about 1.5 mW/g, 30 dB to about 5  $\mu$ W/g. The given temperatures are sample temperatures, which can be higher than the surrounding liquid temperature owing to microwave heating.

### 3.4 Proton spin lattice relaxation

The proton spin lattice relaxation time  $T_{1H}$  in normal 1,2-propanediol was measured at various magnetic fields and temperatures by following the decay of the enhanced NMR signal; this was found to be exponential<sup>29</sup>).

The temperature dependence of  $T_{1H}$  below 1 K is shown in Fig. III.11 at two different magnetic fields, while the field dependence of  $T_{1H}$  is shown in Fig. III.12 at three different temperatures. The curves drawn there obey the equation

$$T_{1H}^{-1} = \left[ A T_{1e} H^2 \cosh^2 \left( \frac{h\nu_e}{2kT} \right) \right]^{-1} + \left[ 0.19 \frac{H^{1.32}}{T^{1.64}} \right]^{-1}, \quad (\text{III.8})$$

where

$$A T_{1e} = 225 \left[ H^5 \coth \left( \frac{h\nu_e}{2kT} \right) + 6.75 \times 10^5 \exp \left( - \frac{0.5}{T} \right) \right]^{-1}. \quad (\text{III.9})$$

In these equations  $T_{1H}$  is expressed in hours, the magnetic field  $H$  is expressed in kG, and the temperature  $T$  in K;  $A$  is a constant and  $T_{1e}$  is the electron spin lattice relaxation time.

The first term in Eq. (III.8) shows the field and temperature dependence of Eq. (I.41), which is valid, if the nuclear relaxation occurs via the forbidden transitions. This term

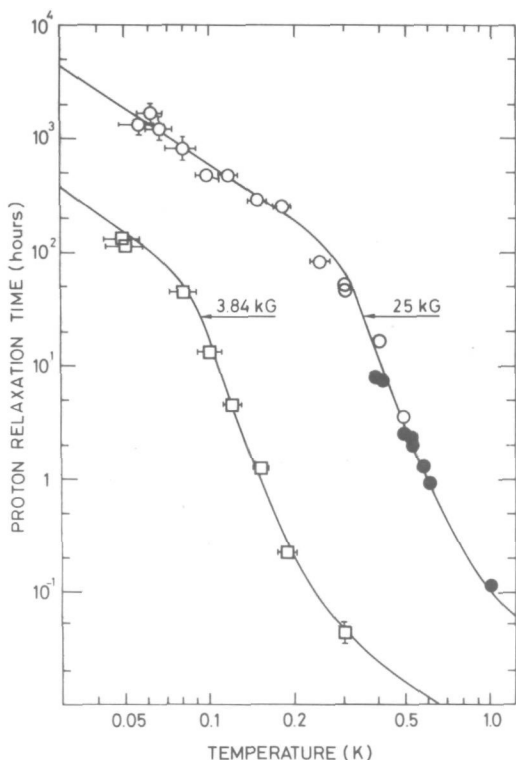


Fig. III.11

The temperature dependence of the proton spin lattice relaxation time  $T_{1H}$  in 1,2-propanediol for magnetic fields of 25 kG (○) and 3.84 kG (□). Some points (●) were obtained in <sup>3</sup>He or <sup>4</sup>He evaporation cryostats for the same sample. The curves are calculated from Eqs. (III.8) and (III.9). Error bars are only shown where they exceed the size of the symbols.

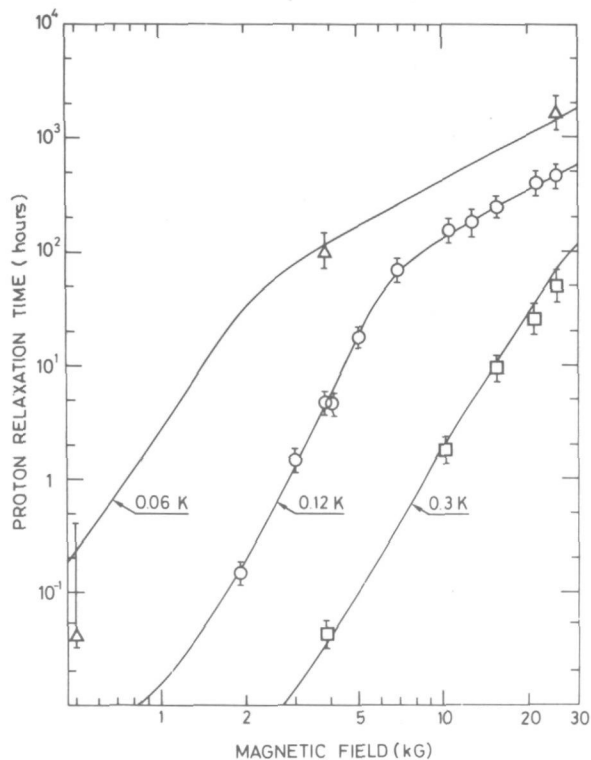


Fig. III.12

The magnetic field dependence of the proton spin-lattice relaxation time  $T_{1H}$  of 1,2-propanediol at temperatures of 0.3 K (□), 0.12 K (○) and 0.06 K (Δ). The error bars also include possible errors of temperature. The curves are calculated from Eqs. (III.8) and (III.9).

causes the steep increase of the relaxation time in Fig. III.11. However, for values of  $T_{1H}$  larger than 50 h, such a steep temperature dependence was no longer observed and we had to add the second purely empirical term in Eq. (III.8).

The first term in Eq. (III.9) has the field and temperature dependence of the direct process for electron spin lattice relaxation [see Eq. (I.39)]. This term fits well with the measured points at high fields, but it becomes too small at lower field values, which is usually observed if one extrapolated  $T_{1e}$  from high fields to low fields. We could fit our low field measurements by adding to Eq. (III.9) an exponential field-independent term proportional to  $e^{-(b/T)}$ , with  $b = 0.5 \pm 0.05$  K. If one now extrapolates  $T_{1e}$  from 25 kG and 0.5 K to 3 kG and 1 K, one expects  $T_{1e} = 40$  msec, which is the right order of magnitude<sup>117)</sup>. Harris and Yngvesson<sup>118)</sup> found such an exponential term for the spin lattice relaxation in some iridium salts, and they explained it by a relaxation process between the manifolds of exchange-coupled clusters.

As was described in the previous section, there exists a strong thermal coupling between different nuclear spin species. Therefore the relaxation via the electron spin-spin interaction reservoir is likely to play some role; however, we do not know how to separate the various possible contributions.

In high magnetic fields the nuclear relaxation time was roughly proportional to the inverse of the  $Cr^V$  concentration, as expected<sup>72)</sup>, but at lower fields a stronger concentration dependence was observed, which may be related to cluster formation<sup>119,120)</sup>.

#### 4. COMPARISON WITH THE SPIN TEMPERATURE THEORY

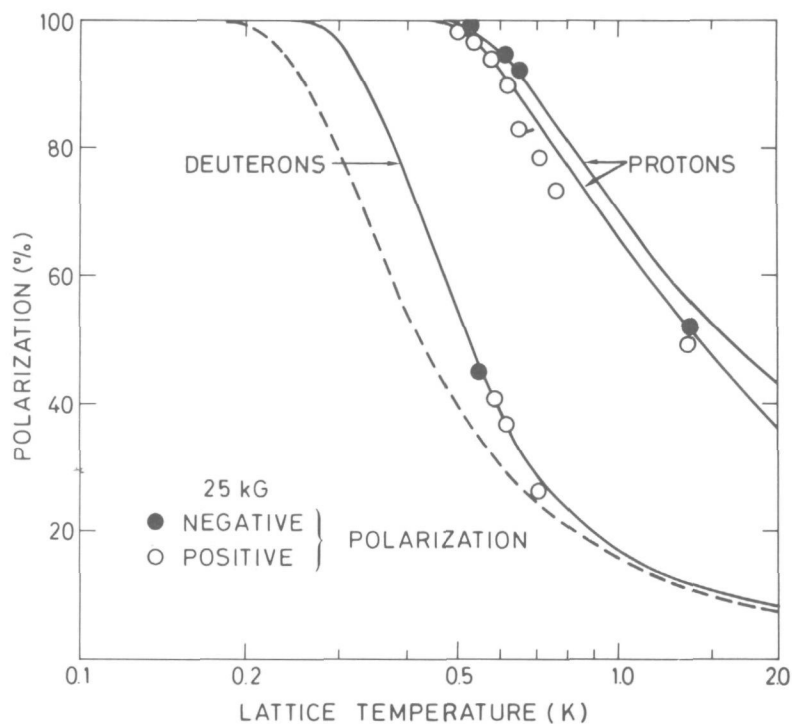
In Chapter I we calculated the magnetic field and temperature dependence of the polarization in 1,2-propanediol. However, an accurate experimental verification of the temperature dependence is difficult, because the sample temperature is unknown during dynamic polarization owing to microwave heating. Fortunately, one thing can be measured rather precisely, namely the slope  $\partial P/\partial T$ , because at low temperatures the thermal contact between the sample and the He bath is mainly limited by the Kapitza boundary resistance<sup>121)</sup>. Then the rate of change of energy  $\dot{Q}$  between the sample and the bath, which have temperatures  $T_S$  and  $T_L$ , respectively, is given by

$$\dot{Q} \propto (T_S^4 - T_L^4) \quad (III.10)$$

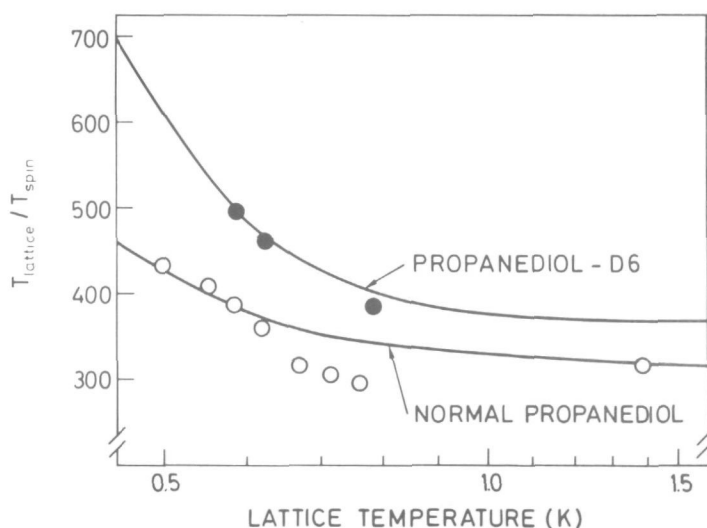
or

$$T_S = C\dot{Q}^{\frac{1}{4}} \quad (III.11)$$

at low temperatures. This means that  $T_S$  is mainly determined by the microwave power, at least if  $C$  is constant. This relation was verified by measuring the difference between  $T_S$  and  $T_L$  as a function of microwave power<sup>29)</sup>. By using a microwave frequency far from paramagnetic resonance, the sample temperature could be determined accurately from the nuclear spin lattice relaxation time. The microwave power was determined by comparing it with the power of an electrical heater wrapped around the mixing chamber. We determined the maximum proton polarization for different microwave power levels<sup>29)</sup>. The sample temperature was calculated from Eq. (III.11), using a value of  $C$  equal to  $2.9 \text{ K/W}^{\frac{1}{4}}$  in order to get a good agreement with the polarizations as calculated from Eq. (I.31). The results are shown in Fig. III.13. The sample temperature around 1 K was determined by using the Kapitza



- a) The temperature dependence of the proton and deuteron polarization. The curves were calculated from Eq. (I.31). The upper curve corresponds to the calculated negative proton polarizations, which are seen to be slightly higher than the positive polarizations. The leakage term was determined from the measured relaxation times; in the calculation of the deuteron polarization curve, the reduced heat capacity of the nuclear Zeeman reservoirs was taken into account. For comparison the deuteron polarization is also shown, if the reduced heat capacity for the deuterated sample was not taken into account (dashed line).



- b) The "enhancement" of the inverse spin temperatures for normal and partially deuterated propanediol. The difference between the two samples arises from the smaller heat capacity of the nuclear Zeeman reservoirs in the deuterated sample. The curves are calculated ones.

Fig. III.13

resistance coefficient given in Ref. 84. At the highest polarizations the microwave power was about 0.5 mW/g and the temperature of the He mixture in the dilution refrigerator was 0.2 K.

At a constant temperature the negative polarization was observed to be slightly higher than the positive one, as was expected from the calculations (the upper curve in Fig. III.13 corresponds to the calculated negative polarizations). This difference is connected with the asymmetric ESR line<sup>30</sup>).

The optimum polarizations were obtained at a microwave frequency, for which  $|\Delta| = 200$  MHz, which is in good agreement with the calculated value of  $|\Delta|$ . Of course the constant C could have been chosen different, which would shift the experimental points by a constant factor. However, this retains the rather steep temperature dependence of the polarizations, which is seen to be in good quantitative agreement with the spin temperature model described before. Also the magnitude of the polarization corresponds well with the calculated one.

For the calculations of the curve for the deuteron polarization we used a slightly lower value of f corresponding to the reduced heat capacity of the nuclear Zeeman reservoirs in the partially deuterated sample as compared to a normal sample (about a factor three lower). As was calculated in Chapter I.3.3, a small difference in the leakage term should still give appreciable variations, even at low temperatures. In Fig. III.13 the calculated enhancement of the inverse spin temperatures is shown for a normal and a deuterated propanediol sample together with the experimental points. The expected increase of the enhancement and the difference between a normal and a deuterated sample are evident. This latter fact has also been observed in 1-butanol<sup>106</sup>).

Some measurements were done at different magnetic fields<sup>99,122</sup>), namely at 48, 25, and 17 kG, at an estimated sample temperature of 0.7 K. The points are shown in Fig. III.14 together with the calculated curves. A rather large deviation is found at 48 kG. There

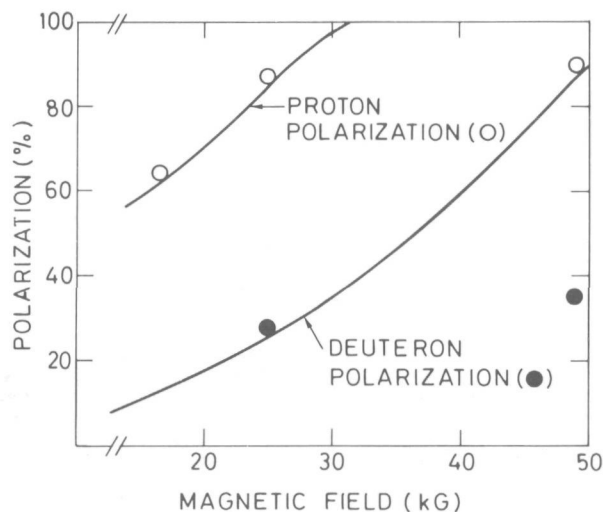


Fig. III.14

The proton and deuteron polarization at 0.7 K as a function of magnetic field. The polarization was measured at three field values (17, 25 and 48 kG). The large deviation at 48 kG is discussed in the text.

may be several reasons for this: the electron spin system is not completely saturated, because of the short electron spin lattice relaxation time [about 1 msec, if we extrapolate the value at 25 kG by using the expression (I.39)] or the thermal contact of the nuclei with the electron spin-spin interaction reservoir became too bad. The latter may be due to a slow cross-relaxation within the electron spin system, since the g-factor anisotropy will cause an appreciable inhomogeneous broadening at 50 kG. Also the factor  $(1 - P_e P_0)$  then becomes very small. As said before, this factor arises simply from the fact that at high polarizations there are hardly any electrons with spin up, thus reducing the cross-relaxation rate, since a combination of spin up and spin down is a necessary condition for a flip-flop transition. By using a higher microwave power at 48 kG (6 mW/g instead of 1 mW/g at 25 kG) the proton polarization reached about 90%, but the sample temperature was then about 0.9 K, and the use of a  $^3\text{He}$  evaporation cryostat had little advantage over a  $^4\text{He}$  cryostat, in which similar polarizations have been observed at 50 kG <sup>95</sup>).

## CHAPTER IV

### A PURE TENSOR POLARIZATION OF THE DEUTERON SPIN SYSTEM

#### 1. INTRODUCTION

A new scheme of dynamic orientation of the deuteron spin system was found. It allows one to vary the deuteron tensor polarization or alignment independently of its vector polarization. This can be done by slightly off-resonance RF irradiation of a surrounding, polarized proton system, which cools the proton spin-spin interaction reservoir. It appeared that in a high magnetic field the RF field provides a rather strong thermal contact between this reservoir and the deuteron quadrupole interaction reservoir. The quadrupole interaction energy is proportional to the alignment, namely

$$\langle H_Q \rangle = h\nu_Q \{3 \cos^2(\theta) - 1\} \langle 3I_Z^2 - I(I+1) \rangle = h\nu_Q \{3 \cos^2(\theta) - 1\} A(D), \quad (\text{IV.1})$$

thus a change of the quadrupole energy will change  $A(D)$ . This mechanism is then analogous to that of dynamic polarization, where the cooling of the electron spin-spin interaction reservoir is transmitted to the nuclear Zeeman reservoirs. If the experiment is performed in a dilution refrigerator, then the nuclear spin lattice relaxation times are sufficiently long to obtain easily the strong saturation conditions under which the Zeeman and spin-spin interaction reservoir obtain an equal spin temperature in the rotating frame. First I will make some simple estimates of the possible values of the alignment, assuming the previous sentence to be true in our case. The results will then be compared with experiments performed with propanediol-D6<sup>32)</sup>. Some preliminary results obtained with ethanediol-D4 were published elsewhere<sup>31)</sup>.

#### 2. SIMPLE ESTIMATES FROM THE SPIN TEMPERATURE THEORY

##### 2.1 Steady-state values of the proton polarization and deuteron alignment

We assume that our system of protons and deuterons in a high magnetic field and at low temperatures can be described by the following density matrix

$$\rho = \frac{\exp(-\alpha_H H_{ZH} - \beta_H H_{SSH} - \beta_H H_Q - \gamma_D H_{ZD})}{\text{Tr} [\exp(-\alpha_H H_{ZH} - \beta_H H_{SSH} - \beta_H H_Q - \gamma_D H_{ZD})]}, \quad (\text{IV.2})$$

where  $H_{ZH}$ ,  $H_{ZD}$ ,  $H_{SSH}$ , and  $H_Q$  are the Hamiltonians for the proton and deuteron Zeeman energies, the proton spin-spin, and deuteron quadrupole interaction energy, respectively;  $\alpha_H$ ,  $\gamma_D$ , and  $\beta_H$  are the corresponding inverse temperatures, where we assumed that the proton spin-spin interaction reservoir and the deuteron quadrupole interaction reservoir are in good thermal contact with each other<sup>123)</sup>.

In our experiments we reduced the deuteron polarization to zero in order to simplify the analysis, hence  $\gamma_D = 0$ . We further assume that under strong irradiation  $\alpha_H$  and  $\beta_H$  tend to a common value  $\beta_f$  in the rotating frame, while energy is conserved. Since the spin lattice relaxation times are normally much longer than the time span for these experiments, we can neglect them now, and eventually make a correction in the experimental results.

Energy conservation then ensures that

$$-\frac{1}{2} \Delta_n \left[ P(H)_i - P(H)_f \right] = -\frac{1}{4} \beta_f \Omega_n^2, \quad (IV.3)$$

where  $i$  and  $f$  denote initial and final states, respectively, and  $\Delta_n$  is the difference between the proton Larmor frequency and the RF frequency;  $\Omega_n^2$  is defined by the relation

$$-\frac{1}{4} \beta_H \Omega_n^2 n_H = \text{Tr} \left[ \rho \left( H_Q + H_{SSH} \right) \right]; \quad (IV.4)$$

$n_H$  is the number of protons. The left-hand side of Eq. (IV.3) is exactly equal to the difference in Zeeman energy between the initial and final state; at the right-hand side we neglected  $\beta_i$  compared with  $\beta_f$ , as well as higher-order terms. However, a simple estimate yields that the errors introduced in this way are of the order of the experimental ones, which are about 10% (mainly owing to finite spin lattice relaxation).

After reaching thermal equilibrium,  $P(H)_f$  is normally so small that we can write it as

$$P(H)_f = \frac{1}{2} \Delta_n \beta_f. \quad (IV.5)$$

Substitution in Eq. (IV.3) gives

$$\beta_f = \frac{2 \Delta_n P(H)_i}{\Omega_n^2 + \Delta_n^2}. \quad (IV.6)$$

Equations (IV.5) and (IV.6) combined yield

$$P(H)_f = \frac{\Delta_n^2 P(H)_i}{\Omega_n^2 + \Delta_n^2}. \quad (IV.7)$$

When the vector polarization is 0, the alignment is directly related to the inverse spin temperature  $\beta_H$  of the quadrupole interaction reservoir by

$$A(D) = \text{Tr} \rho \left[ 3I_z^2 - I(I+1) \right], \quad (IV.8)$$

which reduces to

$$A(D) = \frac{2 \exp(-\beta_H X) - 2 \exp(2\beta_H X)}{2 \exp(-\beta_H X) + \exp(2\beta_H X)}, \quad (IV.9)$$

where  $X = \nu_Q [3 \cos^2(\theta) - 1]$ ;  $A(D)$  can vary between 1 and -2 and is different for peaks and pedestals for a constant value of  $\beta$ , because of their different values of  $X$ , which are  $-\nu_Q$  and  $2\nu_Q$ , respectively. We denote them by  $A_{\text{peak}}$  and  $A_{\text{ped}}$ , respectively.

## 2.2 Transient behaviour of P(H) and A(D)

### 2.2.1 Thermal mixing rate

In the case that  $P(H) \propto \alpha_H$ , the Provotorov equations show that  $\alpha_H$  and  $\beta_H$  vary exponentially to a common value with a rate given by

$$\tau_{\text{mix}}^{-1} = W \left[ 1 + \frac{\Delta_n^2}{\Omega_n^2} \right]. \quad (\text{IV.10})$$

W is a constant proportional to the line-shape function  $h(\nu)$  of the proton spin system.

### 2.2.2 Spin lattice relaxation in the rotating frame

After reaching a common spin temperature,  $\alpha_H$  and  $\beta_H$  decay with a common rate  $\tau_{\text{RF}}^{-1}$ , given by the weighted average of the proton spin lattice relaxation time  $T_{1H}$  and  $\tau(D, D)$ <sup>3)</sup>:

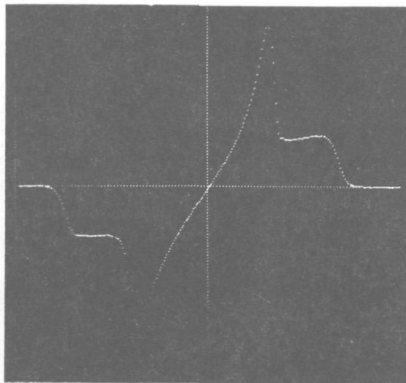
$$\tau_{\text{RF}}^{-1} = \frac{\Delta_n^2 T_{1H}^{-1} + \Omega_n^2 \tau(D, D)^{-1}}{\Delta_n^2 + \Omega_n^2}, \quad (\text{IV.11})$$

or since  $T_{1H} \gg \tau(D, D)$  (see Chapter III.3),

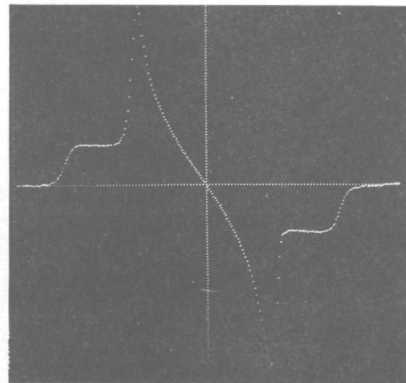
$$\tau_{\text{RF}} = \tau(D, D) \left[ 1 + \frac{\Delta_n^2}{\Omega_n^2} \right]. \quad (\text{IV.12})$$

## 3. EXPERIMENTAL RESULTS

The experimental sequence was as follows: after dynamically polarizing a partially deuterated propanediol sample at 25 kG, the microwaves were switched off and the deuteron polarization was reduced to zero by a saturating RF field. Then the still highly polarized proton system was irradiated by a slightly off-resonance RF field, which caused the deuteron magnetic resonance signal to grow with an antisymmetrical shape, as shown in Fig. IV.1. The RF field strength was estimated to be a few mG. We repeated this experiment for several values of the initial proton polarization and for different  $\Delta_n$ 's.



a) Deuteron signal after RF irradiation at 106.640 MHz of the proton spin system with initial conditions:  $P(H) = -89\%$  and  $P(D) = 0\%$ . The peak alignment is +25%, the pedestal alignment is -58%.



b) Deuteron signal after RF irradiation at 106.410 MHz with initial conditions:  $P(H) = -88\%$  and  $P(D) = 0\%$ . The peak alignment is -30%; the pedestal alignment is +48%.

Fig. IV.1

In Fig. IV.2 we plotted the values of  $A_{\text{peak}}$  and  $A_{\text{ped}}$  corresponding to the same spin temperature together with the experiment values of the alignment in the steady state, which was taken as the time when  $A_{\text{ped}}$  passed through its maximum; it decayed afterwards owing to finite spin lattice relaxation. It can be seen that in the steady state the deuteron quadrupole reservoir can be described by one single spin temperature.

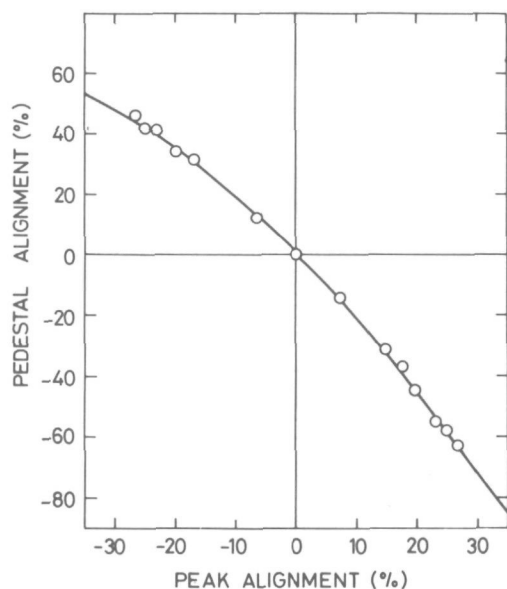


Fig. IV.2

The steady-state values of pedestal alignment versus "peak alignment". The curve corresponds to equal quadrupole spin temperatures [deduced from Eq. (IV.9)].

The experimental values of the final proton polarization are plotted in Fig. IV.3 together with a curve deduced from Eq. (IV.7) with a value of  $\Omega_n$  equal to 130 kHz. With this value the best fit to the experimental points was obtained. This value of  $\Omega_n$  was also used for calculating the curves of the following figures, unless stated differently. The two highest points were corrected for spin lattice relaxation.

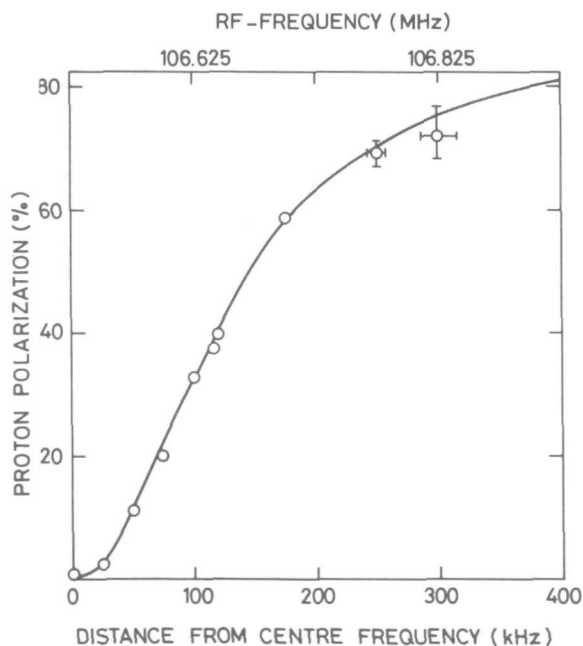


Fig. IV.3

The steady-state value of the final proton polarization under RF-irradiation as a function of the RF frequency. The initial polarization was 90% each time. The curve was deduced from Eq. (IV.7).

Figure IV.4 shows the steady-state values of  $A_{\text{peak}}$  and  $A_{\text{ped}}$  as function of  $\Delta$ , which is the difference between proton Larmor frequency and RF frequency. The absolute values of the alignment can be determined from the DMR line, since  $A_{\text{peak}}$  and  $A_{\text{ped}}$  are proportional to the difference in intensity between the two peaks and between the outside part of the pedestals, respectively (see Chapter I.5). The constants of proportionality can be determined from a calibration signal at a known spin temperature (or polarization; the latter can be determined quite accurately by the method described in Chapter III.2.3). The initial proton polarization was -90%. The curve was calculated with the aid of Eqs. (IV.6) and (IV.9). The points for  $|\Delta_n| > 150$  kHz were corrected for spin lattice relaxation, because the alignment

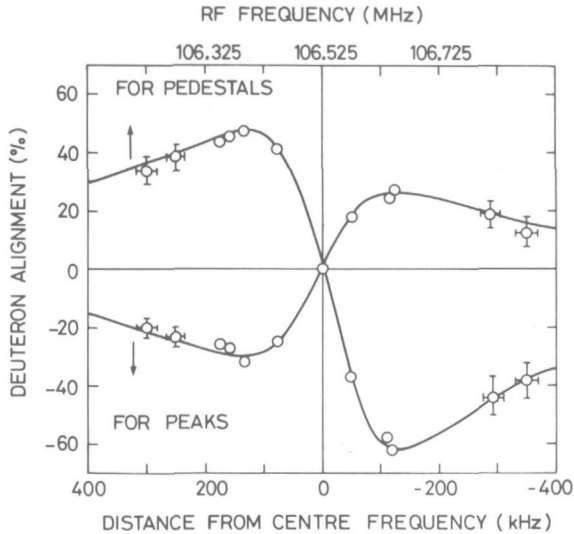


Fig. IV.4

The steady-state values of the alignment as function of the RF frequency. The initial proton polarization was -90%. The curves were deduced from Eqs. (IV.6) and (IV.9). The error bars are only shown when they exceed a relative error of 10%.

time strongly increased for larger  $\Delta_n$ , as can be seen from Fig. IV.5. Here we plotted the inverse of the time constants of the exponential development of  $\alpha_H$  and  $\beta_H$ . The spin lattice relaxation time of the common inverse spin temperature  $\beta_H$  as function of  $\Delta_n$  is shown in Fig. IV.6, together with the theoretical curve, deduced from Eq. (IV.12).

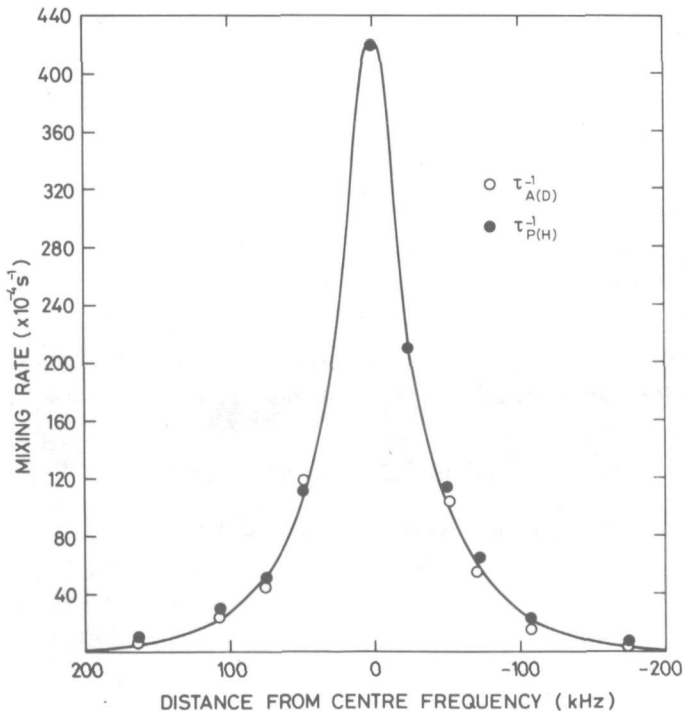


Fig. IV.5

Inverse of decay time of the proton polarization (●) and build-up time of the alignment (O) versus  $\Delta_n$ . The curve was calculated from Eq. (IV.10), using the measured proton NMR line shape.

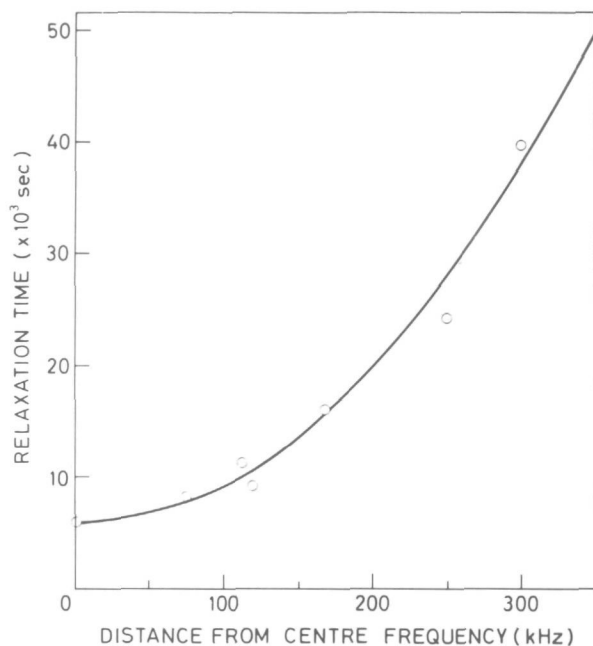


Fig. IV.6

The relaxation time of the common inverse spin temperature  $\beta_H$  in the rotating frame as calculated from Eq. (IV.12) together with the experimental points.

The mixing rate was determined by neglecting the initial non-exponential variation of  $P(H)$  and  $A(D)$ . The curve in Fig. IV.5 was calculated from Eq. (IV.10), using for  $h(\nu)$  an experimental line shape. The first non-exponential behaviour is attributed to the following facts: i) from the Provotorov equations an exponential behaviour is only expected if Eq. (IV.5) is fulfilled; that is if  $P(H) \leq 50\%$ , which is not true for the initial period; ii) when  $\Delta_n$  is much smaller than the total line width of the deuteron line (230 kHz), the build-up of the alignment for the peaks is slightly shorter than for the pedestals in the beginning, indicating that the RF field plays an important role in establishing the thermal contact between the proton spin-spin interaction reservoir and the deuteron quadrupole interaction reservoir. It can occur, for example, through processes in which a photon-induced proton spin-flip is accompanied by two deuteron spin-flips in opposite directions. If the difference in quadrupole energy is about equal to the difference between photon and Zeeman energy, the total angular momentum and energy can be easily conserved. Note that such processes change only the deuteron tensor polarization and not the vector polarization, as was observed.

For deuterons belonging to the pedestals, the mentioned processes will be less frequent, if the difference between photon and proton Zeeman energy is too small to balance the difference in quadrupole energy. The pedestals may, however, reach the same quadrupole spin temperature as that of the peaks by means of various cross-relaxation transitions within the deuteron spin system; in spite of the inhomogeneous character of the deuteron spin system these are still quite effective, as was evident from the fast recovery of "burned holes" (see Chapter III.3.3). We found indeed that when  $\Delta_n$  was equal to or larger than the deuteron line width, the alignment times for peaks and pedestals were equal.

The steady-state values of  $\beta_H$  are plotted as a function of the RF frequency in Fig. IV.7. The lowest absolute value of  $\beta_H$  was  $7 \pm 0.7 \mu K$  for positive as well as for negative  $\Delta_n$ . The errors for large values of  $\Delta_n$  are mainly due to finite relaxation: since the aligned deuteron spin system does not correspond to a homogeneous Zeeman spin temperature, the thermal contact with the electron spin-spin interaction reservoir made that the

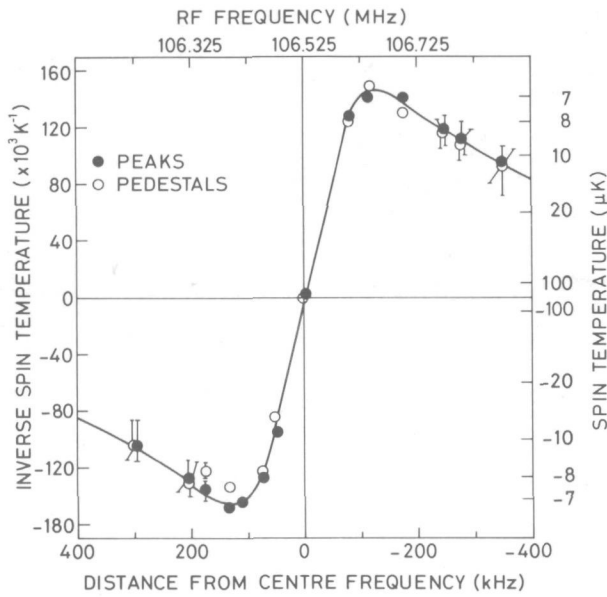


Fig. IV.7

The inverse spin temperature  $\beta_H$  as a function of the RF frequency. The curve was calculated from Eq. (IV.6). The initial proton polarization was -90% each time.

alignment decayed with a time constant of a few hours, which is much shorter than the spin lattice relaxation time (see Fig. III.7).

Figure IV.8 shows the deuteron alignment as function of the initial proton polarization; during each measurement  $\Delta_n$  was -80 kHz. These measurements were done in ethanediol-D4 (contrary to the previous measurements), and in order to calculate the curves [from Eqs. (IV.6) and (IV.9)] we used slightly different values of  $\Omega_n$  and  $\nu_Q$ , these being 140 and +18.5 kHz, respectively. The value of  $\Omega_n$  was again chosen to give the best fit to the experimental points.

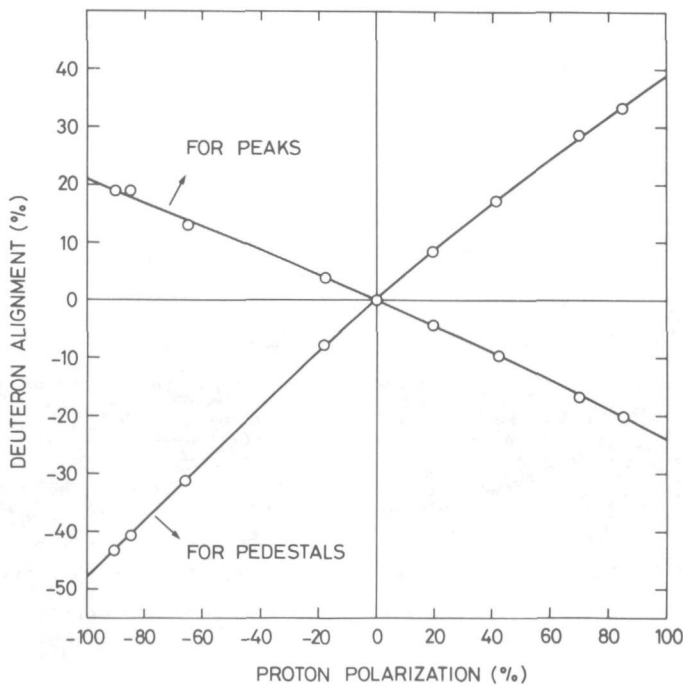


Fig. IV.8

The final deuteron alignment as function of the initial proton polarization with a constant  $\Delta_n$  equal to -80 kHz. The curves were deduced from Eqs. (IV.6) and (IV.9). The relative errors are less than 10%.

As has already been mentioned, for small values of  $\Delta_n$  the build-up time of the alignment for the peaks is slightly shorter than for the pedestals. This allows one to create a non-equilibrium within the deuteron quadrupole reservoir and to perform thermal mixing experiments analogous to those observed for the nuclear Zeeman reservoirs in the presence of a microwave field (Chapter III.3.3). The experiment is done as follows: starting from an initial proton polarization of -91%, an RF field with a frequency of 106.410 MHz is applied during 10 minutes. This results in  $A_{\text{peak}} = -20\%$  and  $A_{\text{ped}} = +20\%$ . The RF frequency is then changed to 106.755 MHz, where  $|\Delta_n|$  is equal to the total deuteron line width. The evolution of the alignment is then as shown in Fig. IV.9: instead of decreasing,  $A_{\text{ped}}$  first increases owing to the fact that the RF field now provides a strong thermal coupling between the pedestal deuterons and the "cold" peak deuterons. It then starts to decrease to its equilibrium value, which is of the opposite sign because  $\Delta_n$  has changed sign.

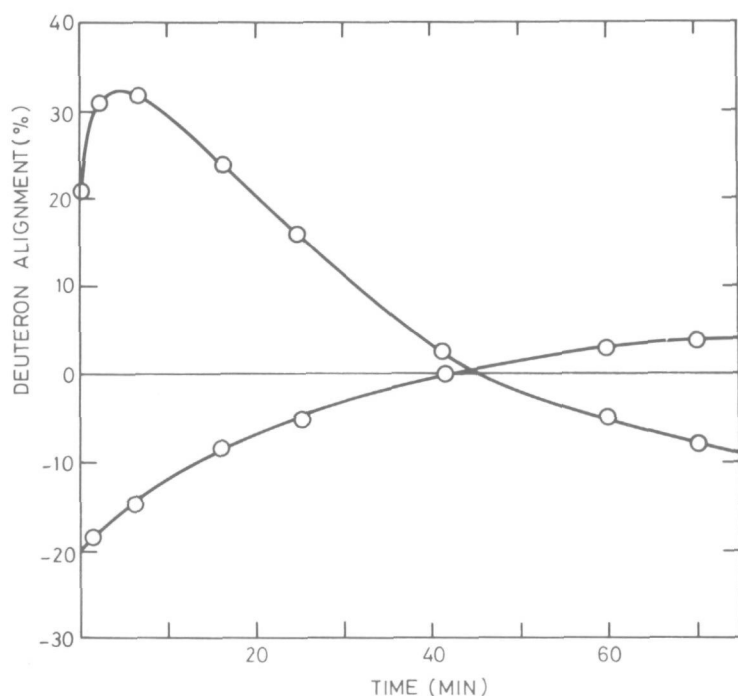


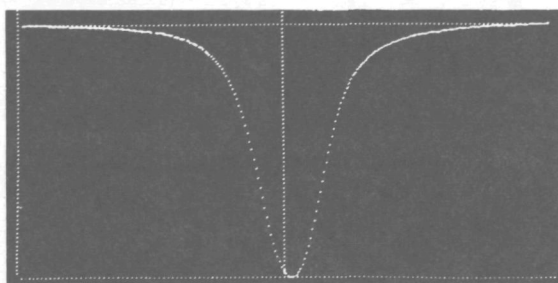
Fig. IV.9

Evolution of pedestal alignment and peak alignment, starting from a non-equilibrium state of the deuteron quadrupole reservoir (see text).

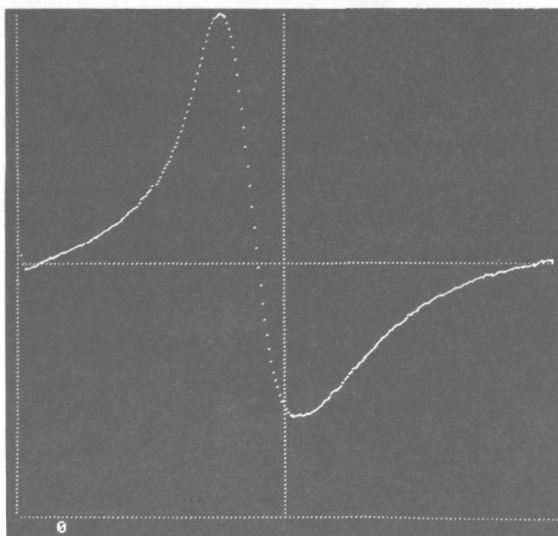
The influence of the proton spin-spin interaction reservoir was also evident from the change in the proton NMR signal during irradiation. It became zero at the irradiation frequency, but sometimes negative below this frequency and positive above, or the opposite way around according to the case. Such a behaviour was expected for homogeneous spin systems under strong saturation conditions<sup>5,19)</sup>, because the absorption signal is not proportional to the factor  $\alpha_{\text{H}}^{\mu}$ , but to the sum of two factors, as follows from Eq. (I.11):

$$h(\nu) \propto (P_{\text{H}} - \beta_{\text{H}} \Delta_n).$$

If the spin system is in internal thermal equilibrium the second term can be neglected compared with the first one. However, during irradiation the second term may become very large and dependent on the sign of  $\Delta_n$ ; it may be of an opposite sign compared with the first one, thus changing the sign of  $h(\nu)$ . Figure IV.10 shows the proton NMR signal after irradiation at the frequency where the signal is zero. It was initially -90% polarized.



a) NMR signal of -96% polarized protons in 1,2-propanediol. The frequency sweep on the horizontal axis is 400 kHz.

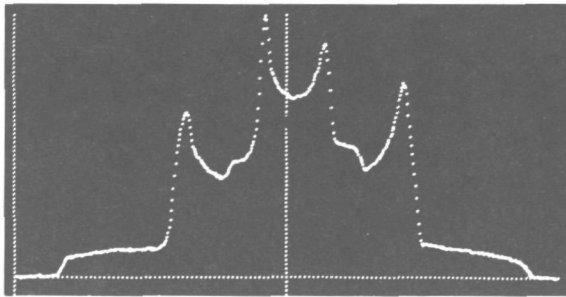


b) NMR signal of -90% polarized protons after saturating it at the frequency where it crosses zero.

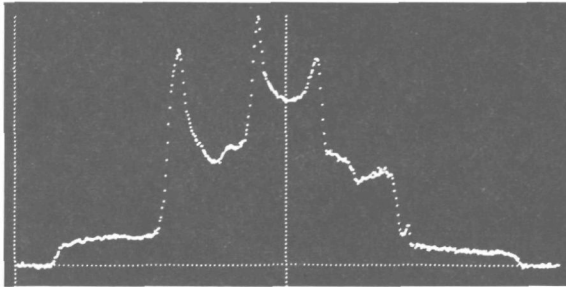
Fig. IV.10

Another method of enhancing the alignment consists of simply saturating one of the peaks of the DMR line. This always changes the population  $n_0$  of the level with  $m = 0$ <sup>124</sup>), thus changing  $A(D) = 1 - 3n_0$  (see Chapter I.5). Of course, the alignment cannot be changed independently of the vector polarization by this method, which is most clearly illustrated in toluol-D8. The DMR line consists then of four peaks, corresponding to different positions of deuterons in the methyl group and in the plane of the benzene ring (see Fig. IV.11a). From Fig. IV.11b it can be seen that if the line is saturated at a frequency  $\nu = \nu_D + \delta$  (in this case the peak on the right), this increases  $n_0$  of the corresponding deuterons, thus enhancing the line at  $\nu = \nu_D - \delta$  (peak on the left). This is apparent from a comparison with the intensity of the inner peaks, which are hardly affected by the saturation. The inner peaks are normally attributed to the methyl group, which is rotating, thus averaging the quadrupole splitting to a lower value<sup>125</sup>). However, this explanation is in contradiction to our observation of the DMR signal in m-xylene-D6, in which only the methyl groups were deuterated. Then still four peaks were observed<sup>126</sup>).

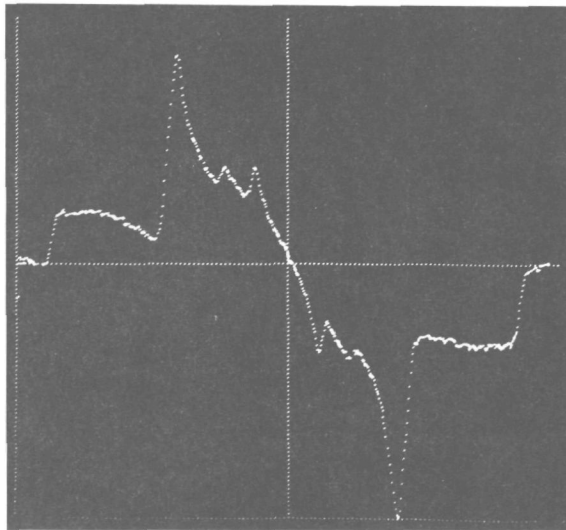
Figure IV.11c shows the alignment, obtained by RF irradiation, of the remaining protons (about 10%) in the deuterated toluol sample. Since the alignment is proportional to the quadrupole splitting for small values of  $A(D)$ , the alignment for the inner peaks is about three times lower than the alignment of the outer peaks, which is about 3%. This rather low value is mainly limited by the short value of the spin lattice relaxation time  $\tau(D, D)$ , being about 10 minutes at 120 mK.



a) Deuteron magnetic resonance signal in toluol-D8. The inner peaks are due to the fact, that there are deuterons in the methyl group, which experience an electric field gradient different from the ring deuterons.



b) Deuteron magnetic resonance signal in toluol-D8 after application of a saturating RF field at the frequency of the peak on the right-hand side. This causes an increase of the peak on the left-hand side (see text).



c) Deuteron magnetic resonance signal in toluol-D8 after slightly off-resonance irradiation of the remaining protons in this sample with initial conditions:  $P(H) = 30\%$  and  $P(D) = 0\%$ .

Fig. IV.11

#### 4. DISCUSSION

The fact that the inhomogeneous deuteron quadrupole interaction reservoir can be described by one single spin temperature makes it possible to apply the spin temperature theory, although the Zeeman energy reservoir cannot be described by a spin temperature at all (the aligned DMR signal has positive and negative parts!). This latter fact clearly shows that the energies of the two reservoirs are separately constants of motion in a high magnetic field.

This experiment provides a good quantitative agreement with several aspects of the spin temperature theory, namely:

- a) cooling of a spin-spin interaction reservoir by slightly off-resonance RF irradiation;
- b) thermal mixing between reservoirs, having similar frequency spectra in the rotating frame;
- c) saturation of a nuclear spin system as function of the RF frequency;
- d) spin lattice relaxation in the rotating frame.

Cooling of a quadrupole reservoir has been observed in a paradichlorobenzene, which was irradiated near the chlorine quadrupole resonance frequency<sup>18</sup>). The cooling was apparent from the observed proton polarization. This experiment can be compared with ours in the respect that there a spin-spin order produced polarization (or Zeeman order), while we first polarized and then transformed the Zeeman order into spin-spin order. However, our experiment provided quantitative results in contrast to the above-mentioned experiments, where only qualitative features were observed. Furthermore, by using the technique of dynamic polarization we could choose the initial spin temperatures in a wide range, positive as well as negative.

## CHAPTER V

### DYNAMIC POLARIZATION EXPERIMENTS WITH THE FREE RADICAL BDPA

#### 1. INTRODUCTION

We have studied dynamic polarization of protons, deuterons, and carbon-13 nuclei at 25 kG in organic samples, doped with 1,2-bis-diphenylene-1-phenylallyl (BDPA), a free radical.

This radical shows a resonance absorption line width of only 20 MHz at 0.5 K in a 25 kG magnetic field (see Fig. V.1). This width is about the same as the one in a frozen sample at 3 kG and a temperature of about  $-100^{\circ}\text{C}$ , thus in a high magnetic field the g-factor anisotropy is not the dominant broadening mechanism.

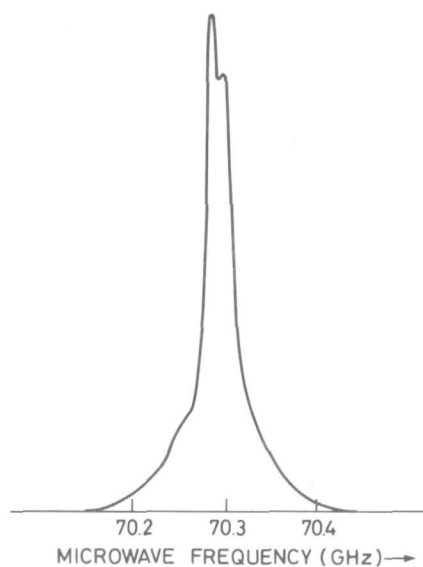


Fig. V.1

ESR signal of toluol doped with BDPA ( $5 \times 10^{19}$  spins/cm<sup>3</sup>) in a 25 kG magnetic field at 0.5 K.

As mentioned in Chapter I.3.3, one expects for protons a resolved solid-state effect in a 25 kG magnetic field, eventually accompanied with dynamic polarization by cooling of the electron spin-spin interaction reservoir. Only this latter mechanism is expected for deuterons and carbon-13 nuclei, because their Larmor frequencies are of the same order as the ESR line width. A differential solid effect is not expected, since the cross-relaxation within the narrow ESR line will be fast compared with the electron spin lattice relaxation time, which was measured to be  $1.6 \pm 0.2$  msec in a toluol sample doped with  $5 \times 10^{19}$  spins/cm<sup>3</sup> at a temperature of 0.5 K in a 25 kG magnetic field. Since the nuclear spin lattice relaxation times were measured to be at least several minutes under the experimental conditions, the leakage factor is smaller than  $10^{-2}$  and we therefore neglect it. The qualitative features of experiments with this free radical have been given before<sup>(127,128)</sup>. However, then no detailed comparison with the ESR line shape was made.

2. RESULTS

We measured the polarization of protons and deuterons as function of the microwave frequency in partially deuterated m-xylene(2,2-D6), doped with BDPA ( $6 \times 10^{18}$  spins/cm<sup>3</sup>). The sample temperature during dynamic polarization was estimated to be 0.75 K.

The results for protons are shown in Fig. V.2. The large peaks, occurring at frequencies for which  $|\Delta| = \nu_H$ , correspond to the resolved solid-state effect, while the inner ones are attributed to cooling of the electron spin-spin interaction reservoir. Two small peaks were observed at microwave frequencies around  $\nu = \nu_e \pm 2\nu_H$ . These are due to a "double" solid-state effect, in which two proton spins flip simultaneously with an electron spin in opposite direction. Such an effect has been observed before in a 3 kG magnetic field<sup>1,2,9</sup>). The curve was calculated from the following formula (see Chapter I.3.3.3):

$$P(H) = \frac{(S^- + s^-) - (S^+ + s^+) + \Delta\nu_H S_1 S_4 / \Omega^2}{1 + S^+ + S^- + S_4} \quad (V.1)$$

The terms  $s^\pm \ll 1$  were added to take the "double" solid-state effect into account.

In this calculation the ESR line shape was approximated by a Lorentzian with a half-width of 10 MHz. The various saturation parameters are not known precisely. Therefore they were obtained by making a rough estimate and then adjusting them to fit the experimental points.

$S^+$  and  $S^-$  with maxima at  $\nu_e + \nu_H$  and  $\nu_e - \nu_H$  MHz were taken proportional to  $g(\Delta)$ . Absolute values for them were obtained by determining the maximum values of  $S^\pm$  from the measured polarization time  $\tau_\pm$  at the solid-state effect frequencies, using the expression<sup>2</sup>)

$$\tau_\pm = T_{1H} \left[ \frac{1}{S^\pm + 1} \right] \quad (V.2)$$

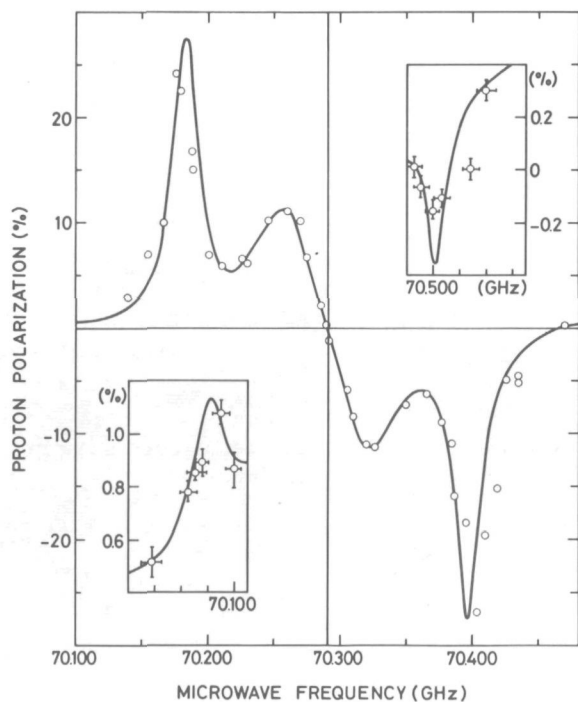


Fig. V.2  
Proton polarization versus microwave frequency in m-xylene-D6, doped with BDPA ( $6 \times 10^{18}$  spins/cm<sup>3</sup>). The curve was calculated from Eq. (V.1). The insets show the double solid-state effect on an enlarged scale.

The polarization time was measured to be 20 minutes with a microwave power of 7 mW/g, while  $T_{1H}$  was 30 minutes at 0.75 K, yielding a maximum value of  $S^\pm = 0.5$ .

The determination of  $S_1$  as function of microwave frequency is difficult, since the average microwave field strength in the cavity will decrease, if the frequency is near paramagnetic resonance. This effect may be appreciable, because of the high filling factor of the cavity ( $\approx 0.5$ ) and the high concentration of paramagnetic centres. The variation of the microwave field strength was measured as function of microwave frequency with a bolometer, consisting of a carbon resistor; this had a resolution better than 0.5 dB. This variation made  $S_1$  a slightly broader function than  $g(\Delta)$ . It could be approximated rather well by a Gaussian function with a half-width of 35 MHz.

Absolute values of the ratio  $S_1/\Omega^2$  were obtained by fitting these values to the measured deuteron polarization, since in that case there are no other unknown quantities for microwave frequencies around  $\nu_e$  (see below). This yielded

$$\frac{S_1}{\Omega^2} = (3 \times 10^{-4}) \exp\left(\frac{-\Delta^2}{1800}\right) \quad (V.3)$$

where  $\Delta$  is expressed in MHz.

Since the value of  $\Omega^2$  is of the order of  $100 \text{ MHz}^2$ , the value of  $S_1$  is rather low compared with  $S^\pm$ . This should not be surprising, since at low temperatures  $T_{1H} \propto T_{1e} F(P_e)$ ; thus  $S^\pm \approx S_1 F(P_e)$ , where  $F(P_e) = 1/(1 - P_0 P_e)$  may vary between 1 and 20. Such a low value of  $S_1$  justifies the use of Eqs. (I.35), (I.37) and (I.38), which were derived under the assumption of weak saturation.

The value of  $S_4$  was taken to be 0.25 in order to fit the experimental points of  $P(H)$  at the inner peaks. This rather low value expresses that the thermal contact of the proton spin system with the lattice is four times stronger than the contact with the electron spin-spin interaction reservoir. This is not surprising, since the proton Larmor frequency  $\nu_H$  is large compared with the ESR line width. Therefore it will be difficult to find two electron spins with a frequency difference of the order of  $\nu_H$ , which are at the same time sufficiently close in space to perform a flip-flop transition.

The saturation parameters  $s^\pm$  of the double solid-state effect were taken proportional to  $g(\Delta)$  with maxima at  $\nu_e \pm 2\nu_H$  equal to 0.007, which is two orders of magnitude lower than  $S^\pm$ .

The deuteron polarization as function of microwave frequency is shown in Fig. V.3. Besides the two expected peaks at frequencies around  $\nu_e$ , four additional peaks were observed at frequencies for which  $|\Delta| = \nu_H \pm \nu_D$ . They are attributed to a double solid-state effect, in which one electron, one proton, and one deuteron spin flip simultaneously.

The curve drawn there was calculated from Eq. (I.37), in which four terms corresponding to this double solid-state effect were added:

$$P(D) = + \frac{4}{3} \Delta \nu_D S_1 / \Omega^2 + S_{D1}^- - S_{D1}^+ + S_{D2}^- - S_{D2}^+ \quad (V.4)$$

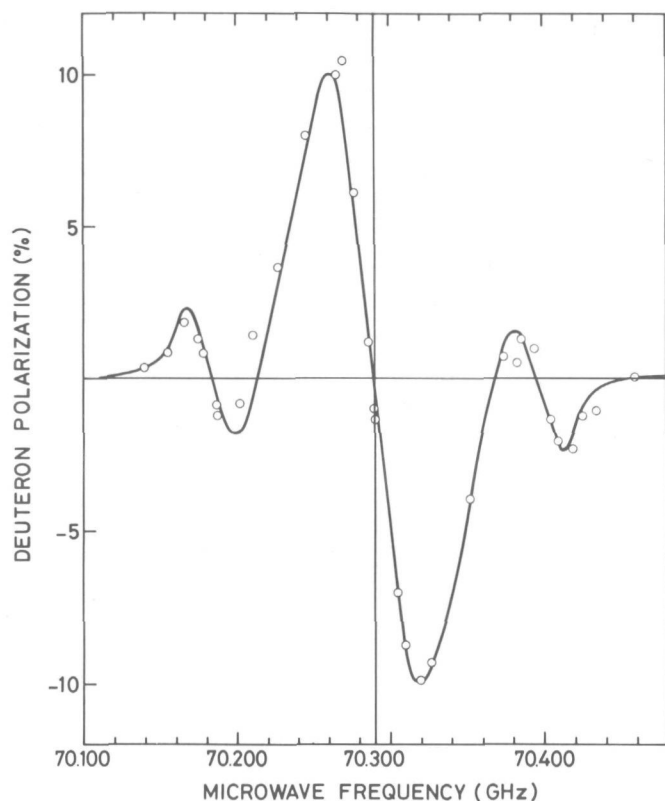


Fig. V.3

Deuteron polarization versus microwave frequency in *m*-xylene-D<sub>6</sub>, doped with BDPA ( $6 \times 10^{18}$  spins/cm<sup>3</sup>). The curve was calculated from Eq. (V.4).

The saturation parameters  $S_{D1}^{\pm}$  and  $S_{D2}^{\pm}$  were taken proportional to  $g(\Delta)$  with a maximum value of 0.03 at  $\nu_e - \nu_H \pm \nu_D$  and  $\nu_e + \nu_H \pm \nu_D$ , respectively. Of course the double solid-state effect depends also on the proton polarization, but since this is small compared with the electron polarization,  $S_{D1}$  and  $S_{D2}$  were simply taken proportional to  $P_e \approx -1$ .

The ratio of  $S_{D1}^{\pm}/s^{\pm}$  is about 4. This order of magnitude was expected from the factor  $I(I+1)$  in the expressions for the transition probabilities [see Eq. (I.21)]. This factor is about three times larger for deuterons than for protons.

By using Eq. (V.4) it was assumed that for deuterons the thermal contact with the electron spin-spin interactions occurs mainly via cross-relaxation transitions, which are proportional to  $\int_0^{\infty} g(\nu) g(\nu - \nu_n) d\nu$  for a homogeneous ESR line [see Eq. (I.23)]. By using the value of  $S_4$  for protons ( $\sim 0.25$ ), one can estimate the corresponding factor for deuterons to be 20, which is indeed much larger than the saturation parameters for the forbidden transitions, so that condition (I.36) will be fulfilled.

It is interesting to compare the spin temperatures of protons and deuterons. As shown in Chapter III.2, these become equal in the case of a strong thermal contact with the electron spin-spin interaction reservoir. Figure V.4 shows the inverse spin temperatures of protons and deuterons as function of microwave frequency as calculated from Eqs. (V.1) and (V.4) and using the relations

$$T(H)^{-1} = 2kP(H)/h\nu_H \quad (V.5)$$

$$T(D)^{-1} = 3kP(D)/2h\nu_D \quad (V.6)$$

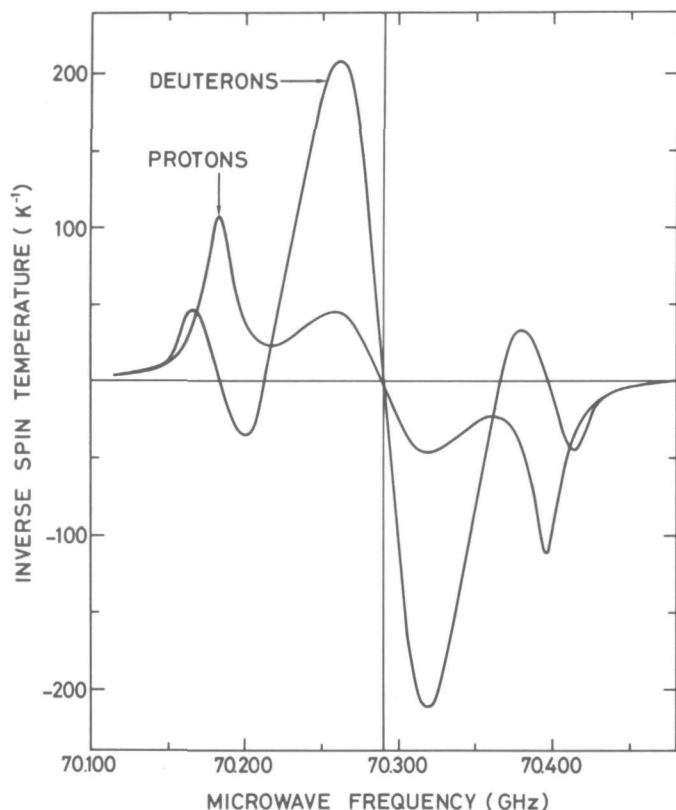


Fig.V.4

The inverse spin temperature of protons and deuterons in m-xylene, doped with BDPA, as calculated from Eqs. (V.1), (V.4), (V.5) and (V.6).

It can be seen that the deuteron spin temperature is about five times lower than the proton spin temperature at frequencies around  $\nu_e$ ; this is attributed to the poor thermal contact of the protons with the electron spin-spin interaction reservoir.

In order to check this explanation more carefully, we studied a sample of toluol-D8 with a higher concentration of BDPA ( $5 \times 10^{19}$  spins/cm<sup>3</sup>). Because of this higher concentration, the wings of the ESR line will extend further from the centre. Then the thermal contact with the protons is increased, first because of the wider frequency spectrum of the electron spin-spin interaction reservoir, and secondly because of a stronger overlap between the forbidden and allowed transitions. In Figure V.5 we plotted the inverse spin temperatures of the different nuclei. The same features as in m-xylene were observed, but this time the spin temperature of the protons approached the one of deuterons and carbon-13 nuclei. The carbon-13 polarization was determined in a way described in Chapter III.2. The curves in Fig. V.5 are drawn to guide the eye, since we did not attempt to calculate them because of the stronger overlap between the forbidden and allowed transitions; this makes the curves sensitive to the tails of the ESR line, which are not known so precisely.

The role of the electron spin-spin interaction reservoir was also apparent from thermal mixing experiments, analogous to those described in Chapter III.3. After, for example, positive polarization, the microwave power was switched off and one of the spin species, say the deuterons, had its polarization reduced to zero by RF irradiation. Then the application of microwave power at a frequency corresponding to negative polarization produced at first a positive increase of the deuteron polarization owing to the thermal contact with the still positively polarized protons; then both polarizations changed sign. When the microwave power was applied at the solid-state effect frequencies, the thermal mixing was slightly obscured by the "direct processes".

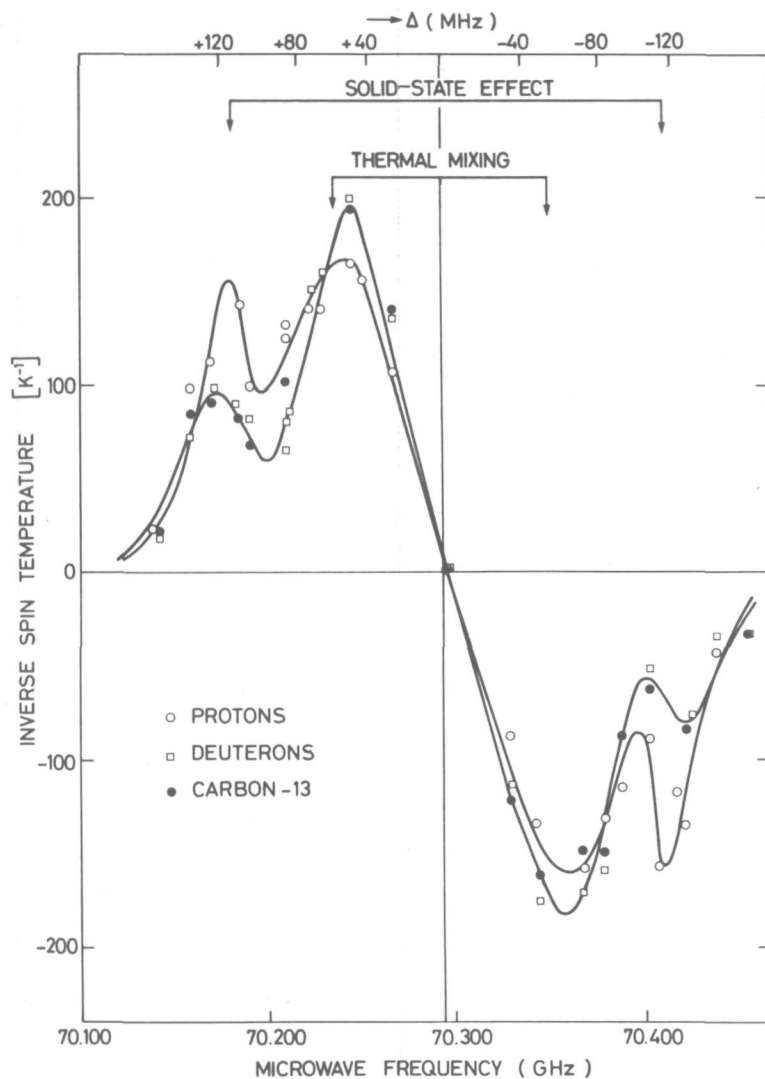


Fig. V.5

The inverse spin temperatures of protons, deuterons and carbon-13 nuclei in toluol-D8, doped with BDPA ( $5 \times 10^{19}$  spins/cm<sup>3</sup>). The curves were drawn to guide the eye (see text).

To conclude, we may say that these samples clearly exhibit the contributions of different mechanisms of dynamic polarization in a high magnetic field, namely the solid-state effect, the double solid-state effect, and the polarization arising from the thermal contact with a dynamically cooled electron spin-spin interaction reservoir. The comparison with the theoretical curves should be considered as qualitative, because of the various assumptions made, in both the theory and experimental quantities. However, the qualitative behaviour as well as the orders of magnitude show a reasonable agreement with what was expected, thus leaving little doubt about the contributions of the various mechanisms. A similar separation of the solid-state effect and thermal mixing with a spin-spin interaction reservoir has been done for nuclear spin systems<sup>18)</sup>, however without relating the various curves to the resonance absorption line shape.

## FINAL CONCLUSIONS

In previous chapters we compared the spin temperature theory with the dynamic nuclear orientation experiments, performed in organic materials at low temperatures and in high magnetic fields.

In all these experiments the important role of the spin-spin interaction energy reservoir was apparent from the transient behaviour of the different nuclear spin species. Therefore the concept of such a reservoir seems to be valid, even under conditions where the polarization approaches 1.

The order of magnitude of the calculated maximum polarization values of protons, deuterons, and carbon-13 nuclei in 1,2-propanediol doped with  $\text{Cr}^{\text{V}}$ -complexes, as calculated from Borghini's spin temperature model, is in good agreement with the observed ones. An exact comparison is difficult, because of the uncertainty in the leakage factors and in the sample temperature during dynamic polarization. However, the relative values of the polarizations of different nuclei agree within a few per cent with the ratios expected from the "equal spin temperature hypothesis". Also several other features such as the steep temperature dependence and the increase of the enhancement factor at low temperatures are quite well reproduced by the measurements. This is the first time that a reasonable agreement with this model, which is valid at low temperatures, has been obtained. It was also the first time that such high polarizations have been observed, as far as we know.

The observed high polarizations in 1,2-propanediol make it an attractive material for polarized targets, in spite of the slightly higher ratio of bound to free protons as compared, for example, to 1-butanol doped with porphyraxide, which has been widely used as a target material<sup>100,101</sup>). These bound protons in carbon and oxygen nuclei cause an unwanted background in the scattering experiments.

The observed long spin lattice relaxation times make 1,2-propanediol also a suitable candidate for so-called spin-frozen targets<sup>78,130</sup>). This type of target is first dynamically polarized and then moved into the magnet of the spectrometer, where the scattering experiment is done. A long relaxation time then prevents a quick decay of the polarization during the scattering experiment.

We observed a pure tensor polarization of deuterons in a solid, obtained by slightly off-resonance irradiation of the proton spin system in partially deuterated diols. This was attributed to a thermal contact between the proton spin-spin interaction reservoir, and the reservoir made up of the deuteron quadrupole interactions. It appeared that most times the inhomogeneous deuteron quadrupole interaction reservoir could be described by one single spin temperature; this made it possible to apply the spin temperature theory, which provided an elegant description of the rather complicated processes.

For the deuterons, in which the C-D bond is roughly parallel to the external magnetic field, a maximum alignment of about 60% was observed. However, the averaged alignment in our glassy samples was much lower, about 10%. This value is too low for use in a scattering experiment, but it is not excluded that a crystalline material is found in which the same method can be applied. Then the angular averaging does not occur, thus yielding probably a higher alignment.

Different mechanisms of dynamic polarization could be distinguished from one another in samples doped with the free radical BDPA. The various shapes of the proton, deuteron, and carbon-13 polarization versus microwave frequency show the contribution of different polarization schemes in high fields for the case of nuclear spin systems in dipolar interaction with an electron spin system. By making a few simplifying assumptions the steady-state solutions of the proton, deuteron and carbon-13 polarization as function of microwave frequency were obtained from the basic set of Eqs. (I.19) (see Chapter I). The solutions were in reasonable agreement with the measurements, which showed clearly the different features of each term in these equations. These features can be summarized as follows: saturation of the forbidden transitions causes dynamic polarization by the solid-state effect or double solid-state effect and the thermal contact with the electron spin-spin interaction reservoir causes polarization, if this reservoir is cooled by off-resonance saturation of the allowed transitions.

Acknowledgements

I wish to express my sincere thanks to the members of the Polarized Target Group at CERN, whose help and experience in the field of dynamic polarization were indispensable during the course of this work.

Especially, I wish to thank Drs. M. Borghini, K. Morimoto, T.O. Niinikoski and F. Udo for many useful discussions, and for their help during parts of the experiments.

The accuracy of the experiments described before could not have been obtained without the effort of Mr. H. Ponssen, who provided the link between the NMR electronics and the computer.

Furthermore, I am indebted to Mr. G. Gattone for the preparation of several free radicals, and to Mr. M. Rieubland for teaching me the techniques of operating a  $^3\text{He}$  cryostat.

The award of a Fellowship from CERN during my stay there is gratefully acknowledged, as well as the efficient handling of the manuscript by the CERN Scientific Reports Typing Service.

Last, but not least, I wish to thank my family, for their understanding in allowing me to use part of my spare time for the experiments and analysis in order to finish them within the restricted time available.

#### REFERENCES

- 1) A. Abragam, Principles of nuclear magnetism (Oxford Univ. Press, London, 1961).
- 2) C.D. Jeffries, Dynamic nuclear orientation (Interscience Publishers, New York, 1963).
- 3) M. Goldman, Spin temperature and magnetic resonance in solids (Oxford Univ. Press, London, 1970), and references quoted therein.
- 4) M. Borghini, Proc. 2nd Int. Conf. on Polarized Targets, Berkeley, 1971 (ed. G. Shapiro) (LBL 500, UC-34 Physics, National Technical Information Service, Springfield, Virginia, 1972), p. 1, and references quoted therein.
- 5) V.A. Atsarkin and M.I. Rodak, Uspekhi Fiz. Nauk 107, 3 (1972); [Soviet Phys. Uspekhi 15, 251 (1973)], and references quoted therein.
- 6) W.Th. Wenckebach and N.J. Poulis, 17th Congress Ampère, Turku, Finland, 1972 (ed. V. Hovi) (North-Holland Publishing Co., Amsterdam, 1973), p. 120, and references quoted therein.  
T.J.B. Swanenburg, thesis, Leiden (1967).  
W.Th. Wenckebach, thesis, Leiden (1970).
- 7) A. Abragam and M. Borghini, Progress in low temperature physics (ed. C.J. Gorter) (North-Holland Publishing Co., Amsterdam, 1964), Vol. IV, Chapter 8.
- 8) Proc. 1st Int. Conf. on Polarized Targets and Ion Sources, Saclay, 1966 (ed. La Direction de la Physique, CEN) (La Documentation Française, Saclay, 1966).
- 9) Proc. 2nd Int. Conf. on Polarized Targets, Berkeley, 1971 (ed. G. Shapiro) (LBL 500, UC-34 Physics, National Technical Information Service, Springfield, Virginia, 1972).
- 10) A. Kastler, CR Acad. Sci. B 233, 1444 (1951).
- 11) A.W. Overhauser, Phys. Rev. 89, 689 (1953); *ibid.* 92, 411 (1953).
- 12) J. Korryng, Phys. Rev. 94, 1388 (1954).
- 13) H.G. Beljers, L. van der Kint and J.S. van Wieringen, Phys. Rev. 95, 1683 (1954).
- 14) A. Abragam, Phys. Rev. 98, 1729 (1955).
- 15) C.D. Jeffries, Phys. Rev. 106, 164 (1957).
- 16) N. Bloembergen and P.P. Sorokin, Phys. Rev. 110, 865 (1958).
- 17) A. Abragam and W.G. Proctor, CR Acad. Sci. B 246, 2253 (1958).
- 18) M. Goldman and A. Landesman, Phys. Rev. 132, 610 (1963).
- 19) B.N. Provotorov, Zh. Eksper. Teor. Fiz. 41, 1582 (1961); [Soviet Phys. JETP 14, 1126 (1962)]; Fiz. Tverdogo Tela 4, 2940 (1962); [Soviet Phys. Solid State 4, 2155 (1963)]; Phys. Rev. 128, 75 (1962).
- 20) B.N. Provotorov, Zh. Eksper. Teor. Fiz. 42, 882 (1962); [Soviet Phys. JETP 15, 611 (1962)].
- 21) A.G. Anderson and S.R. Hartmann, Phys. Rev. 120, 2023 (1962).

- 22) J. Philippot, Phys. Rev. 133, A471 (1964).
- 23) J. Jeener, Advances in magnetic resonance (ed. J.S. Waugh) (Academic Press, Inc., New York, 1968), Vol. 3, pp. 206-320.
- 24) L.C. Hebel, Solid state physics (eds. F. Seitz and D. Turnbull) (Academic Press, Inc., New York, 1963), Vol. 15, p. 409.
- 25) H. Glättli, M. Odehmal, J. Ezratty, A. Malinovski and A. Abragam, Phys. Letters 29 A, 5 (1969).
- 26) A. Mसाike, H. Glättli, J. Ezratty and A. Malinovski, Phys. Letters 30 A, 63 (1969).
- 27) W. de Boer, M. Borghini, K. Morimoto, T.O. Niinikoski and F. Udo, J. Low Temp. Phys. 15, 249 (1974).
- 28) W. de Boer, Nuclear Instrum. Methods 107, 99 (1973).
- 29) W. de Boer and T.O. Niinikoski, Nuclear Instrum. Methods 114, 495 (1974).
- 30) M. Borghini, Phys. Rev. Letters 20, 419 (1968).
- 31) W. de Boer, M. Borghini, K. Morimoto, T.O. Niinikoski and F. Udo, Phys. Letters 46 A, 143 (1973).
- 32) W. de Boer, Proc. 1st Specialized Colloque Ampère, Kraków, 1973 (ed. J.W. Hennel) (Inst. of Nuclear Physics, Kraków, Poland, 1973), p. 228.
- 33) R.J. Blin-Stoyle and M.A. Grace, Handb. Phys. 42, 555 (1957); and references quoted therein.
- 34) C.J. Gorter, Physica 14, 504 (1948).
- 35) M.E. Rose, Phys. Rev. 75, 213 (1949).
- 36) M.A. Grace, C.E. Johnson, N. Kurti, R.G. Schurlock and R.T. Taylor, Phil. Mag. 4, 948 (1959).
- 37) B.N. Samoilov, V.V. Sklyarevskii and E.P. Stepanov, Soviet Phys. JETP 38, 359 (1960).
- 38) D.A. Shirley, Annu. Rev. Nuclear Sci. 16, 89 (1966); and Proc. 2nd Int. Conf. on Polarized Targets, Berkeley, 1971 (ed. G. Shapiro) (LBL 500, UC-34 Physics, National Technical Information Service, Springfield, Virginia, 1972), p. 223.
- 39) J.M. Daniels, see above Conference, p. 77.
- 40) C.D. Jeffries, see above Conference, p. 381.
- 41) R.T. Johnson, D.N. Paulson, R.P. Giffard and J.C. Wheatley, J. Low Temp. Phys. 10, 35 (1973).
- 42) C.D. Jeffries, Cryogenics 3, 41 (1963).
- 43) A. Abragam, Cryogenics 3, 42 (1963).
- 44) T.R. Carver and C.P. Slichter, Phys. Rev. 92, 212 (1953).
- 45) M. Abraham, R.W. Kedzie and C.D. Jeffries, Phys. Rev. 106, 165 (1957).
- 46) F.M. Pipkin and J.W. Culvahouse, Phys. Rev. 106, 1102 (1957).
- 47) C.D. Jeffries, Phys. Rev. 117, 1056 (1960).
- 48) E. Erb, J.L. Motchane and J. Uebersfeld, CR Acad. Sci. B 246, 2121, 3050 (1958).
- 49) A. Abragam, J. Combrisson and I. Solomon, CR Acad. Sci. B 247, 2237 (1958).
- 50) N. Bloembergen, Physica 15, 386 (1949).

- 51) A.M. Portis, Phys. Rev. 91, 1070 (1953); 104, 584 (1956).
- 52) M. Abraham, M.A.H. McCausland and F.N.H. Robinson, Phys. Rev. Letters 2, 449 (1959).
- 53) N. Bloembergen, E.M. Purcell and R.V. Pound, Phys. Rev. 73, 679 (1948).
- 54) A.V. Kessenikh and A.A. Manenkov, Fiz. Tverdogo Tela 5, 1143 (1963); [Soviet Phys. Solid State 5, 835 (1963)].
- 55) C.F. Hwang and D.A. Hill, Phys. Rev. Letters 19, 1011 (1967).
- 56) N. Bloembergen, S. Shapiro, P.S. Pershan and J.O. Artman, Phys. Rev. 114, 445 (1959).
- 57) A.G. Redfield, Phys. Rev. 98, 1787 (1955).  
A.G. Redfield, Science 164, 1015 (1969).
- 58) I. Solomon, Magnetic and electric resonance and relaxation, Proc. 11th Colloque Ampère, Eindhoven, 1962 (ed. J. Smidt) (North-Holland Publishing Co., Amsterdam, 1963), p. 25.
- 59) M.A. Kozhushner, Zh. Eksper. Teor. Fiz. 56, 246 (1969); [Soviet Phys. JETP 29, 136 (1969)].
- 60) M. Goldman, M. Chapellier, Vu Hoang Chau and A. Abragam, The principles of nuclear magnetic ordering, to be published.
- 61) M. Odehnal and V. Bouffard, J. Phys. (France) 32, 699 (1971).
- 62) L.L. Buishvili, Zh. Eksper. Teor. Fiz. 49, 1968 (1965); [Soviet Phys. JETP 22, 1277 (1966)].  
L.L. Buishvili, M.D. Zviadadze and G.R. Khutsishvili, Zh. Eksper. Teor. Fiz. 56, 290 (1969); [Soviet Phys. JETP 29, 159 (1969)].
- 63) M. Borghini, Phys. Letters 26 A, 242 (1968).
- 64) M.A. Kozhushner and B.N. Provotorov, Fiz. Tverdogo Tela 6, p. 1152 (1964); [Soviet Phys. Solid State 6, 1152 (1964)].
- 65) A. Abragam, Conf. Proc. of Ref. 8, p. 27.
- 66) W.T. Wenckebach, T.J.B. Swanenburg, H. Hoogstraate and N.J. Poulis, Phys. Letters 26 A, 203 (1968).
- 67) N. Bloembergen, Physica 15, 386 (1949).
- 68) A. Abragam and B. Bleaney, Electron paramagnetic resonance of transition ions (Oxford Univ. Press, London, 1970).
- 69) J.H. van Vleck, Phys. Rev. 57, 426 (1940).
- 70) R. Orbach, Proc. Roy. Soc. A 264, 458 and 485 (1961).
- 71) W.E. Blumberg, Phys. Rev. 119, 79 (1960).
- 72) G.R. Khutsishvili, Uspekhi Fiz. Nauk 87, 211 (1965); [Soviet Phys. Uspekhi 8, 743 (1966)].  
G.R. Khutsishvili, Proc. 17th Colloque Ampère, Turku, 1972 (ed. V. Hovi) (North-Holland Publishing Co., Amsterdam, 1973), p. 35, and references quoted therein.
- 73) O.S. Leifson and C.D. Jeffries, Phys. Rev. 122, 1781 (1961).
- 74) T.J. Schmutge and C.D. Jeffries, Phys. Rev. 138, 1785 (1965).
- 75) T.E. Gunther and C.D. Jeffries, Phys. Rev. 159, 290 (1967).
- 76) G.M. van den Heuvel, T.J.B. Swanenburg and N.J. Poulis, Physica 56, 365 (1971).

- 77) W.G. Williams, D.J. Nicholas, P.H.T. Banks and D.A. Cragg, Nuclear Instrum. Methods 88, 73 (1970).
- 78) M. Borghini, T.O. Niinikoski, F. Udo and P. Weymuth, Nuclear Instrum. Methods 105, 215 (1972).
- 79) E.L. Lucken, Nuclear quadrupole coupling constants (Academic Press, London, 1969), and references quoted therein.
- 80) P. Roubeau, Cryogenics 6, 207 (1966).  
P. Roubeau and J. Vermeulen, Cryogenics 11, 478 (1971).
- 81) T.O. Niinikoski, Nuclear Instrum. Methods 97, 95 (1971).
- 82) T.O. Niinikoski, Cryogenics 11, 232 (1971).
- 83) T.O. Niinikoski, thesis Helsinki University of Technology, Helsinki (1973).
- 84) E. Boyes, G.R. Court, B. Craven, R. Gamet and P.J. Hayman, Proc. 2nd Int. Conf. on Polarized Targets, Berkeley, 1971 (ed. G. Shapiro) (LBL 500, UC-34 Physics, National Technical Information Service, Springfield, Virginia, 1972), p. 403.
- 85) V. Petříček and M. Odehnal, Nuclear Instrum. Methods 52, 197 (1967).  
V. Petříček, Nuclear Instrum. Methods 58, 111 (1968).
- 86) F. Udo, Proc. 2nd Int. Conf. on Polarized Targets, Berkeley, 1971 (ed. G. Shapiro) (LBL 500, UC-34 Physics, National Technical Information Service, Springfield, Virginia, 1972), p. 397.
- 87) J.J. Hill and D.A. Hill, ANL/HEP report 7359, Argonne (1973).
- 88) N.S. Garif'yanov, B.M. Kozyrev and V.N. Fedotov, Dokl. Akad. Nauk SSSR 178, 808 (1968);  
[Soviet Phys. Dokl. 13, 107 (1968)].
- 89) P.R. Bontchev, A. Malinovski, M. Mitewa and K. Kabassanov, Inorg. Chim. Acta 6, 499 (1972).
- 90) M. Mitewa, A. Malinovski, P.R. Bontchev and K. Kabassanov, A study on Cr<sup>V</sup>-complexes formed in the process of photochemical oxidation of diethyleneglycol by dichromate, Inorg. Chim. Acta, to be published.
- 91) D.M. Etheridge, thesis, Oxford Univ., Oxford (1971).
- 92) H. Glättli, Proc. 2nd Int. Conf. on Polarized Targets, Berkeley, 1971 (ed. G. Shapiro) (LBL 500, UC-34 Physics, National Technical Information Service, Springfield, Virginia, 1972), p. 281.
- 93) W.G. Williams and J.L. Thomas, RHEL/R 213, Rutherford Lab. (1971).
- 94) P. Weymuth, Proc. 2nd Int. Conf. on Polarized Targets, Berkeley, 1971 (ed. G. Shapiro) (LBL 500, UC-34 Physics, National Technical Information Service, Springfield, Virginia, 1972), p. 301.
- 95) M. Odehnal and V. Bouffard, Phys. Letters 32 A, 407 (1970).
- 96) D. Hill, private discussion.
- 97) M. Borghini, O. Chamberlain, R.Z. Fuzesy, W. Gorn, C.C. Morehouse, T. Powell, P. Robrish, S. Rock, S. Shannon, G. Shapiro and H. Weisberg, Nuclear Instrum. Methods 84, 168 (1970).
- 98) W. Gorn and P. Robrish, Proc. 2nd Int. Conf. on Polarized Targets, Berkeley, 1971 (ed. G. Shapiro) (LBL 500, UC-34 Physics, National Technical Information Service, Springfield, Virginia, 1972), p. 305.
- 99) W. de Boer, M. Borghini, M. Rieubland and F. Udo, Dynamic polarization at <sup>3</sup>He temperatures in a 50 kG magnetic field, unpublished results.

- 100) S. Mango, Ö. Runolfsson and M. Borghini, Nuclear Instrum. Methods 72, 45 (1969).
- 101) D. Hill, J.B. Ketterson, R.C. Miller, A. Moretti, R.C. Niemann, L.R. Windmiller, Y. Yokosawa and C.F. Hwang, Phys. Rev. Letters 23, 460 (1969).
- 102) D.J. Nicholas, P.H.T. Banks and D.A. Cragg, Nuclear Instrum. Methods 88, 69 (1970).
- 103) S.F.J. Read, G.W.L. Duncan, D.R. Madden, D.J. Nicholas and W.G. Williams, Proc. 16th Colloque Ampère, Bucharest, 1970 (ed. I. Ursu) (North-Holland Publishing Co., Amsterdam, 1971), p. 976.
- 104) G. Hartmann, D. Hubert, S. Mango, C.C. Morehouse and K. Plog, Proc. 2nd Int. Conf. on Polarized Targets, Berkeley, 1971 (ed. G. Shapiro) (LBL 500, UC-34 Physics, National Technical Information Service, Springfield, Virginia, 1972), p. 289.
- 105) M. Borghini, A. Masaike, K. Scheffler and F. Udo, Nuclear Instrum. Methods 97, 577 (1971).
- 106) M. Borghini and K. Scheffler, Phys. Rev. Letters 26, 1362 (1971).  
M. Borghini and K. Scheffler, Nuclear Instrum. Methods 95, 93 (1971).
- 107) M. Borghini and F. Udo, Phys. Letters 43 A, 93 (1973).
- 108) K. Scheffler, Proc. 2nd Int. Conf. on Polarized Targets, Berkeley, 1971 (ed. G. Shapiro) (LBL 500, UC-34 Physics, National Technical Information Service, Springfield, Virginia, 1972), p. 271.
- 109) K. Scheffler, Nuclear Instrum. Methods 82, 205 (1970).
- 110) V.A. Atsarkin, A.E. Mefed and M.I. Rodak, Zh. Eksper. Teor. Fiz. 55, 1871 (1968);  
[Soviet Phys. JETP 28, 877 (1969)].  
H.H. Niebuhr, E.E. Hundt and E. Brun, Helv. Phys. Acta 43, 778 (1970).
- 111) Ch. Gabathuler and E. Brun, Proc. 1st Specialized Colloque Ampère, Kraków, 1973 (ed. J.W. Hennel) (Inst. of Nuclear Physics, Kraków, Poland, 1973), p. 176.
- 112) A. Abragam, M. Chapellier, M. Goldman, J.F. Jacquinet and Vu Hoang Chau, Proc. 2nd Int. Conf. on Polarized Targets, Berkeley, 1971 (ed. G. Shapiro) (LBL 500, UC-34 Physics, National Technical Information Service, Springfield, Virginia, 1972), p. 247.
- 113) M. Borghini and K. Scheffler, see above Conference, p. 303.
- 114) R.L. Kuhl and B.D. Nageswara-Rao, Phys. Rev. 158, 284 (1967).  
V.A. Atsarkin, A.E. Mefed and M.I. Rodak, Zh. Eksper. Teor. Fiz. 55, 1671 (1968);  
[Soviet Phys. JETP 28, 877 (1969)].
- 115) G.M. Van de Heuvel, C.T.C. Heyning, T.J.B. Swanenburg and N.J. Poulis, Phys. Letters 27 A, 38 (1968).
- 116) S.F.J. Cox, V. Bouffard and M. Goldman, J. Phys. C 6, L100 (1973).
- 117) A. Malinovski and H. Glättli, private communication. At 1.2 K and 3 kG they measured an electron spin lattice relaxation time of 40 msec in ethanediol, if one disregarded the initial non-exponential part of the recovery signal. This non-exponential behaviour may be due to microwave heating of the sample, since  $T_{1e}$  showed a strong temperature dependence at 3 kG. Our measurements of  $T_{1e}$  at 25 kG were only weakly dependent on temperature around 0.5 K. Such a different temperature dependence of  $T_{1e}$  in low and high magnetic fields is in agreement with Eq. (III.9).
- 118) E.A. Harris and K.S. Yngvesson, Proc. Phys. Soc. Ser. 2, 1, 990 (1968).
- 119) V.A. Atsarkin, P.E. Budkovskiy, G.A. Vasneva, V.V. Demidov, E.A. Novikov, O.A. Ryabushkin and Yu. V. Funtikov, 17th Colloque Ampère, Turku, 1972 (ed. V. Hovi) (North-Holland Publishing Co., Amsterdam, 1973), p. 502.
- 120) J. Svoboda and M. Odehnal, Czech. J. Phys. B24, 93 (1974).

- 121) For definition see, for example, G.L. Pollack, Rev. Mod. Phys. 41, 1, 48 (1969).
- 122) The author is indebted to S. Mango for the measurements at 17 kG, which were performed at SIN, Zürich.
- 123) M.E. Zhabotinskii, A.E. Mefed and M.I. Rodak, Zh. Eksper. Teor. Fiz. Pis'ma 11, 482 (1970); [JETP Letters 11, 328 (1970)].
- 124) R.V. Pound, Phys. Rev. 79, 685 (1950).
- 125) R.G. Barnes and J.W. Bloom, J. Chem. Phys. 57, 3082 (1972).
- 126) M. Borghini, W. de Boer, K. Morimoto and K. Scheffler, CERN, unpublished results.
- 127) M. Borghini, S. Mango, O. Runolfsson and J. Vermeulen, Proc. 1st Int. Conf. on Polarized Targets and Ion Sources, Saclay, 1966 (ed. La Direction de la Physique, CEN) (La Documentation Française, Saclay, 1966), p. 387.  
M. Borghini, see Fig. 14, by M. Borghini and P. Weymuth, *in* Proc. 2nd Int. Conf. on Polarized Targets, Berkeley, 1971 (ed. G. Shapiro) (LBL 500, UC-34 Physics, National Technical Information Service, Springfield, Virginia, 1972), p. 1.
- 128) M. Borghini, W. de Boer and K. Morimoto, Dynamic polarization by a resolved solid-state effect and thermal mixing with an electron spin-spin interaction reservoir, submitted to Physics Letters.
- 129) S.F. Read, Thesis, Oxford University (1962).
- 130) F.M. Russel, Proc. 2nd Int. Conf. on Polarized Targets, Berkeley, 1971 (ed. G. Shapiro) (LBL 500, UC-34 Physics, National Technical Information Service, Springfield, Virginia, 1972), p. 89.

## APPENDIX

For the convenience of the reader we shall give here the derivation of Eq. (I.31), which was at first derived by Borghini<sup>4</sup>).

If we assume, that the amplitude of the microwave field is small and that the ESR line width arises mainly from g-factor anisotropy (thus hyperfine- and spin-spin interactions are negligible), then the Hamiltonian for the electron spin system can be written as

$$H = \sum_i h\nu_i S_z^i . \quad (\text{A.1})$$

The total variation of  $\langle H \rangle$  arises from spin lattice relaxation and saturation owing to an RF field:

$$\left(\frac{d}{dt}\right)_{\text{tot}} \langle H \rangle = \left[ \left(\frac{\partial}{\partial t}\right)_L + \left(\frac{\partial}{\partial t}\right)_{\text{RF}} \right] \langle H \rangle . \quad (\text{A.2})$$

There is no variation of  $\langle H \rangle$  arising from the spin-spin interactions, since energy is always conserved in pure spin-spin processes.

The exchange of energy between the RF field and the spin system occurs via the absorption or emission of photons with energy  $h\nu$ . Therefore

$$\left(\frac{\partial}{\partial t}\right)_{\text{RF}} \langle H \rangle = h\nu \left(\frac{\partial}{\partial t}\right)_{\text{RF}} \langle S_z \rangle . \quad (\text{A.3})$$

Furthermore, cross-relaxation transitions do not change  $\langle S_z \rangle$ , since they involve an even number of electron spins, thus  $(\partial/\partial t)_{\text{SS}} \langle S_z \rangle = 0$ . Then, since  $\langle S_z \rangle$  is constant in steady-state:

$$\left(\frac{\partial}{\partial t}\right)_{\text{RF}} \langle S_z \rangle = -\left(\frac{\partial}{\partial t}\right)_L \langle S_z \rangle . \quad (\text{A.4})$$

A combination of this result with Eqs. (A.2) and (A.3) gives in steady-state [when  $(d/dt)_{\text{tot}} \langle H \rangle = 0$ ]:

$$\left(\frac{\partial}{\partial t}\right)_L \langle H - h\nu S_z \rangle = 0 , \quad (\text{A.5})$$

or in our case [see Eq. (A.1)]:

$$\left(\frac{\partial}{\partial t}\right)_L \left\langle \sum_i h(\nu_i - \nu) S_z^i \right\rangle = 0 . \quad (\text{A.6})$$

This result means that the value of  $\langle \sum_i h\Delta_i S_z^i \rangle$  in steady-state equalizes its thermal equilibrium value, or

$$\sum_i \Delta_i P_i = \sum_i \Delta_i P_0 = \Delta P_0 \quad . \quad (\text{A.7})$$

If there are nuclei surrounding the electron spins, Eq. (A.5) reads:

$$\left( \frac{\partial}{\partial t} \right)_L \left[ \left\langle \sum_i h\Delta_i S_z^i \right\rangle + \left\langle \sum_j h\nu_n I_z^j \right\rangle \right] = 0 \quad , \quad (\text{A.8})$$

or

$$\sum_i \left[ \Delta_i P_i + f\nu_n P_n (1 - P_0 P_i) \right] = \Delta P_0 \quad . \quad (\text{A.9})$$

Here we neglected the thermal equilibrium polarization of  $P_n$ .

## SAMENVATTING

Dit proefschrift beschrijft de dynamische polarisatie experimenten, die gedurende de laatste 2 à 3 jaar uitgevoerd zijn in de Polarized Target groep bij CERN.

Behalve op het bereiken van hoge polarisaties, was de aandacht vooral gericht op het verkrijgen van inzicht in de mechanismen van dynamische polarisatie.

In Hoofdstuk I worden verschillende mechanismen beschreven in termen van de spin-temperatuur theorie; de wisselwerkingen tussen gelijke spins, die in vaste stoffen aanleiding kunnen geven tot een collectief gedrag worden in deze quantum-statistische theorie in rekening gebracht door de introductie van een spin-spin interactie reservoir met een eigen temperatuur, die verschillend kan zijn van de temperatuur van het Zeeman energie reservoir. Het blijkt, dat het spin-spin interactie reservoir een fundamentele rol speelt in de verklaring van vele experimenten op het gebied van dynamische polarisatie, spin-rooster relaxatie, adiabatische demagnetisatie, cross-relaxatie e.a.

In Hoofdstuk II worden de meetmethoden en de apparatuur besproken. De experimenten werden uitgevoerd bij magneetveldwaarden tot 50 kG en temperaturen beneden 1 K ( $^3\text{He}$  verdampingscryostaten en een  $^3\text{He}$ - $^4\text{He}$  mengcryostaat).

Hoofdstuk III beschrijft de dynamische polarisatie experimenten in diolen, waarin kleine hoeveelheden paramagnetische  $\text{Cr}^{\text{V}}$ -complexen voorkomen. Deze organische verbindingen zijn interessant voor het gebruik in verstrooiingsexperimenten vanwege de hoge kern-spin polarisaties, die we erin bereikt hebben:  $\sim 80$ - $90\%$  voor protonen,  $\sim 40\%$  voor deuterium - en  $50\%$  voor koolstof-13 kernen.

In een magneetveld van 25 kG werd een sterke thermische koppeling tussen de kern-spin systemen waargenomen, die vanwege de sterke temperatuur-afhankelijkheid van de overgangverschijnselen aan de invloed van het electron spin-spin interactie reservoir moet worden toegeschreven.

Dynamische polarisatie werd verkregen door verzadiging van het electron-spin systeem met behulp van microgolven, die een frequentie juist naast de electron-spin resonantie-frequentie hadden. Het verschil tussen de photon - en electron Zeeman energie wordt dan opgenomen door het electron spin-spin interactie reservoir, wat hierdoor een temperatuur verschillend van de rooster temperatuur krijgt. Dit temperatuurverschil kan naar de kern-spin systemen overgebracht worden door, bijvoorbeeld, cross-relaxatie overgangen tussen twee electron-spins, waarbij tevens een kern-spin omklapt.

De gemeten proton-, deuterium-en koolstof-13 polarisatie werden vergeleken met een spin temperatuur model van Borghini, dat geldig is bij lage temperaturen. Verschillende kenmerken, zoals gelijke spin-temperaturen voor alle kernen, een sterke temperatuur-afhankelijkheid van de polarisaties en een toename van de verhouding van rooster-temperatuur en

de "steady-state" spin-temperatuur by spin-temperaturen beneden 2 mK, stemmen quantitatief goed overeen met de metingen. Dit is de eerste keer, dat deze theorie experimenteel geverifieerd werd bij zulke lage temperaturen en dat de berekende hoge polarisaties inderdaad bereikt werden.

In gedeeltelijk gedeutereerde diolen werd een nieuwe methode van orientatie van het deuterium-spin systeem gevonden, waarmee de tensor-polarisatie (= alignering) onafhankelijk van de vector-polarisatie gevarieerd kan worden (zie Hoofdstuk IV). Dit gebeurt bij niet-resonante verzadiging van het gepolariseerde proton-spin systeem, wat een koeling van het proton spin-spin interactie reservoir ten gevolge heeft. De waarnemingen werden geïnterpreteerd als een thermisch contact tussen dit reservoir en het deutron "quadrupole interactie reservoir". De resultaten stemmen verrassend goed overeen met quantitative berekeningen op grond van de spin-temperatuur theorie. Dit mechanisme vertoont een grote analogie met het hierboven omschreven mechanisme van dynamische polarisatie: daar werd de dynamische koeling van het electron spin-spin interactie reservoir overgebracht op de kernen, hier wordt de koeling van het proton spin-spin interactie reservoir overgebracht op het deutron quadrupole interactie reservoir.

In Hoofdstuk V worden de experimenten met het vrije radicaal 1,2-bis-diphenylene-1-phenylallyl beschreven. Deze zijn vooral interessant, omdat verschillende dynamische polarisatie mechanismen experimenteel van elkaar gescheiden kunnen worden ten gevolge van de nauwe electron spin resonantie lijn van dit vrije radicaal. De proton-, deuterium-en koolstof-13 polarisatie, gemeten als functie van de microgolf-frequentie, vertonen duidelijk de bijdragen van het "solid-state effect", het "double" solid-state effect en van dynamische polarisatie door koeling van het electron spin-spin interactie reservoir.

## Stellingen

- 1) De beschrijving, die Hill and Hwang geven voor het mechanisme van dynamische polarisatie in 1-butanol, verzadigd met het vrije radicaal porphyrexide, is onvolledig<sup>1)</sup>.
  - 1) C.F. Hwang and D.A. Hill, Phys. Rev. Letters 19, 1011 (1967).
- 2) Gezien de bestaande gegevens en technieken is het verwonderlijk, dat de polarisatie in elastische verstrooiing van positieve hadronen nog niet gemeten is bij kleine verstrooiingshoeken.
- 3) Het is in het algemeen moeilijk om de proton polarisatie met een absolute nauwkeurigheid beter dan 2% te bepalen, uitgezonderd in stoffen waar dynamische polarisatie door koeling van het electron spin-spin interactie reservoir optreedt.  
Dit proefschrift, Hoofdstuk III.2.3.
- 4) Het is interessant gepolariseerd propaandiol als koelmiddel in een adiabatische demagnetisatie cryostaat te proberen, o.a met het oog op mogelijk nieuwe fase-overgangen in vloeibaar <sup>3</sup>He beneden 1 mK.
- 5) De interpretatie van de complexe deutron magnetische resonantie lijn in toluol-D8 is in strijd met de door ons waargenomen deutron magnetische resonantie lijn in m-xylool-D6.  
R.G. Barnes en J.W. Bloom, J. Chem. Phys. 57, 3082 (1972)  
Dit proefschrift, Hoofdstuk IV.3.
- 6) De waarnemingen van Henaux en Conard vormen geen duidelijke illustratie van dynamische polarisatie door koeling van het electron spin-spin interactie reservoir, dit in tegenstelling tot wat de schrijvers stellen.
  - 1) J.Cl. Henaux and J. Conard, 17th Congress Ampere, Turku, 1972 (ed. V. Hovi) (North Holland Publ. Co.), Amsterdam, 1973, p. 509.
- 7) Nu er gepolariseerde deuterium targets beschikbaar zijn, verdient het aanbeveling de reactie  $\pi^+n^+ \rightarrow \pi^0p$  te bestuderen, dit om de controverses in de metingen van verschillende groepen<sup>1,2)</sup> in de ladingssymmetrische reactie  $\pi^-p^+ \rightarrow \pi^0n$  weg te nemen.
  - 1) P. Bonamy et al. Nucl. Phys. B52, 392 (1973)
  - 2) D. Hill et al. Phys. Rev. Lett. 30, 239 (1973).
- 8) De mogelijkheid van een cryogene detectie van neutrino's, zoals voorgesteld door Lubkin<sup>1)</sup>, is realistischer dan uit zijn schattingen blijkt.
- 9) De impuls van een geladen deeltje in een bekend magneetveld wordt dikwijls bepaald uit enkele gemeten punten van de baan m.b.v. een iteratieve Runge-Kutta integratie. Het is computer-tijd besparend om deze methode te vervangen door de "quintic spline" methode<sup>1)</sup>.
  - 1) H. Wind, Nucl. Instr. and Methods, 115, 431 (1974).
- 10) Van de Meerssche stelt in zijn proefschrift: "Het blijkt, dat bij de aanstelling van de Europese ambtenaren de nationale invloeden omgekeerd evenredig toenemen met de improvisatie-talenten van de betrokken organisaties en instellingen en recht evenredig met de belangrijkheid van de te begeben posten" <sup>1)</sup>. De wetenschappelijkheid van deze stelling dient betwijfeld te worden.
  - 1) P. van de Meerssche, proefschrift "Het Europees openbaar ambt", Katholieke Universiteit van Leuven, Leuven (1965), p. 182.